# APPLICATIONS OF PHOTODYNAMIC EFFECTS IN DERMATOLOGY

*By*

**KHAGESWAR SAHU**

**LIFE03200904002**

**Raja Ramanna Centre for Advanced Technology,**

**Indore-452013, India**

***A Thesis submitted to the***

***Board of Studies in Life Sciences***

***In Partial Fulfilment of requirements***

***for the degree of***

**DOCTOR OF PHILOSOPHY**

***Of***

**HOMI BHABA NATIONAL INSTITUTE**

***August 2014***

# Homi Bhabha National Institute

## Recommendations of the Viva Voce Committee

As members of the Viva Voce Committee, we certify that we have read the dissertation prepared by **Khageswar Sahu** entitled "**Applications of photodynamic effects in dermatology**" and recommend that it may be accepted as fulfilling the thesis requirement for the award of Degree of Doctor of Philosophy.

**Chairman – Dr. S.K. Apte** **Date:** 14/10/2015

**Guide / Convener – Dr. M. Sharma** **Date:** 14/10/15

**Co-guide – Dr. P.K. Gupta** **Date:** 14/10/15

**Member 1– Dr. A. Dube** **Date:** 14/10/15

**Member 2–Dr. A. Ghosh** **Date:** 14/10/15

**External Examiner Dr. J. Gowrishankar** **Date:**

Final approval and acceptance of this thesis is contingent upon the candidate's submission of the final copies of the thesis to HBNI.

We hereby certify that we have read this thesis prepared under our direction and recommend that it may be accepted as fulfilling the thesis requirement.

**Date:** 14/10/15

**Place: RRCAT, Indore**

**Guide**
**(Dr. M. Sharma)**

**Co-guide**
**(Dr. P.K. Gupta)**

## STATEMENT BY AUTHOR

This dissertation has been submitted in partial fulfillment of requirements for an advanced degree at Homi Bhabha National Institute (HBNI) and is deposited in the Library to be made available to borrowers under rules of the HBNI.

Brief quotations from this dissertation are allowable without special permission, provided that accurate acknowledgment of source is made. Requests for permission for extended quotation from or reproduction of this manuscript in whole or in part may be granted by the Competent Authority of HBNI when in his or her judgment the proposed use of the material is in the interests of scholarship. In all other instances, however, permission must be obtained from the author.

Khageswar sahu.

(Khageswar Sahu)

## DECLARATION

I, hereby declare that the investigation presented in the thesis has been carried out by me. The work is original and has not been submitted earlier as a whole or in part for a degree / diploma at this or any other Institution / University.

Khageswar sahu.

(Khageswar Sahu)

# LIST OF PUBLICATIONS ARISING FROM THE WORKS PRESENTED IN THE THESIS

## I. Publications in referred Journals:

1. **K. Sahu**, M.Sharma, A. Dube and P. K. Gupta, "Topical antimicrobial photodynamic therapy improves angiogenesis in wounds of diabetic mice", Lasers Med Sci. **30**,1923-9 (2015).
2. **K. Sahu**, M. Sharma, P. Sharma, Y. Verma, K.D. Rao, H. Bansal, A. Dube and P. K Gupta."Effect of poly-L-lysine-chlorin p6 mediated antimicrobial photodynamic treatment on collagen restoration in bacteria infected wounds." Photomed Laser Surg. **32**, 23-29 (2014).
3. **K. Sahu**, M. Sharma, H. Bansal, A. Dube and P.K. Gupta, "Topical photodynamic treatment with poly-L-lysine chlorin p6 conjugate improves wound healing by reducing hyperinflammatory response in *Pseudomonas aeruginosa* infected wounds of mice." Lasers Med Sci. **28**, 465-471 (2013).
4. **K. Sahu**, H. Bansal, C. Mukharjee, M. Sharma and P.K. Gupta, "Atomic force microscopic study on morphological alterations induced by photodynamic action of Toluidine Blue O in *Staphylococcus aureus* and *Escherichia coli*." J Photochem Photobiol. B **96**, 9–16 (2009).

## II. Conferences presentations

1. **K. Sahu**, M. Sharma, A. Dube and P. K. Gupta. "Antimicrobial photodynamic therapy for wound healing ". Presentation in 21$^{st}$ International Conference on Lasers in Surgery and medicine, Aug 18-21$^{st}$ , Indore, Madhya Pradesh (2015) .

2. **K. Sahu**, H. Bansal, M. Sharma, A. Dube and P. K. Gupta. "Antimicrobial photodynamic treatment induced by red light and poly-L- lysin conjugated chlorine p6 leads to enhanced nitrite level and healing in Methicillin resistant *Staphylococcus aureus* infected wounds of diabetic mice". Presentation in National Laser Symposium 2014, Jan 7-10$^{th}$ , Manipal, Udupi (2014) .
3. **K. Sahu**, M. Sharma, H. Bansal, A. Dube and P. K. Gupta. "Antimicrobial photodynamic treatment induced oxidative stress reduces inflammatory response in Methicillin resistant *Staphylococcus aureus* infected wounds in diabetic mice". Presentation in 9$^{th}$ DAE-BRNS Life Science Symposium 2013, Nov 28$^{th}$- 30$^{th}$, Bhaba Atomic Research Centre, Mumbai (2013).
4. **K. Sahu**, M.Sharma, A. Dube and P. K. Gupta "Effect of photodynamic therapy on inflammatory response of *Pseudomonas aeruginosa* infected wounds". Presentation in FIMSA Advanced course on "Basic and translational immunology", Institute for Defence Studies and Analyses, New Delhi during Mar 18-20$^{th}$ (2012).
5. **K. Sahu**, M.Sharma, P. Kakani, A. Dube, P. K. Gupta. "Photodynamic treatment induced changes in expression of inflammatory cytokines and growth factors in *Pseudomonas aeruginosa* infected excisional wounds of mice" Presentation in 5$^{th}$ Annual Meeting of Federation of Immunological Society of Asia and Oceania , Mar 14-17$^{th}$ , New delhi (2012).
6. **K. Sahu**, Y. Verma, M. Sharma, K.D. Rao, A. Dube, P. K. Gupta "Optical Coherence Tomography for Non-invasive Assessment of Wound Healing Response in *Pseudomonas aeruginosa* infected excisional wounds subjected to Photodynamic Treatment". Presentation in XXXVI Optical Society of India

conference " Frontiers in Optics and photonics 2011", Dec 3-5th,Indian Institute of Technology, New Delhi (2011).

7. **K. Sahu**, M. Sharma, H. Bansal, A.Dube and P.K. Gupta, "Evaluation of photobactericidal effect of poly-L-lysine conjugated chlorine p6 on *Pseudomonas aeruginosa* infected wounds." Presentation (oral) in International Conferences on Antimicrobial Research-2010, Nov 3 -5th ,Valladolid, Spain ( 2010) .

Khageswar Sahu.

(Khageswar Sahu)

*I dedicate this work to my family and my school*

# ACKNOWLEDGEMENT

*My supervisors Prof M. Sharma and Prof. P. K. Gupta have been the guiding forces in shaping up of the thesis. I express my deep sense of gratitude to both them for their erudite guidance, continuous support in the planning of experiments, and analysis of the experimental data. I also thank both of them for proofreading of various drafts of this thesis, the synopsis and of the manuscripts, which helped me, immensely. The journey had been smoother because of the presence of both of them, from whom I have learnt many lessons, the most important one being the desire to work hard.*

*I would like to thank my colleagues especially Mrs. H. Bansal, Dr. Y. Verma, Dr. A. Dube, Dr. K. D. Rao, Ms. P. Sharma, Mr. M. K. Swami and Mr. H. S. Patel for the discussions, suggestions during the work and for participating in some of the studies included in this dissertation. I am especially grateful to Mr. M. K. Swami for his suggestions and help in formatting the thesis.*

*I would like to thank Mr. Anupam Chowdhury for his help in some of the works on animal models. I acknowledge the support of Mr. Gyan Singh and Mr. Yeshwant Deshpande in the day-to-day maintenance of the animal house and the help of Mr. V. Sharma in repair and maintenance of the instruments. I also appreciate the helps of my project trainees Ms. H. Jain and Ms. S. Pathak for helping me in some of the studies of this dissertation.*

*Appreciations are also due for Ms. P. Patheja, Dr. K. Das, Dr. B. Bose, Dr. R. Dasgupta for their involvements in general discussions which in some or other way helped in the thesis work. I duly acknowledge the support from Dr S. Raja and his*

*colleagues, for their help.I thank the other colleagues of LBAID,RRCAT for their support.*

*I express my gratitude to doctoral committee members Prof. S. K. Apte, Prof. T. P. A. Devasagayam and Dr S.Santosh Kumar for their suggestions and involvement in discussions during the progress of the thesis work.*

*Culmination of this thesis is also a result of the inspirations I have received from my family. I am indebted to my wife for her constant encouragements to complete my thesis work in a stipulated period. My parents, brothers, parents-in-laws and my sister-in-law have also played important roles in motivating me and I sincerely acknowledge their support .*

*Khageswar Sahu*

## CONTENTS

# SYNOPSIS

**Name of the Constituent Institution:** Raja Ramanna Centre for Advanced Technology

**Name of the Student:** Khageswar Sahu

**Enrolment No:** LIFE03200904002

**Title of the Thesis:** Applications of photodynamic effects in dermatology

In today's society, chronic wounds represent a major health care burden. Normally wounds heal in about 2-3 weeks and the healing has four overlapping phases: coagulation, inflammation, proliferation, and remodeling. Abnormality in any of these phases, caused by either systemic factors like vascular insufficiency, diabetes, neuropathy, or local factors such as pressure and infection of wounds can cause delay in healing. The growing emergence of antibiotic resistance in bacteria commonly infecting wounds is another concern particularly in diabetic and immunocompromised conditions. To overcome this problem various alternative strategies are being explored. These include use of (i) antimicrobial peptides, (ii) efflux pump inhibitors, and (iii) antimicrobial photodynamic therapy (APDT). Of these, APDT is particularly attractive, because, while bacteria are expected to develop resistance mechanisms against the other approaches, the possibility of developing resistance against APDT is considered remote.

APDT involves excitation of an exogenously applied or endogenously synthesized photosensitizer (PS) by visible light. This can lead to generation of lethal level of

singlet oxygen via energy transfer to molecular oxygen present in the wound tissue. This is referred to as type II process. The other process contributing to the inactivation of microbes, referred to as type I process, involves generation of radicals through electron transfer to nearby molecules. In contrast to the conventional antibiotics that are designed to target a specific bacterial site, in APDT, the generated reactive oxygen species (ROS) destroy all cellular components and are not target specific. This is the reason why it is considered highly unlikely that bacteria could evolve resistance mechanisms against APDT. In addition, PDT can inactivate bacterial virulent factors, biofilms and proinflammatory cytokines, which also can contribute to faster healing.

The important parameters that an ideal PS for APDT should have include (i) high ROS quantum yield, (ii) cationic charge as well as amphiphilic nature to ensure higher accumulation at the polyanionic microbial cell surfaces and (iii) a strong absorbance in the red region to minimize the energy deposition in tissue. Cationic phenothiaziniums, like methylene blue and toluidine blue have been the most widely investigated photosensitive drugs currently being investigated for APDT. However, these have relatively lower triplet yield, hydrophilic nature, and efflux pump dependent uptake into bacterial cells. Therefore there is interest in exploring other PS. Chlorophyll derivatives like chlorine p6 (cp6) are particularly attractive because these have good triplet yield, amphiphilicity and strong absorbance in the red (660 nm) region. Since cp6 is anionic, its conjugation with cationic peptides like poly-L-lysin (pl-cp6) is therefore expected to enhance the targeting of the cp6 to bacterial cells. The objective of the thesis was to explore the photobactericidal efficacy of cp6 and pl-cp6 for both Gram positive and negative bacteria and investigate the use of pl-cp6

mediated APDT for the healing of bacteria infected and uninfected wounds in normal and diabetic mice.

The thesis is organized as follows.

**In Chapter 1,** we provide a brief overview of the processes involved in the healing of wounds and the factors that can lead to the development of the chronic wounds. Therapeutic modalities for the management of antibiotic resistant bacteria, with particular emphasis to APDT, are discussed next

In **chapter 2,** we describe the strains of bacteria used for our studies, photoirradiation protocol, procedure for synthesis of pl-cp6 and establishment of wound infection in normal as well as diabetic mice model. A brief overview of biochemical techniques such as immunoblotting, hydroxyproline assay, that were used for our studies on wound healing, is also provided in the chapter.

In **chapter 3,** we present the results of the investigations carried out to study the phototoxicity of cp6 and pl-cp6 against *Staphylococcus aureus* (Gram positive), *Pseudomonas aeruginosa* (Gram negative) and keratinocyte cell line (HaCaT). The latter was used as a model for host cell.

In **chapter 4,** we present the results of the studies carried out by us towards understanding the mechanism of bacterial cell damage induced by APDT mediated by different photosensitizers, cp6, pl-cp6 and a standard phenothiazinium, toluidine blue O (TBO). Changes in cellular morphology resulting from APDT were monitored using atomic force microscopy. Fluorescence microscopy of cell impermeable dye (Propidium Iodide) uptake and absorbance spectroscopy were used to monitor damage to cell membrane and leakage of intracellular contents, respectively. As noted in

chapter 3, for *S.aureus* and *P. aeruginosa,* cp6 showed lower phototoxicity and did not result in significant morphological alterations. APDT mediated by both TBO and pl-cp6 resulted in a significant reduction in the mean cell height, flattening of Gram negative bacteria (*P.aeruginosa, E.coli*) suggesting damage to the bacterial membrane and reduction of cell volume due to the loss of cytoplasmic materials. For *S.aureus,* the change in morphology observed subsequent to APDT mediated by TBO and pl-cp6 was significantly different. While the major effect of TBO mediated APDT was breakage in the contact between the cell wall and the membrane, pl-cp6 mediated APDT resulted in damage primarily to outer peptidoglycan layer.

In **chapter 5,** we describe the results of the studies carried out to investigate the effect of pl-cp6 mediated topical APDT on the healing of *P. aeruginosa* infected wounds in mice. Apart from monitoring the decrease in bacterial load, the levels of different cytokines like interleukin-6 (IL-6), Tumor necrosis factor-α (TNF-α) were measured to quantitate the effect of APDT on the inflammatory response. The results showed that 96 hr post APDT, bacteria load, IL-6 and, TNF-α level in the infected wounds were reduced by ~1.5 log, ~6 times and ~ 4 times, respectively. The resulting reduction in hyperinflammatory response in wounds may also be contributing to the observed faster healing.

In **chapter 6,** we present the results of the studies carried out to investigate the effect of pl-cp6 mediated topical APDT on collagen remodeling response of methicillin resistant *Staphylococcus aureus* (MRSA) and *P. aeruginosa* infected wounds. Collagen remodeling was monitored by measurement of tissue retardance using Polarization sensitive Optical Coherence Tomography (PSOCT) as well as by measurements on hydroxyproline content and matrix metalloproteases (MMP-8 and

MMP-9) level in wounds. As expected, compared to the uninfected wounds, slower collagen restoration and higher MMP-8,9 expressions were observed in infected wounds. Further, compared to the infected wounds treated with pl-cp6 alone, in infected wounds treated with both pl-cp6 and light the hydroxyproline content and retardance were higher by a factor of ~3 and ~2 respectively but MMP 8, 9 levels were lower. This suggests that APDT leads to promotion of collagen remodeling of wounds.

In **chapter 7**, we present results of the studies carried out to investigate the effect of single or multiple APDT on the healing response of MRSA infected and uninfected wounds of diabetic mice. The parameters monitored include bacteria regrowth, thiobarbituric acid reactive substrates (TBARS), protein carbonyl (PC) and glutathione (GSH) levels in wound tissues. Further, to quantify the effect of APDT on inflammatory cells of wounds, measurements were also made on the level of myeloperoxidase (MPO) and neutrophil elastase (NE). Results show that, compared to untreated wounds, in MRSA infected wounds of diabetic mice subjected to APDT at a fluence of ~120 J/cm$^2$ there was ~ 1.5 log decrease in bacteria load after APDT. However, at 24h post APDT (day 3) there was ~ 5-fold bacteria regrowth. The use of APDT repeated at 24 hr intervals for 3 days was investigated to address this issue. APDT at a higher fluence of ~120 J/cm$^2$ led to a significant increase in TBARS (~70 %), PC (~ 25 %) and a decrease in MPO, while there was no change in NE and GSH levels. Multiple APDT at fluence of ~60 J/cm$^2$ led to better responses like reduction in bacterial regrowth by a factor of ~ 2.5, increased levels of MPO (~50%), NE (~35 %), GSH (~35%), moderate increase in TBARS (~ 40 %) but no change in PC levels.

Further, effect of multiple APDT at a fluence of ~60 J/cm$^2$ on angiogenesis in wounds of diabetic mice was also investigated. Measurements were made on the levels of nitric oxide (NO) and vascular endothelial growth factor-A (VEGF-A) of wound tissue, which play important role in angiogenesis and healing of wounds. Results show that multiple APDT leads to an increase in the levels of NO and VEGF-A by factor of ~3.5 and ~60 %, respectively, on day 3. Furthermore, a good correlation was observed between NO concentration and wound closure time ($R^2$ = -0.90, $p < 0.05$). These results suggest that enhanced angiogenesis caused by APDT may also lead to improvement in wound healing.

Finally, in the **chapter 8**, we provide a brief summary of the findings of the studies included in the thesis and discuss the future potential.

***List of Abbreviations***

AFM Atomic Force Microscopy

AGE Advanced glycated end products

AG Aminoguanidine

$AgNO_3$ Silver nitrate

APDT Antimicrobial photodynamic therapy

CFU Colony forming units

Cp6 Chlorin p6

Ce6 Chlorin e6

DAQ Data acquisition board

EGF Epidermal growth factor

GAPDH Glyceral dehyde-3-phosphate dehydrogenase

GSH Reduced glutathione

*HaCaT* Human keratinocyte cell line

IL Interleukin

IGF-1 Insulin-like growth factor-1

Inf Infected

L+S+ Light+ photosensitizer

M Mirror

MRSA Methicillin resistant *Staphylococcus aureus*

MMP  Matix metalloprotease

MPO Myeloperoxidase

NPBS  Nonpolarizing beam splitter

NE Neutrophil elastase

NBT Nitroblue tetrazolium

NO Nitric oxide

PBS  Phosphate buffered saline

PC Protein carbonyl

PDGF  Platelet-derived growth factor

PI  Propidium iodide

Pl-cp6  Poly-L-lysin conjugated chlorin p6

PSOCT  Polarization sensitive Optical Coherence Tomography

PS  Photosensitizer

RNO p-nitrosodimethylaniline

ROS Reactive oxygen species

SC Stratum corneum

SD  Standard deviation

SEM  Standard error of mean

STZ  Streptozotocin

TBARS Thiobarbituric acid reactive substrates

TBO Toluidine blue O

TNF-α Tumor necrosis factor-α

VEGF-A Vascular endothelial growth factor-A

# LIST OF TABLES

## LIST OF FIGURES

# 1. Introduction


## Abstract

In this chapter we provide a brief overview of the processes involved in the healing of wounds and the factors that can lead to the development of the chronic wounds. Therapeutic modalities for the management of antibiotic resistant bacteria, with particular emphasis to APDT, are discussed next. Finally, a brief account of the results of studies on use of APDT for wound infections in animal models is presented and the major objectives of the thesis are discussed.

## 1.1 Introduction

Photodynamic therapy (PDT) is a therapeutic approach, which involves interaction of light with an exogenously administered or endogenously synthesized photosensitizer (PS) that preferentially gets localized in the diseased tissue, leading to generation of reactive oxygen species (ROS) that is cytotoxic to diseased cells. PDT provides a selective way of treating carcinoma *in situ* and other diseases like macular degeneration and has been used successfully in clinical medicine for more than 2 decades for the management of tumor related pathologies in head and neck, gastrointestinal tract, skin and bladder with promising results. Even tumors of bone marrow and hepatobilliary organs have responded well.

In the last one decade, there is a considerable interest to use PDT as an alternative to antibiotics for management of localized infections such as dental and skin related infections. Application of PDT is a promising approach particularly for promotion of healing of acute and chronic wounds infected with antibiotic resistant bacteria.It is believed that PDT can benefit patients who suffer from localized infections of wounds caused by antibiotic resistant bacteria and those who require prolonged antimicrobial therapy.

## 1.2 Basics of Wound Healing

In this section, we provide a brief overview of the different phases of wound healing and the different factors like inflammatory cytokines, ROS and growth factors in wound healing.

### 1.2.1 *Different phases of Acute wound healing*

The main cellular events involved in acute wound healing are haemostasis, inflammation, cell proliferation and collagen remodeling [1, 2].

#### 1.2.1.1 Haemostasis (immediate)

This phase is initiated immediately after wounding and lasts up to 6 h. The tissue injury causes microvascular injury and extravasation of blood into the wound, which is followed by clot formation and platelet aggregation. The platelets trapped in the clot degranulate and release alpha granules [3], which contain several growth factors and chemotactic factors such as platelet-derived growth factor (PDGF), insulin-like growth factor-1 (IGF-1), epidermal growth factor (EGF) and transforming growth factor-β (TGF- β). This helps in initiation of the inflammation response.

#### 1.2.1.2 Inflammation

Early inflammatory phase begins with infiltration of the wound by neutrophils, which are attracted to the wound site within 6 to 24 h post wounding (p.w.), by a number of chemoattractants such as fragments of extracellular matrix proteins that are released upon injury, TGF- β , complement components (e.g. C3a, C5a) and products released from bacteria like formyl-methionyl peptide [1, 4].

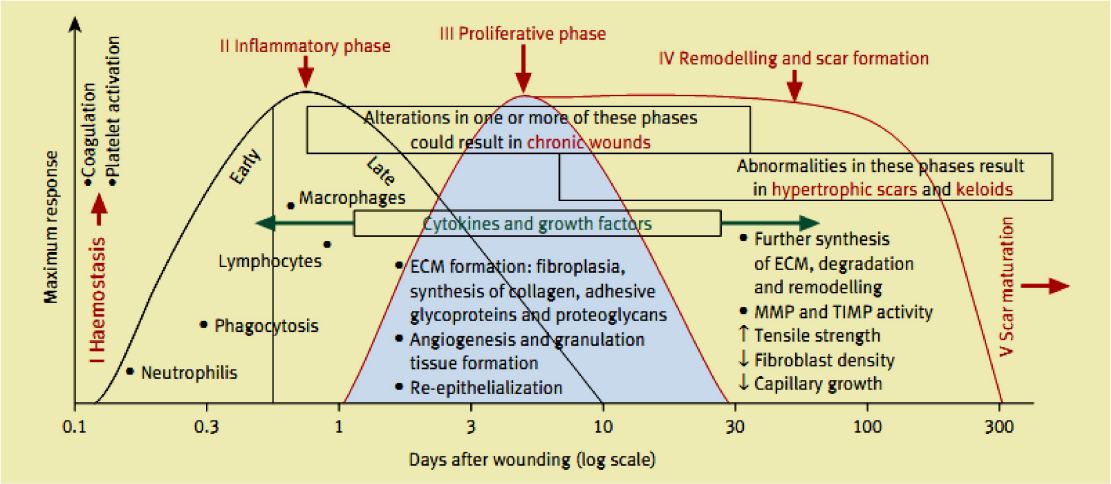


**Figure 1.1:** Stages of acute wound healing, reprinted from reference 1 with permission from Elsevier.

The infiltration of neutrophils begins with their adherence to the endothelial cells in the adjacent blood vessels (margination) followed by their active movement through blood vessels (diapedesis) towards the wound. In the wounds, they phagocytose bacteria and other foreign particles and destroy them by releasing degrading enzymes and reactive oxygen species (ROS). Once the contaminating bacteria and damaged cells are cleared, the neutrophils are disposed of by extrusion to the wound surface as slough and by apoptosis. The cell remnants and apoptotic bodies are phagocytosed by macrophages which arrive at the wound site around day 1 p.w. Macrophages are attracted to the wound site by a variety of chemoattractants, like clotting components, fragments of immunoglobulin G, breakdown products of collagen and cytokines (e.g. leukotrine B4, platelet factor IV, PDGF, TGF-β) and complements [4].

| Growth factors | Source(s) | Function in wound healing |
|---|---|---|
| PDGF | Platelet, fibroblast, macrophage, endothelial cells | Mitogenic for smooth muscle, endothelial cells and fibroblasts.<br>Chemoattractant for neutrophils, fibroblasts. Fibroblast proliferation and collagen metabolism. |
| FGF | Fibroblast, endothelial cell, smooth muscle cell, macrophage. | Proliferation of fibroblasts, epithelial cells, matrix deposition, wound contraction, angiogenesis.<br>Formation of granulation tissue. |
| EGF | Platelet, macrophage, keratinocytes, fibroblast, endothelial cell, smooth muscle cell. | Differentiation, Proliferation and migration, adhesion of keratinocytes.<br>Formation of granulation tissue. |
| VEGF | Platelet, neutrophil, macrophage. | Stimulates angiogenesis in granulation tissue, formation of collateral blood vessels in peripheral vascular disease, macrophage apoptosis, chemotaxis (integrins), Increasing vascular permeability. |
| KGF | Fibroblast | Proliferation and migration of keratinocytes. |
| G-CSF | Monocyte, fibroblast lymphocyte. | Stimulates production of neutrophils.<br>Enhances function of neutrophils and monocytes. |
| GMCSF | Keratinocytes, macrophage, lymphocyte, fibroblast | Mediates proliferation of epidermal cells. |
| TGF-β | Platelet,macrophage, fibroblast, neutrophils, keratinocytes. | Fibroplasia, matrix production.<br>Chemotaxis for macrophages, inhibition of reepithelialization. |

| | | |
|---|---|---|
| IL-1 | Neutrophils, monocytes macrophages. | Inflammation, reepithelialization. |
| IL-6 | Neutrophils macrophages. | Inflammation, reepithelialization. |
| IL-8 | Keratinocytes, fibroblasts, endothelial cell. | Keratinocyte proliferation.<br>Chemotaxis of PMNs. |
| IL-10 | fibroblasts, endothelial cell | Growth and/or differentiation of<br>immune cells, keratinocytes and endothelial cell.<br>Anti-inflammatory action. |
| TNF-α | Neutrophils macrophages. | Inflammation, reepithelialization. |

**Table 1.1** Important cytokines, growth factors,their sources and role in wound healing , adapted from reference 1 and 8 .

The macrophages function as phagocytic cells and also secrete growth factors like PDGF, VEGF, TGF-β, FGF, interleukins (IL) and tumor necrosis factor-α (TNF-α).These cytokines and growth factors carry out multiple regulatory roles such as fibroblast chemotaxis, production of the extracellular matrix, proliferation of smooth muscle cells and endothelial cells (table 1.1. and fig. 1.2). Macrophages also release proteolytic enzymes like matrix metalloproteases (MMP) which help in debridement of the dead, necrotic tissue of wound. However, prolonged presence of high number of neutrophils and macrophages, observed in infected and chronic wounds, leads to excessive production of proinflammatory cytokines like IL-6, TNF- α and MMPs, that delay the onset of cell proliferation.

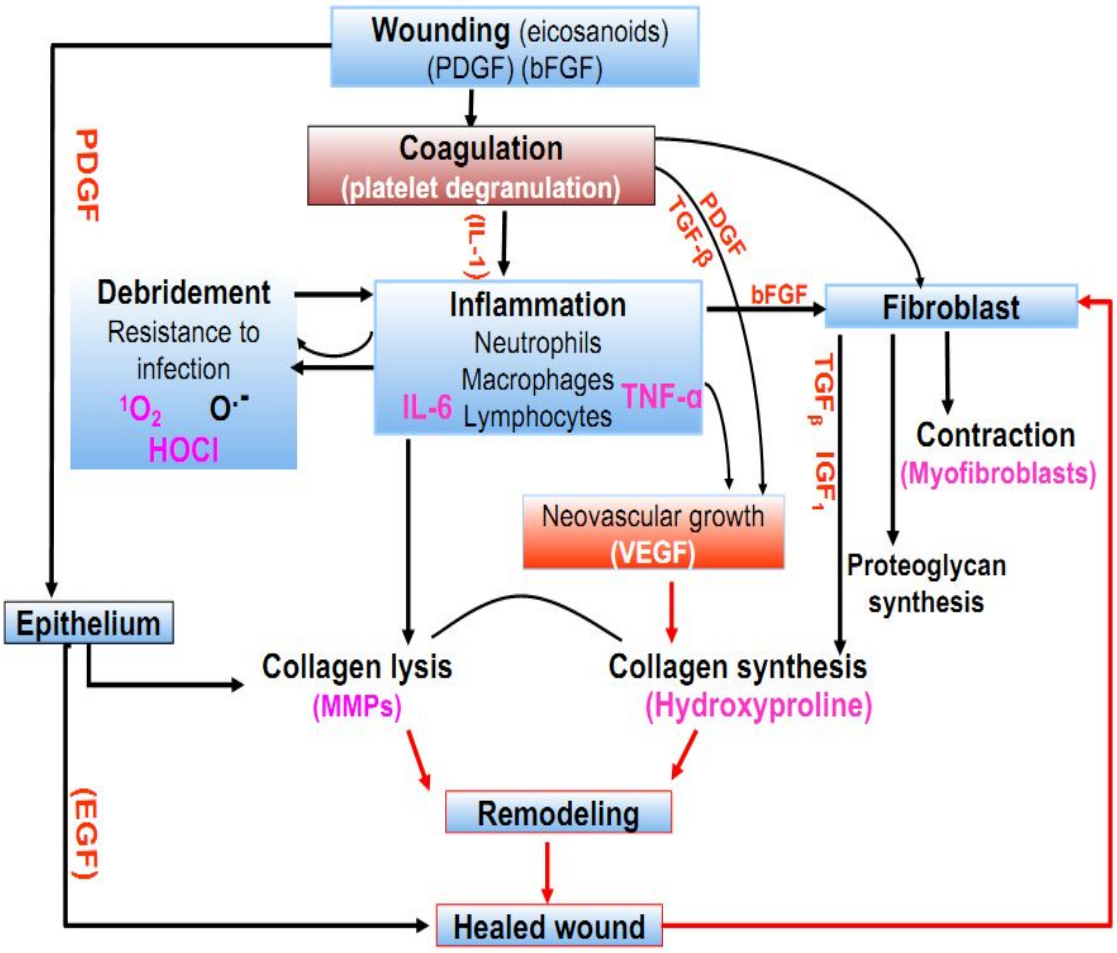


**Figure 1.2** Regulation of healing of acute wounds by growth factors, cytokines and oxidative species. HOCl: Hypochlorous acid. Adapted from reference 8 .

### 1.2.1.3 Cell proliferation

Cell proliferation phase starts around day 1 p.w. and involves epithelialization, angiogenesis, extracellular matrix (ECM) formation that ultimately leads to granulation tissue formation. Epithelialization begins with dissolution of cell-cell, cell-basement membrane contact followed by mitotic division of keratinocytes followed by theirmigration from the wound edge towards to the wound bed around

day 2 p.w. that establishes a protective barrier against fluid loss and further contamination. The signal for epithelialization comes from EGF and TGF secreted by the activated platelets and the macrophages.

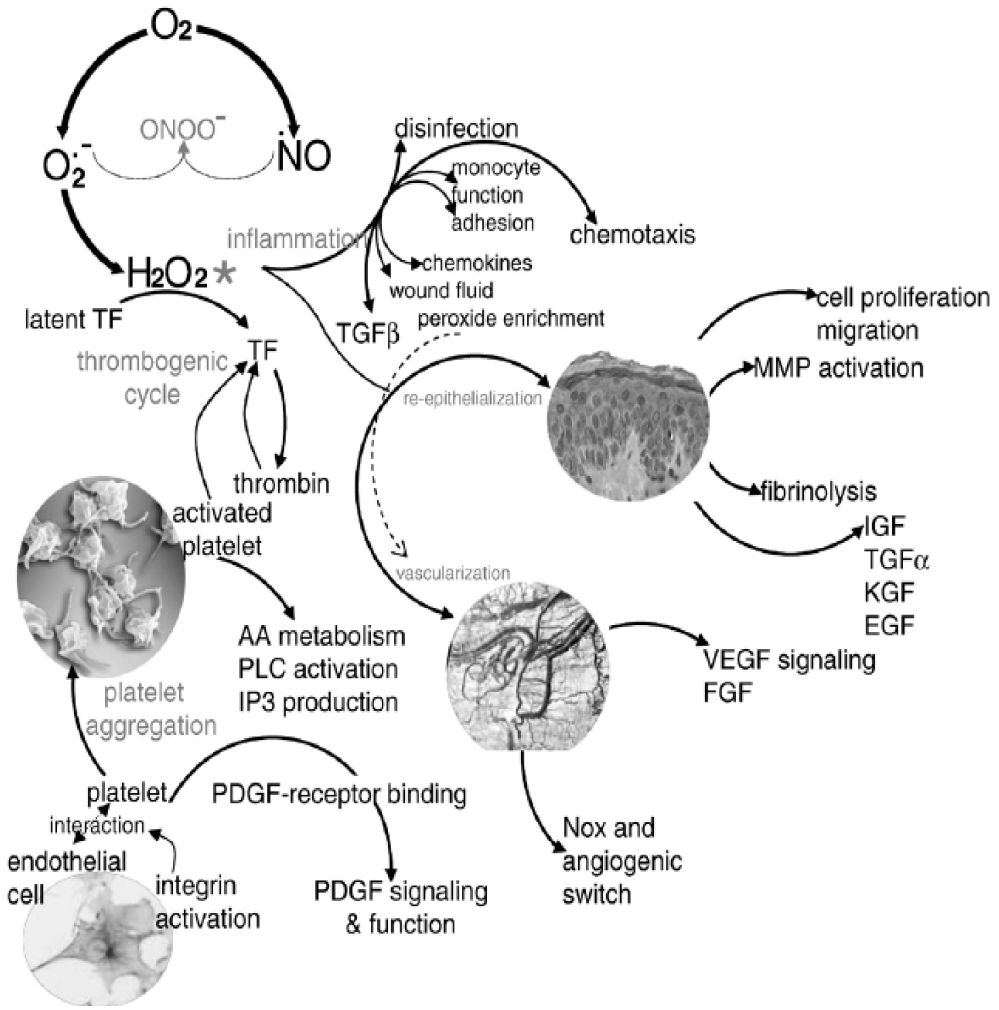


**Figure 1.3** Redox regulation of wound healing. ROS is involved in diverse processes such as inflammation, chemotaxis, platelet aggregation, angiogenesis, NO production and MMP activation. Reprinted from reference 5 with permission from Elsevier.

Fibroblasts then proliferate and migrate (fibroplasia) to the wound bed under the new epithelium layer during day 2 p.w. Several growth factors like PDGF, FGF (table 1.1), ROS (fig. 1.3) and NO are also produced during this time (fig. 1.4.) which regulate

crucial phases of wound healing like angiogenesis, cell proliferation (fig. 1.3) and MMP production [5].

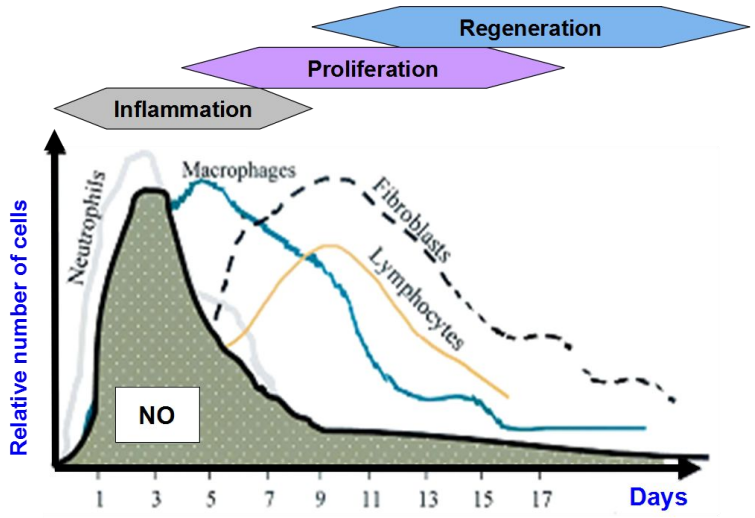


**Figure 1.4** Kinetics of cellular response in wound healing. NO synthesis peaks around day 3 p.w. and coincides with the inflammatory phase of wounds. Reprinted from reference 7 with permission from Elsevier.

Angiogenesis starts around day 2, accompanying fibroplasia and is essential for both granulation tissue formation and scar maturation. This process is initiated when endothelial cells sprout from preexisting blood vessels, which then migrate and proliferate to form a cord-like structure. Several factors such as hypoxia, tissue damage products and denatured type I collagen are the inducers of angiogenesis at the wound site. Injured parenchymal cells at the site of a wound also release basic fibroblast growth factor (bFGF), which is essential for angiogenesis during the first 3 days of wound repair. Keratinocytes and macrophages at the wound edge secret

VEGF during low oxygen tension (hypoxia) resulting from rapid cell proliferation. VEGF increases angiogenesis by vasodilation, degradation of basement membrane, increasing endothelial cell migration and stimulation of endothelial cell proliferation [6]. It has been observed that NO produced during this phase (fig 1.3) by macrophages [7] contributes to cell proliferation, VEGF production and collagen deposition.

MMPs digest the endothelial basement membrane, followed by digestion of the surrounding ECM. This allows endothelial cells to proliferate and migrate via a gradient of cytokines such as bFGF and VEGF to the site of the digested basement membrane. Integrin receptors like αυ/β3, αυ/β5 which are present on the endothelial cells, mediate the cell-matrix interactions and allow this migration. Fibroblasts also synthesize and deposit proteoglycans, glycosaminoglycans and collagens, particularly, collagen III which form a provisional matrix. All these processes lead to completion of granulation tissue formation which comprises inflammatory cells, fibroblasts, endothelial cells, the newly formed capillaries and the collagen III.

#### 1.2.1.4 Maturation and Collagen remodeling

At the end of granulation phase differentiation of myofibroblasts ( fig 1.2) occurs which is required for wound contraction. Concomitant to the wound contraction, the provisional matrix rich in collagen of type III is gradually replaced by more complex and cross linked collagen type I . The originally disorganized collagens are now arranged in an ordered fashion, which results in recovery of the tissue tensile strength.

Ordering of collagen fibres also contributes to their birefringence property, a feature exploited by optical imaging techniques to assess wound healing and therapeutic efficacy. The second feature of this phase is the well coordinated apoptosis of fibroblasts, macrophages, keratinocytes and myofibroblasts, that converts the highly cellular granulation tissue into a collagen rich tissue [8-10]. Some of the blood capillaries are also removed by apoptosis during this phase.

### 1.2.2 *Regulation of wound healing*

Timely completion of wound healing requires participation of different biochemical intermediates like growth factors, cytokines, enzymes, ROS and NO etc. A sound understanding of the factors that influence healing is vital for the successful management of any type of wound. In this section we provide a brief overview of some of the important regulators of wound healing.

#### 1.2.2.1 Growth Factors and cytokines

Several growth factors like PDGF, FGF,VEGF, KGF, EGF, TGF play important role in timely completion of healing. Role of these growth factors in wound healing is summarized in table 1.1 and figure 1.2. In addition to the growth factors, many cytokines also play important role in wound healing [9]. Of these cytokines, IL-6 and TNF-α have prominent role in inflammation.

IL-6 is mitogenic for keratinocytes, and also acts as chemoattractant for neutrophils [8,10]. Level of IL-6 is two to four times higher in chronic wounds [11] and the excessive level is associated with cutaneous scarring, and excessive MMP production.

IL-6 gene expression is under the influence of Nuclear Factor kappa beta (NF-kB), the later being overexpressed in response to bacterial components. It has been reported that in bacteria infected wounds IL-6 is overexpressed [12].

During wound healing, TNF- α is primarily released by mononuclear cells after their stimulation by bacterial and matrix products. It up regulates its own synthesis in macrophages and also stimulates macrophages to express other cytokines like IL-6, IL-8, GM-CSF, G-CSF, MCP-1 and IL-1. TNF- α is also implicated as a possible mediator of angiogenesis and can activate monocytes to mature into macrophages [8, 9]. The level of TNF- α in chronic wounds is higher than in acute wounds. In addition, excessive TNF- α triggers the activation of MMPs [13] , inhibition of angiogenesis and ECM formation.

### 1.2.2.2 MMPs and Wound Healing

Healing of acute wounds involves the formation of fibrin clot, which physically impedes the epithelial layer migration. Clot degradation occurs through the action of MMPs. During wound healing several MMPs like MMP-1 (interstitial collagenase), MMP-8 (collagenase), MMP-9 (gelatinase B), and, MMP-10 (stomelysin-2) are produced. Out of these MMP-8, 9 play more important role than other MMPS in wound healing. MMP-8 is expressed mainly by neutrophils and is important for collagen matrix remodeling. MMP-9, produced by migrating keratinocytes and macrophages, degrades collagen IV and laminins present in the basement membrane. This allows epithelial cells to leave the basement membrane and migrate towards the wound. VEGF also activates MMP-1, 2 and 9 that are required for degradation of

endothelial basement membrane. When reepithelialization is completed the production of MMP by keratinocytes is turned off allowing formation of hemidesmosomal adhesions between the keratinocytes and the basal lamina. MMPs also activate some of the inflammatory cytokines and generate chemokine gradients [14]. Although the presence of MMP is essential for wound maturation, the presence of high amount may lead to delay in healing of wounds. In chronic wounds, MMPs such as MMP-8, 9 are observed to be over expressed [15], as a result of which there is continued degradation of endogenous as well as supplemental growth factors, thus arresting the healing at the inflammation phase.

#### 1.2.2.3 ROS and wound healing

ROS are generated predominantly during inflammatory phase by the neutrophils and macrophages for pathogen clearance. ROS also regulate key processes during wound healing (fig. 1.4.) like monocyte function, chemotaxis, neutrophil degranulation, VEGF production and MMP production [5]. It is also believed that one of the ways by which some of the cytokines and growth factors like PDGF, FGF regulate wound healing is by stimulating ROS generation. ROS are rapidly removed by intracellular antioxidant enzymes like superoxide dismutase, catalase and non enzymatic antioxidants like glutathione. When ROS production exceeds the capacity of the antioxidant molecules, it may induce oxidative modification of signaling proteins (e.g., RTKs and MAP3Ks). High concentration of ROS are also detrimental to cells, as these can induce lipid peroxidation, protein carbonyl formation, DNA damage leading to cell death either by apoptosis or necrosis.

### 1.2.2.4 NO and wound healing

NO is a key mediator of cutaneous physiology. Expression of NO is controlled by tissue-specific stimuli, such as inflammatory cytokines or exogenous materials, such as bacterial lipopolysaccharide (LPS), lipoteichoic acid (LTA). In human skin, keratinocytes, fibroblasts, and endothelial cells can produce NO. Epithelial migration, wound angiogenesis, and granulation tissue formation are primarily influenced by the activation and upregulation of the NO. At low concentrations NO promotes gene expression of growth factors like VEGF, nitrosylation of NF-kB, inhibition of MMPs, collagen synthesis via protein kinase C activation. In diabetic ulcers, reduced NO level is one of the reasons for reduced VEGF, cell proliferation and delayed healing response [5,6,7]. At the same time, at very high levels, NO is known to induce inflammation and cell death response.

#### 1.2.2.5 NF-kB and wound healing

NF-kB, the central regulator of stress response also plays determinant role in wound healing, by regulating transcriptional expression of inflammatory cytokines like IL-6, TNF-α. NF-kB influences generation of ROS and various growth factors by various cells [5]. Also, activation of NF-kB is influenced by bacterial infection, NO and ROS [16,17]. In hyperinflammatory conditions, down regualting the excess level of NF-kB to physiological level, therefore might be one of the ways to ensure timely wound healing.

## 1.3 Problems associated with chronic wounds

Chronic wounds can be perpetuated by many factors, which include vascular insufficiency (venous or arterial), prolonged inflammation, pressure necrosis, infection, radiation therapy and cancer. It is estimated that nearly seventy percent of skin wounds, however, are due to pressure ulcers, venous ulcers, and diabetic foot ulcers. Chronic wounds have high incidence of bacterial biofilms.This leads to persistent inflammation, excessive proteolysis mediated by MMPs (fig. 1.5), degradation of crucial growth factors, receptors, the ECM and degradation of the tissue inhibitors of matrix TIMP.

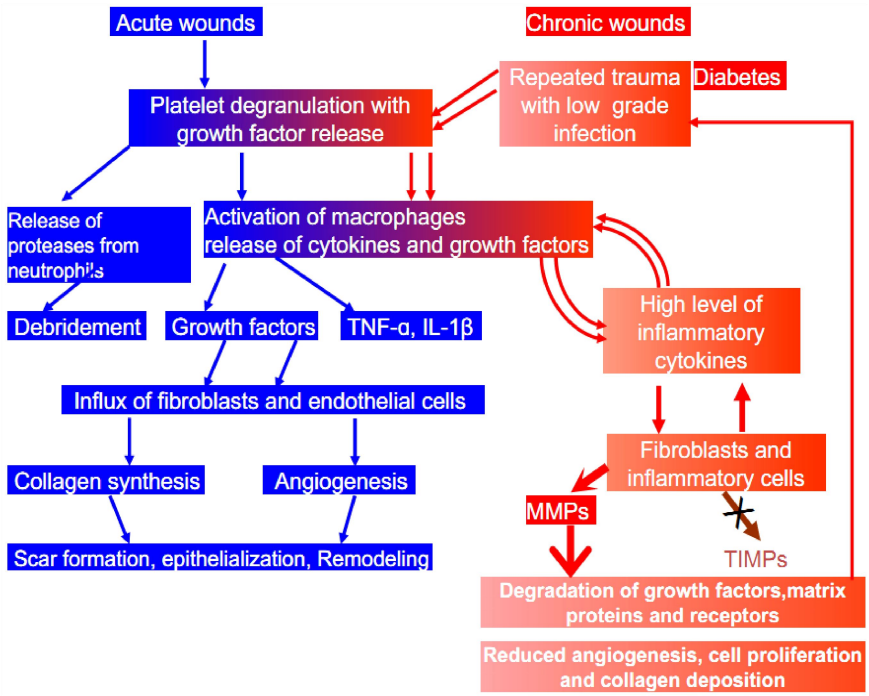


**Figure 1.5** Probable mechanisms of chronic wound formation. In the chronic wounds there is overexpression of TNF -α, IL -1β, MMPs, excess proteolysis. The blue and red marked regions demonstrate the features of acute and chronic wounds,respectively. Some of the steps which are common to both the pathways are also shown here (both

blue and red color). TIMP = Tissue inhibitors of matrix metalloproteases. Adapted from reference 11.

In addition to the presence of biofilms, in chronic wounds the cell proliferation and migration response are reduced because of the absence of functional receptors or appropriate matrix substrates. Also, angiogenesis and neovascularization are impaired in chronic wounds, resulting in insufficient oxygen and nutrient supply for the cells residing within the wound bed [11,18]. Effective therapeutic approaches for management of chronic ulcers should not only reduce the bacterial load but also should the hyperinflammatory cytokines and excessive MMPs produced by the inflammatory cells.

## 1.4 Diabetes and delayed healing

Wound healing is impaired in diabetes due to several factors associated with hyperglycemia.Formation of advanced glycated end products during prolonged hyperglycemia is one of the major reasons for the complications of delayed healing. The other key reasons include persistent inflammation [19,20,21], excessive proteolysis by MMPs, reduced cell proliferation, impaired cell migration response, downregulated angiogenesis, reduced growth factor and NO production [21, 22]. Diabetic patients also show increased susceptibility to infection due to impaired microbicidal function of the immune cells e.g; reduced phagocytic and decreased respiratory burst capability [20].

## 1.5 Wound infection and their management

Microbial infection prolongs the wound healing and predisposes the wounds towards a chronic state [fig 1.6] due to overexpression of proinflammatory cytokines [23], delayed cell proliferation and excessive MMP production [24]. Bacterial toxins also elicit death of fibroblast and endothelial cells. Normally, infection of wounds occur when contaminating microorganisms overcome the host defense,and subsequently invade viable tissues thus provoking both local and systemic host responses. The local response to infection often involves cellulitis, which manifests because of either the direct action of bacterial virulent factors or the host mediated excess inflammatory cytokines and proteases production [24, 25, 26]. The systemic response involves sepsis which sometimes proves fatal. In case of diabetes, the infection persists longer because of the incapability of the immune cells to clear the pathogens from the wounds. This adds to the already existent complications such as reduced growth factor level and cell proliferation response.

Chronic wounds are inhabited by multiple species of microbial organisms. The incidences of infection of ulcers by drug resistant bacteria are increasing world wide. The common drug resistant pathogens encountered in chronic wounds include the methicillin resistant *Staphylococcus aureus (MRSA)*, multidrug resistant *Streptococcus pneumoniae*, and vancomycin resistant *Enterococcus* spp. among the Gram positive bacteria and multidrug resistant *A. baumannii*, *K. pneumoniae*, and *P. aeruginosa* [27] among the Gram negative bacteria.

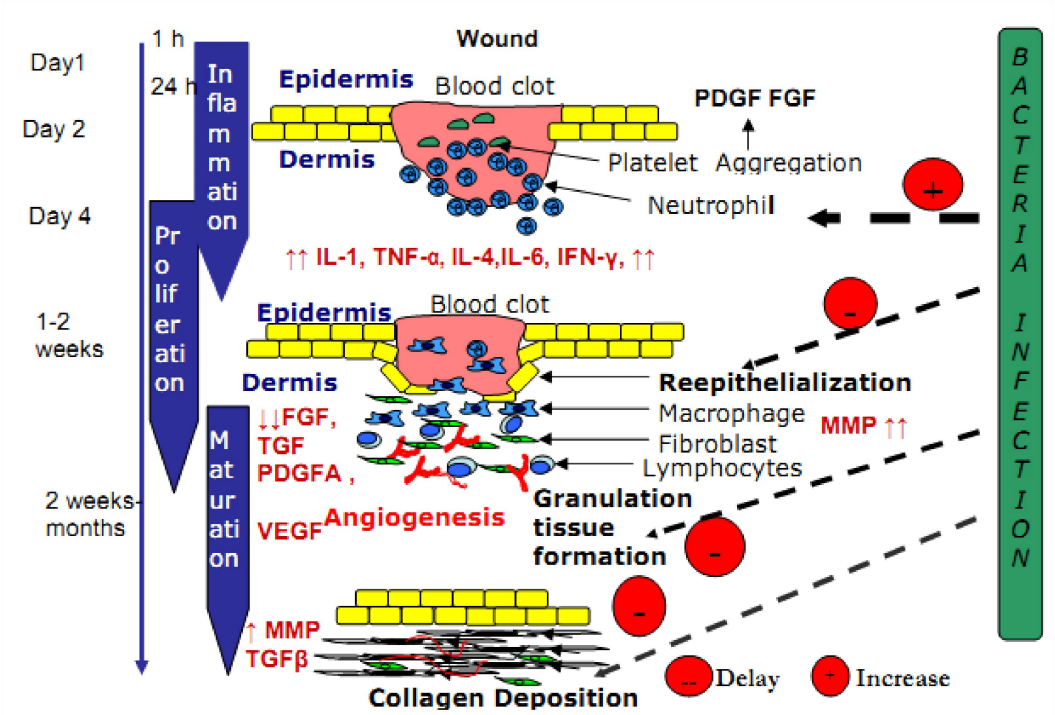


**Figure 1.6** Putative mechanisms of impaired wound healing in bacteria infected wounds. The important responses might be increased or delayed because of either over expression or (↑↑) down regulation (↓↓) of the cytokines and growth factors.

### 1.5.1 Infection of wounds caused by *S.aureus*

*S. aureus* is a major cause of community acquired and nosocomial infections. *S.aureus* employs a wide variety of defensive mechanisms to develop antibiotic resistance and produces many virulent factors for evasion of the immune systems. These include proteases and toxins which can kill leukocytes, inhibit neutrophil chemotaxis, resist phagocytosis, inactivate complement and neutralise host antimicrobial peptides [28, 29]. It has been shown that wound infections caused by this bacteria often result in hyperinflammation and impairment of wound healing. Rise in incidences of infections by *S.aureus* is a matter of great concern worldwide,

specially, amongst the diabetic mellitus patients [30]. It has been reported that diabetic foot ulcers infected by MRSA, multidrug resistant organisms (MDRO) are associated with a higher incidence of lower limb amputation (36 % versus 11 % in non-MDRO infection)[31, 32].

### 1.5.2 Infection of wounds by *P. aeruginosa*

*P.aeruginosa* infection is common among patients who have experienced trauma or a breach in cutaneous or mucosal barriers as observed in severe burns and surgical wounds. *P.aeruginosa* is often associated with refractory skin infections because of its intrinsic resistance to many antibiotics [33], ability to produce virulent factors [34] including collagenases [35, 36] and existence in form of biofilms on ulcer surface. Quorum sensing molecules produced by biofilms of this bacterium can also act directly on host cells to induce expression of proinflammatory cytokines [37]. In addition, the type III secretion systems produced by these bacteria inject protein effectors into host immune cells, inhibit phagocytosis and induce the release of proinflammatory cytokines into the wounds [38].

One of the causes of increased inflammation in infections caused by *P.aeruginosa* and other Gram negative bacteria can occur due to release of LPS either spontaneously from bacterial biofilms in from of membrane vesicles [39] or due to antibiotics or antiseptics treatment induced lysis of bacteria [40]. LPS elicits proinflammatory cytokines production, ROS generation and NF-kB activation via its direct interaction with membrane receptor, toll like receptor-4. Overexpression of NF-kB and proinflammatory cytokines upregulate MMPs causing delayed collagen remodeling.

In addition, bacterial LPS interfere with the membrane-associated phosphatidylserine in neutrophils, because of which the macrophages do not recognize and phagocytose the neutrophils. The latter then disintegrate by necrosis in the wound environment and release elastase, which can cleave cells and extracellular matrix. The soluble fragments from the host elastase-degraded neutrophils/other cells stimulate additional proinflammatory response [41]. The elevated proinflammatory cytokines present in the wound, interfere further with the cellular signaling of neutrophils [42] inducing a delayed apoptotic [43] response resulting in more and more necrotic cell death [44]. All these processes ultimately lead to release of very high levels of proteases in wounds, thereby the host's antiprotease defense mechanisms [45] are overwhelmed. Excess proteases also induce apoptosis of other host cell types, for example in endothelial cells, causing further delay in the wound repair [46].

## 1.6 Management of wound infections

Controlling the microbial load in wounds is crucial for healing, and this can be achieved in several ways. Antibiotics can be used either prophylactically for the treatment of wounds that are likely to be contaminated following surgery or therapeutically in the treatment of clinically infected wounds. Since wounds are infected by both the Gram positive and negative bacteria, broad-spectrum antibiotics are often the choice. However, the indiscriminate use of broad spectrum antibiotics contribute to development of resistance which is a matter of concern world wide.

Antibiotic resistance arises mainly because of the following reasons: (1) drug inactivation or modification (penicillin resistant bacteria),(2) alteration of metabolic

pathways (sulphonamide resistant bacteria), (3) alteration of target sites (MRSA) and (4) reduced drug accumulation [47]. It may be noted that the increasing bacterial resistance to antibiotics also limits the exploitable target sites and hence the development of new class of antibiotics has become more difficult. For instance, in the last 20 years, just two antibacterial agents, linezolid and daptomycin, with novel mechanisms of action have been developed [48]. In India, in recent decades, both MRSA and metallo- β- lactamases producing *P. aeruginosa* are emerging as important cause of nosocomial infections [49].

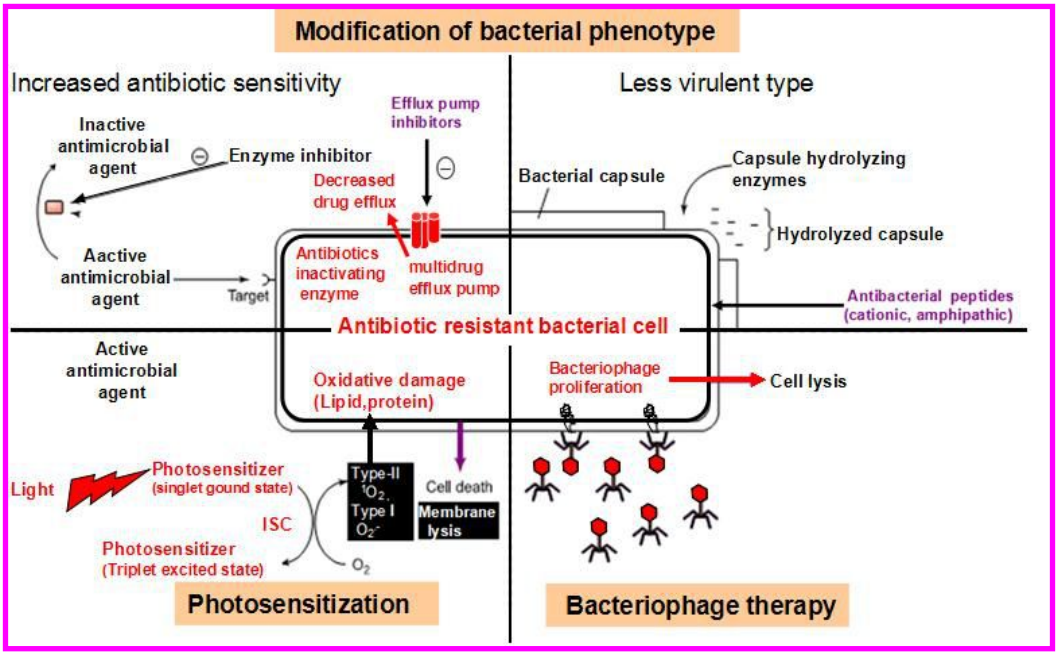


**Figure 1.7** Approaches to control infections caused by drug resistant bacteria. ISC : Intersystem crossing. Adapted from reference 50.

To overcome the problems of antibiotic resistance, alternative strategies (fig. 1.7) such as phenotypic modification, antimicrobial peptides, phage therapy have been investigated [50,51]. Inhibition of antibiotic resistance determinants in genotypically resistant bacterial cells by these methods may help in increasing antibiotic sensitivity so that these can be eliminated by host inflammatory cells. Though these approaches may be effective for antibiotic resistant strains, these methods also act on single target and bacteria may develop resistance to these treatments also. For example, in case of antimicrobial peptides, rapid mutation in bacterial envelope providing resistance against the antimicorbial peptides has also been reported previously[51].

An attractive approach for inactivation of antibiotic resistant bacteria is the photosensitization approach; in which the interaction of visible light and a photosensitive agent could generate lethal level of singlet oxygen and ROS, which can target several bacterial components resulting in rapid cell death (fig 1.7). In the following section of this chapter, brief descriptions of the basics of the antimicrobial photodynamic therapy (APDT), its applications in dermatology have been provided.

## 1.7 Antimicrobial Photodynamic Therapy (APDT)

Use of PDT as an alternative antimicrobial modality was demonstrated in 1980s. Applications of APDT for localized infections have grown rapidly since then. This approach has been explored extensively for treatment of periodontal diseases. However, the studies on APDT for wound infections are not as advanced as in dentistry and is mostly restricted to preclinical studies.

In the following sections we provide overview of the basic mechanism of action of APDT and its applications.

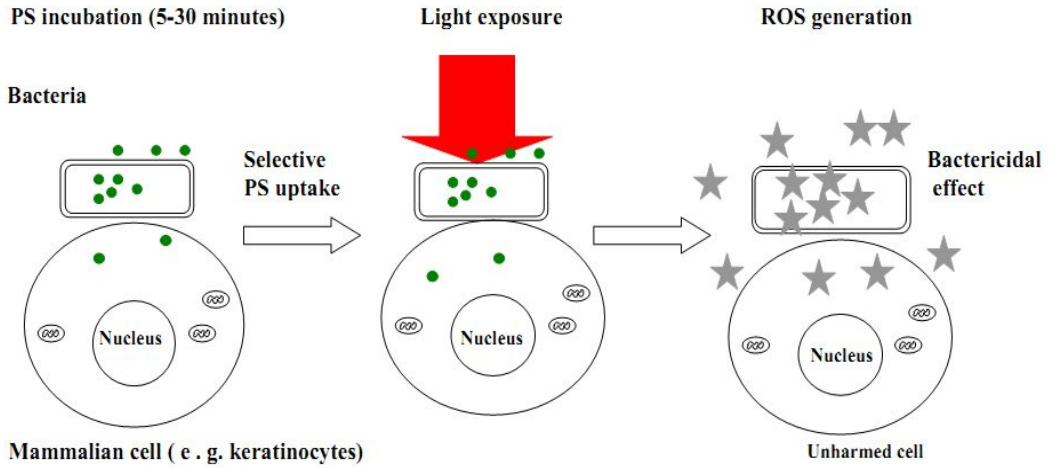


**Figure 1.8** A schematic representation of the basic processes involved in APDT. The figure depicts selective uptake of PS (green circle) by bacterial cell (rectangle). Upon light irradiation there is generation of more amount of ROS (grey stars) in bacterial cells than mammalian cells. Note the presence of intact mitochondria inside mammalian cells even after photoirradiation.

### 1.7.1 *Basic mechanism of APDT*

APDT follows principles similar to that of PDT, which is more widely known for its application in the treatment of cancer and also diseases like macular degeneration, blood sterilization. APDT can be defined as the eradication of microbial cells by the ROS generated during the interaction of a photosensitizer (PS) and light of the appropriate wavelength (ideally at the maximum absorption of the PS). The basic processes involve : excitation of an exogenously applied or endogenously synthesized PS by light of suitable wavelength. This can lead to generation of lethal level of

singlet oxygen via energy transfer to molecular oxygen present in the wound tissue. This is referred to as type II process. The other process contributing to the inactivation of microbes, referred to as type I process, involves generation of free radicals through electron transfer to nearby molecules (fig 1.8). These ROS react with different cellular components and induce oxidative damage to different macromolecules leading to bacterial cell death [52,53]. There are two basic mechanisms that have been proposed to account for the lethal damage caused to bacteria by PDT: 1) damage to the cell envelope which causes leakage of cellular contents or the inactivation of membrane transport systems and enzymes and the other is 2) damage to nucleic acids; DNA and RNA . Because singlet oxygen diffuses very short distance before reacting (<100 nm) with the components of biological tissues, the effects of APDT are highly localized. Also the various cell killing mechanisms act primarily on the cell envelope, hence, the lethality is largely unaffected by growth phase of the bacteria.

### 1.7.2 *Advantages of APDT*

One of the key factors that differentiate APDT from common antibiotic therapy is the that APDT leads to inactivation of the bacterial virulent factors [54] like LPS and proteases that are responsible for triggering inflammation, overexpression of MMPs. In contrast, LPS is released from bacteria during cell lysis induced by conventional antibiotics, antiseptics treatment and results in systemic toxic effects that can prove fatal to a patient [55]. Therefore, inactivation of both the virulence factors [ 56-58] as well as the causative organism are two of the beneficial responses of APDT that can stimulate healing in bacteria infected wounds by controlling inflammation and

possibly attenuating the infection induced collagen degradation, though these aspects need to be confirmed .

The main targets of APDT are the external cell envelope . The PS need not enter into the microorganism and interact with DNA or other intracellular machinery, and its interaction with the structures like LPS, LTA is sufficient for inducing the cell death, upon photoirradiation. Therefore, unlike antibiotics, in case of APDT the target microorganisms/bacteria have lesser chance to develop resistance by reducing uptake, increasing metabolic detoxification or increasing efflux of the drug. In this respect, previous studies have shown that repeated photosensitizations of bacteria do not induce expression of genes that might induce resistance [59] as singlet oxygen and free radicals interact with multiple cell structures and different metabolic pathways in microbial cells. Further, it has been shown that human cells like keratinocytes, blood cells, neutrophils and fibroblasts can survive APDT conditions that are lethal to bacteria.

Inactivation of the bacterial biofilms [60], the activation of both innate and adaptive arms of the immune system [61] and inactivation of pro inflammatory cytokines [62] are amongst some of the other advantages, induced by APDT which might also contribute to wound healing. For instance, in an *in vitro* study, the ability of APDT to directly inactivate proinflammatory cytokines at drug and light fluence resulting in ~99.99 % bacterial survival loss has been studied in detail . This study showed that between APDT and the antibiotics minocyclin , the protease inhibition effect caused by APDT is much superior to that of the antibiotics.As the the level of inflammatory molecules are very high in chronic wounds and suppression of proinflammatory

cytokines is likely to restore cell chemotaxis, there is also a possibility that APDT can elicit such beneficial responses in wounds.

### 1.7.3 *Factors affecting APDT efficacy*

| Nature of PS | Bacterial cell | Mammalian cell |
|---|---|---|
| • Cationic charge/ cationic moiety conjugation (more net positive charge)<br>• Size<br>• Amphiphilicity (leads to better membrane partition)<br>• Self promoted uptake ( in case of cationic, amphipathic peptide-PS conjugate) | • Anionic phospholipids (phosphatidyl ethanol amine, phosphatidyl glycerols but lesser cardiolipins)<br>• Presence of anionic lipopolysaccharide , lipoteichoic acid.<br>• Higher negative transmembrane potential (-130 to -150 mV) compared to mammalian cells | • Zwitterionic cell membrane<br>• Cholesterols on cell membrane<br>• Phosphatidyl glycerols on the inner leaflet of plasma membrane.<br>• Transmembrane potential is within -90 to -110 mV<br>• Endocytosis (lysyl conjugates of PS)<br>• Presence of endomembranes |

**Table 1.2** Some of the factors which may influence the selective localization of the cationic PS or cationic peptide-PS conjugate in bacterial cells during APDT [64, 67,68].

APDT efficacy depends upon the nature of PS and the composition, charge of the bacterial envelope. Gram positive bacteria cell wall constitutes a peptidoglycan wall

constituting molecules like LTA, negatively charged teichuronic acids, and displays a relatively high degree of porosity. Macromolecules with a molecular weight of 30–60 kilodalton (kDa) can diffuse into the inner plasma membrane through the peptidoglycan wall, which does not act as a permeability barrier for the most commonly used PS such as phenothiazines and porphyrins, with molecular weight generally in the range of 1.5–1.8 kDa. In contrast, Gram negative bacteria contains an additional outer membrane outside the peptidoglycan layer, which shows an asymmetric lipid structure composed of anionic LPS, saccharine, protein and proteins with transport function (porins). This layer inhibits the penetration of compounds with MW >700 Da [63] across the outer envelope of these bacteria.

The features that an ideal PS for APDT should possess are cationic charge, good triplet yield, amphiphilic nature, absorbance in red/far red regions and photo stability [64]. Of these, the cationic net charge of the PS is the most crucial feature for efficient binding of the PS to bacteria, especially in case of Gram negative bacteria, because their anionic envelope resists uptake of anionic PS [64]. To circumvent this problem, treatment with penetration boosters like ethylenediamine tetraoxide and Polymyxin B Nonapeptide (PMNB) have been investigated. PMNB, in particular, has also been shown to affect virulence potential [65]. However, one of the concerns with the penetration boosters is the possible mammalian cell toxicity [66]. A cationic PS on the other hand, can achieve bacterial envelope targeting without the need of external penetration boosters [64].

A cationic PS is preferentially taken up by bacterial cells over human cells, because of the differences in cell size and structure (table 1.2). Bacterial outer cell envelope has

predominantly anionic phospholipids and molecules like LPS, LTA. Mammalian cell membranes, in contrast, have mostly zwitterionic phospholipids, cholesterol [67]. Cholesterol imparts rigidity to the cytoplasmic membrane and also acts as a scavenger of ROS [63]. The importance of cholesterol in APDT can be clarified if one considers the lesser photosensitivity of the cholesterol rich Myc*oplasma hominis* than the cholesterol deprived *Acholeplasma laidlawii* [63]. In addition to these structural differences, the trans membrane potential of bacteria is more negative compared to that of mammalian cells (table 1.2), thus providing selectivity for cationic drug/cationic peptide drug conjugate incorporation in the bacterial cell envelope [67].

Amphiphilic PS is preferred over hydrophobic or hydrophobia PS because this helps in partitioning of the cationic amphiphilic PS into microbial membrane. This has been proven in studies comparing the efficiency of synthetic meso substituted cationic porphyrin with tetra-, tri-, di- or monocationic charges on bacterial inactivation. These Results of those studies have shown that di and tri cationic derivatives with aromatic carbon side chains are more efficient than tetracationic ones [64]. Another study in *Staphylococcus warneri* showed that, a tricationic PS (tri-Py+-Me-PF) binds to a lesser extent than its tetracationic counterpart (tetra-Py+-Me) but the amount of PS removed after washing is lower, therefore suggesting that molecules with amphiphilic character remain more tightly bound to bacteria [64], presumably because of a better cell membrane partitioning. The other advantages of amphiphilic PS are that amphiphilicity avoids aggregate formation and ensures effective penetration of the PS through the lipid layer of the cell membrane [64]. In addition to the above discussed factors (such as cationic charge and amphiphilicity), the molecular weight of PS can also be an important factor for the higher accumulation of PS in bacterial cell than the

mammalian cells. For example, because of the increased molecular weight (few kDa) associated with conjugation of the PS to cationic peptides like poly-l-lysine, PS uptake into mammalian cells will occur mostly via phagocytosis [68] which is a time taking process.Therefore, when photoirradiation will be carried out after a shorter incubation time, the uptake of PS into mammalian cells will be lower and hence the ROS generated will be lesser.

Cationic phenothiaziniums, like methylene blue and toluidine blue have been the most widely investigated photosensitive drugs currently being investigated for APDT [69]. However, these have relatively lower triplet yield, hydrophilic nature, and efflux pump dependent uptake into microbial cells [70, 71]. Therefore, there is interest in exploring other PS. Chlorophyll derivatives like chlorine p6 (cp6) are particularly attractive because these have good triplet yield, amphiphilicity and strong absorbance in the red (660 nm) region [72, 73]. Since cp6 is anionic [72], conjugation with cationic peptides like poly-L-lysin (pl) is therefore expected to enhance the targeting of the cp6 to bacterial cells.

### 1.7.4 *Clinical applications of APDT*

APDT is being used clinically for acne treatment and in dentistry using phenothiazinium dyes. In dentistry, APDT has been applied to treat peridontitis, gingivitis etc leading to favorable clinical outcomes such as reduction in periodontal bacteria load and inflammatory cytokines level [61]. It has also been observed that repeated APDT does not adversely affect acute stress markers such as C-reactive protein, serum amyloid A, fibrinogen, procalcitonin, and α-2 macroglobulin in the

gingival crevicular fluid [74]. APDT is also observed to modulate extracellular matrix remodeling by upregulating the levels of tissue inhibitors of MMPs [75] during periodontal wound healing. Further, studies also suggested that a single or double exposure of APDT had some additional benefit over other treatment options like use of multiple ultrasonic treatment for periodontal infections.

### 1.7.5 *Use of APDT for inactivation of bacteria in wound infection models*

There are several reports on use of photodynamic approach to inactivate bacteria infecting wounds in animal models [76-80]. The main observations from these studies are that topical APDT induced by application of PS concentration of 50-300 μM and light fluence in the range ~ 50- 400 J/cm$^2$ led to rapid eradication of different strains of bacteria such as *S. aureus* (MRSA), *V. vulnificus*, *E.coli*, *and P.aeruginosa*. However, despite the encouraging photobactericidal effects observed, the effect of PDT on wound healing is contradictory. There are reports that PDT does not influence wound healing [81,82] or may even lead to epidermal necrosis, decrease in tensile strength and delayed healing [83]. The likely causes of these discrepancies could be oxidative damage to the host cells arising due to accumulation of high concentration of PS in host cells as a result of systemic administration (intraperitoneal/intravenous) of PS and use of high light fluence beyond ~200 J/cm$^2$ [81-83]. It is therefore necessary to optimize the treatment parameters to study the effects on wound healing.

Complete eradication of bacteria in wounds post APDT requires phagocytosis of the survivors by the immune cells. Therefore, bacteria regrowth post APDT is a likely problem in ulcers of diabetic subjects, wherein there is already reduced microbicidal functions of immune cells. In fact, in a placebo controlled phase-II clinical trial, it was demonstrated that APDT can be effective in inducing significant bacterial killing in diabetic foot ulcers (DFU) and leg ulcers colonized with upto $10^5$ CFU/$cm^2$ bacteria. However, there was bacterial regrowth in DFUs at 24 h and 7 day post APDT. Also, improved healing was observed in only ~ 50 % of the treated DFUs [84]. Though the exact reason for these observations are unclear, one of the causes could be bacteria regrowth post PDT, as wound closure is inversely related to bacteria load. It may be expected that multiple PDT may lead to better control over bacteria regrowth. However, one concern pertaining to use of APDT for wound healing of diabetic subjects will be the possible oxidative damage to the inflammatory and other cells of wounds as there is already significantly reduced levels of antioxidants. At the same time, it is known that the low/moderate amount of ROS can lead to increased levels of growth factor [85] and antioxidants in tissues.Therefore, lower amount of ROS generated due to APDT carried out at lower light fluence may also lead to such beneficial responses in wounds which would contribute to healing. However, there are no definitive studies so far.

## 1.8 Summary of the chapter

Wound healing has four overlapping phases: coagulation, inflammation, proliferation, and remodeling. Abnormality in any of these phases, caused by either systemic factors

like vascular insufficiency, diabetes, neuropathy, or local factors such as pressure and infection of wounds can cause delay in healing. The growing emergence of antibiotic resistance in bacteria commonly infecting wounds is another concern, particularly in diabetic and immunocompromised conditions. To overcome this problem various alternative strategies are being explored.

APDT mediated generation of lethal level of singlet oxygen or radicals are not target specific. This is the reason why it is considered highly unlikely that bacteria could evolve resistance mechanisms against APDT. Chlorophyll derivatives like cp6 are attractive PS for APDT because these have good triplet yield, amphiphilicity and strong absorbance in the red (660 nm) region. Further, conjugation with cationic peptides like poly-L-lysin is expected to enhance the targeting of the cp6 to bacterial cells. One of the objectives of the thesis thus was to explore the photobactericidal efficacy of cp6 and pl-cp6 for both Gram positive and negative bacteria.

Though, several published studies show the use of a photodynamic approach to destroy *P.aeruginosa, S.aureus, Vibrio vulnificus* bacteria infecting a wound in animal models, several concerns pertaining to the successful therapeutic outcome need to be addressed. In fact, some contradictory reports are also there. For example, there are reports that PDT does not influence wound healing at all or may even cause epidermal necrosis, decrease in tensile strength, and delayed healing. On the other hand, since APDT can inactivate bacterial virulent factors, it can contribute to faster healing possibly by attenuating the bacterial virulent factors induced over expression of the proinflammatory cytokines and MMPs in infected wounds. Therefore, in this thesis

work, the effect of APDT on wound healing has been studied with particular emphasis on inflammatory and collagen remodeling response.

Both hyperglycemia and oxidative stress can directly activate cell adhesion molecules, pro and anti-inflammatory molecules, vascular endothelial growth factor signaling in cells and neutrophil granulation in inflammatory cells. APDT induced ROS generation thus can generate many beneficial response in wounds. Also, bacterial cell degradation products like DNA, proteins, membrane products released upon APDT induced bacterial cell destruction can generate chemotactic response for inflammatory cells. However, the light fluence and PS concentration that would maximize bacterial inactivation and inflammatory cell accumulation simultaneously in diabetic wounds needs to be carefully optimized. There is also hypothesis that PDT can modulate innate immunity and may lead to increased growth factor production in wounds, thus helping in promotion of wound healing. However, there is no definitive study so far. Therefore, in this thesis while investigating the effect of APDT on wound healing in wounds of the diabetic mice, we have emphasized upon the effect of APDT on levels of markers of oxidative stress , inflammatory cell sequestration and angiogenesis .

## 1.9 Objective

The objective of the thesis was to explore the photobactericidal efficacy of cp6 and pl-cp6 for both Gram positive and negative bacteria and investigate the use of pl-cp6 mediated APDT for the healing of bacteria infected and uninfected wounds in non diabetic and diabetic mice.

# 2. Material and Methods


## Abstract

In this chapter, we describe in detail bacteria used for our studies, experimental protocols of photoirradiation, procedure for synthesis of pl-cp6 and establishment of wound infection in normal as well as diabetic mice model. A brief overview of biochemical techniques such as immunoblotting, hydroxyproline assay, that were used in our studies on wound healing, is also provided in the chapter.

## 2.1 Bacteria and photosensitizer

We have used *S. aureus* (ATCC 43300) and *P. aeruginosa* ( MTCC 3541 ) for our experiments. The MRSA strain was procured from Himedia and is reported to be a clinical isolate. The *P. aeruginosa* strain was obtained from IIMTECH, Chandigarh . This is a pathogenic strain and is reported to express several virulent factors such as exotoxin A, exoenzyme, elastase, protease, phospholipase-C, siderophores.

### 2.1.1 *Staphylococcus aureus*

*S. aureus* is a facultative aerobic, Gram positive coccus of the *Staphylococcaceae* family and is the most common pathogen in community acquired and nosocomial infections. It employs different defensive mechanisms to develop antibiotic resistance and produces many virulent factors like proteases and toxins which play crucial roles in evading immune system [25, 28, 29]. These include wide range of toxins and enzymes such as hemolysins, proteases, lipases and hyaluronidase [86] which can kill leukocytes, inhibit neutrophil chemotaxis, resist phagocytosis, inactivate complement and neutralize host antimicrobial peptides [87,88]. It has been shown that infections caused by this bacteria often result in hyperinflammatory response and impairment of wound healing. Further, the rise in incidence of infections caused by antibiotic resistant strain of *S.aureus* is a matter of great concern worldwide, specially, amongst the diabetic patients [30-32]. Particularly, the diabetic foot ulcers infected by MRSA strains are associated with a slower healing rate. Therefore, a MRSA strain

has been used for both *in vitro* and for studies on wounds of diabetic, non diabetic mice.

### 2.1.2 *Pseudomonas aeruginosa*

*P.aeruginosa* is a bacterium responsible for life threatening infections in immunocompromised patients like burns as well as chronic infections in cystic fibrosis patients. *P.aeruginosa* is often associated with refractory skin infections because of its intrinsic resistance to many antibiotics [33] and its ability to produce virulent factors [34], collagenases [35, 36] and form biofilms on ulcer surface. There are mainly two types of virulent factors secreted by this bacterium. The first category includes factors that are involved in the acute infection. These factors can be either on the surface of *P. aeruginosa* or are secreted. The cell surface factors include pili which allow these bacteria to adhere to the epithelium, enzymes like the exoenzyme S and other adhesins that reinforce the adherence to epithelial cells. This bacterium also produces phospholipase C, exoenzyme S and collagenase which can induce hemolysis, disruption of cytoskeletal organization and tissue necrosis, respectively. The second category of virulent factors are involved in the chronic infection. These include siderophores like pyocyanin which allow the bacteria to multiply in the tissues. Also, the alginate produced by this bacterium protects it from phagocytosis, antibiotics and help in biofilm formation. The quorum sensing molecules produced by *P. aeruginosa* biofilms can induce sustained overexpression of proinflammatory cytokines [37]. LPS is another significant virulent factor for *P.aeruginosa* infection

responsible for inflammatory response [38-40].The *P.aeruginosa* strain used in this study produces pyocyanin, alginate and extracellular proteases.

### 2.1.3 *Photosensitizer preparation*

Chlorins are receiving considerable interest as potential drugs for PDT of cancer and premalignant conditions. These molecules have strong absorption in the therapeutic window (650–900 nm), high singlet oxygen quantum yield (0.7-0.8), low dark toxicity, amphiphilic nature and cost of synthesis is low. Chlorin p6 was prepared following the procedure described by Hoober et al. and the pl-cp6 was prepared by carbodiimide coupling method described in [89] with slight modifications. In brief, cp6 was dissolved in dimethyl sulfoxide (DMSO, Sigma) and an equimolar solution (4.5 mM) of 1-ethyl-3-(3-dimethylaminopropyl) carbodiimide hydrochloride (Sigma-Aldrich) in DMSO was added to it drop-wise under continuous stirring. To this, a known volume of  of poly-L-lysin hydrobromide (average molecular weight 22000 Da, Sigma-Aldrich) prepared in DMSO (25 mg/ml) and 20 µl of tri-ethyl amine was added. After stirring for 48 h in dark, this mixture was diluted with equal volume of 50 % methanol. Poly-L-lysin-cp6 (pl-cp6) conjugate was precipitated from this mixture by addition of chilled acetone (1:9). The green precipitate thus formed was collected by centrifugation at ~1800 g for 10 min, washed again with 90% chilled acetone and evaporated to dryness. The residue was again dissolved in 10 mM sodium acetate buffer (pH 5.0), passed through a column of Sephadex G-25 and eluted using the same buffer. The green fraction containing poly-L-lysine cp6 conjugate (pl– cp6) was collected, reprecipitated with chilled acetone, evaporated to dryness and stored at -20$^{o}$ C until use.  Stock solutions of both the photosensitizers (cp6,pl-cp6) were

prepared in PBS. Absorption spectra of free and conjugated cp6 were measured to determine the concentration.The absorption coefficient of conjugated cp6 was assumed to be the same as that of free cp6 ( 94,600 $M^{-1}cm^{-1}$ at 400 nm).

## 2.2 Establishment of wound infection

Mouse (Swiss albino) was chosen as it is an ideal model for inducing superficial,excisional wounds [90].

### 2.2.1 *Development of diabetes in mice*

The mice strain used in this study is Swiss albino strain which has been widely used for studies on wound healing as well as diabetes related complications.

### 2.2.2 *Rationale for choosing chemical treatment induced diabetic mice model*

There are 4 types of rodent models being used for studies on diabetes which include spontaneous, transgenic, chemical and nutrition based models [91]. The spontaneous diabetic models involve genetic factors and the animals develop characteristic features resembling human type 2 diabetes, allowing genetic studies. However, these rodent models lack the genetic heterogeneity seen in humans, show high mortality due to ketosis and are expensive. The transgenic rodent models of diabetes are useful for mutation studies, and regular screening of type 2 diabetes. These require very sophisticated procedure and are expensive for regular screening experiments. The diet

based models require long dietary treatment and sometimes no clear hyperglycemia develops. Sreptozotocin (STZ) and Alloxan (ALX) treatment induce development of hyperglycemia quickly, the animals live longer without insulin treatment [91]. The procedure is cheaper, easier to develop and maintain. In addition, diabetes induced by this procedure provides a relevant example of endogenous chronic oxidative stress due to hyperglycemia resulting in neuropathy, cardiomyopathy and well marked retinopathy [92]. ALX and STZ treatment induced diabetic animals are most widely used for screening the various drugs for their insulinomimetic, insulinotropic and other hypoglycemic/ antihyperglycemic activities. STZ, because of its relatively longer half life (15 min) and ability to cause sustained hyperglycemia for longer duration, is preferred over ALX.

STZ damages pancreatic β cells, resulting in hypoinsulinemia and hyperglycemia. Its structural similarity with glucose allows STZ binds to GLUT2 glucose transporter receptor and preferential accumulation in β cells. STZ can induce a diabetic state in 2 ways , depending on the dose. At high single dose (150-200 mg/kg) treatment , STZ targets β cells by its alkylating property corresponding to that of cytotoxic nitosurea compounds. At low doses of multiple exposures (40-50 mg/kg, 5 days), STZ elicits an immune and inflammatory reaction. Under this condition, the destruction of β cells and induction of the hyperglycemic state is associated with inflammatory infiltrates including lymphocytes in the pancreatic islets [92]. Also the severity and mortality of diabetes with high STZ dose is more in comparison to multiple sub diabetogenic dose [93]. STZ treated rodents display some of crucial biochemical alterations seen in human diabetic subjects like decreased GSH pool, reduced

angiogenesis, reduced phagocytic function of inflammatory cells , delayed collagen remodeling events crucial to wound healing.

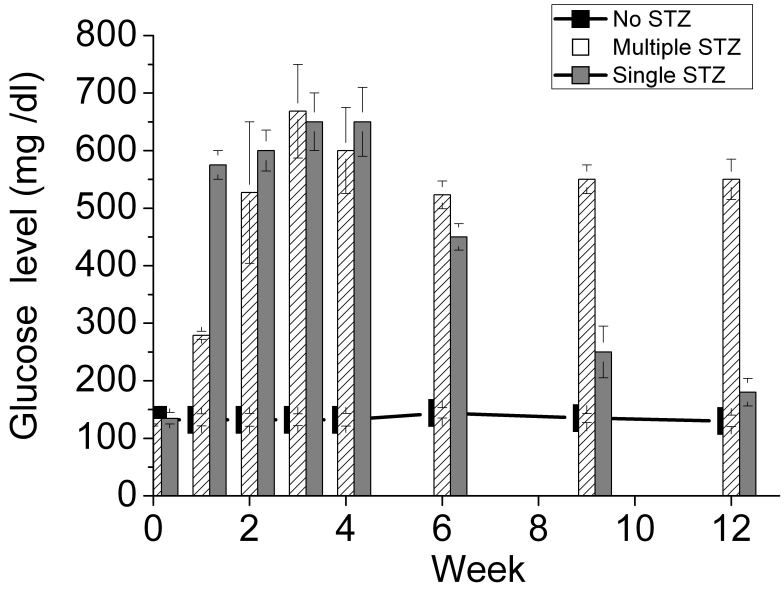


**Figure 2.1:** STZ treatment (single and multiple) induced hyperglycemia in swiss albino mice as function of time.

## 2.2.3 *Establishment of diabetes*

Diabetes was induced by either single high dose (150 mg/kg) or multiple (five) low doses (50 mg/kg/day) of intraperitoneal STZ injection [21]. Blood sugar was assessed at 1 to 12 week post treatment using a commercial glucometer (one touch horizon, Johnson and Johnson). Mice (female and male) with blood sugar > 250 mg/dl were considered diabetic (fig. 2.1). While both the protocols induced diabetes within a week (fig. 2.1), the single STZ protocol induced ~25 % mortality. In addition, mice in which the hyperglycemia was developed by multiple low dose STZ injection, the hyperglycemic state remained stable for 3-4 months. Therefore, multiple STZ induced

diabetic mice model was used for further studies. For experimental purpose both female and male mice with blood glucose level > 250 mg/dl were randomly categorized into the untreated control and other experimental groups.

Total white blood cell (WBC) counts in normal and diabetic mice was determined by drawing blood from the tail vein of mice into vials containing 2.5% sodium citrate. The blood was diluted (1:20) in solution containing 1 % acetic acid and 0.1% crystal violet, so as to cause lysis of the RBCs (i.e. cells are destroyed by bursting), and stain the WBC nuclei. Blood dilution was done very quickly to prevent clotting of the blood and to ensure accuracy. The WBC count was determined manually with a hematocytometer [94]

### 2.2.4 *Wound creation and establishment of infection*

For developing wounds, mice (both immunocompetent and immunocompromised) were anesthetized by intraperitoneal injection of Ketamine (80 mg/kg) and Xylazine (10 mg/kg) cocktail. Subsequently, hair was removed from back of the mice using a depilatory cream. The hairless skin region was then cleansed first with alcohol and then with betadine. A region of defined area was marked and the skin from this region was excised aseptically, down to the region of panniculus carnosus, using sterile surgical scissors and forceps.

Infection of the wounds in mice (both non diabetic and diabetic) was initiated by applying topically bacteria suspension immediately after wounding and spreading the bacterial suspension uniformly over the wound surface with help of a micro pipette tip. Establishment of infection was verified by assessing changes in

wound such as pus formation, edema and inflammatory response, enumeration of bacterial load in wounds.

## 2.3 Photoirradiation

| Parameters | Value |
|---|---|
| Wavelength (nm) | 660 ± 25 |
| Power output (mW) | 260 |
| Spot diameter (cm) | 1.6 |
| Sample distance from probe (cm) | 4.5 |
| Area ($cm^2$) | 2.5 |
| Power density ($mW/cm^2$) | ~ 100 |
| Fluence | Time of irradiation (sec) |
| 2 $J/cm^2$ | 20 |
| 5 $J/cm^2$ | 50 |
| 10 $J/cm^2$ | 100 |
| 20 $J/cm^2$ | 200 |
| 60 $J/cm^2$ | 600 |
| 120 $J/cm^2$ | 1200 |
| 240 $J/cm^2$ | 2400 |

**Table 2.1:** Photoirradiation parameters used for photosensitization (both *in vitro, in vivo* studies on cp6, pl-cp6).

For studies involving (cp6) the light source used was a halogen lamp (LUMACARE, UK). The light fluence delivered during a specified period of irradiation was calculated using the following formula: Light fluence ($J/cm^2$) = power density ($mW/cm^2$) x irradiation time (sec). The light irradiation parameters are given in table 2.1. For all *in vitro* experiments, the sample to be irradiated was placed in well of 24/ 96 well microtitre plates and the adjacent wells were covered with aluminium foil in order to prevent leakage of light. For most of the *in vivo* studies ( in non diabetic mice), following 30 min of application of PS , the wounds were exposed once to red light for 10 or 20 min to achieve light fluence of ~60 or ~ 120 $J/cm^2$ ( fig. 2.2). It may be noted that for some of the experiments, involving the diabetic mice, the wounds were exposed to repeated PDT at 24 h , during day 1-3 p.w. (multiple APDT). During photoirradiation, only wounds were exposed to light and rest of the skin of the back of mice was covered by a black paper. All photoirradiation experiments were carried out in a dark room.

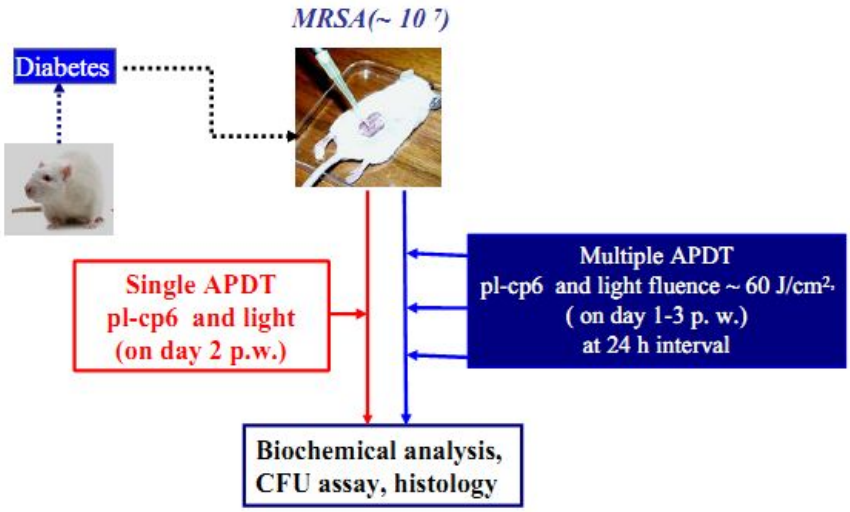


**Figure 2.2:** APDT protocol followed for infected wounds of diabetic mice.

## 2.4 Enumeration of bacterial load of wounds

It is known that bacteria load at a level of $\sim 10^5$ CFU/gm or presence of $\sim 10^6$ CFU/ml wound fluid are signs of infection. Therefore, enumeration of bacterial load in swabs, wound tissue homogenates alongwith histology is carried out to confirm development of infection. Bacterial counts in wounds were determined by quantitative culture of wound tissue homogenates as described in [95]. It is expected that the wound infections in neutropenic [96] and diabetic mice may lead to generalized infections such as sepsis. To ascertain sepsis in distant organs , at predetermined intervals after wound infection, mice were sacrificed by cervical dislocation and liver, spleen were removed aseptically. The organs/ wounds tissues were rinsed with sterile saline, blotted dry, and then minced in PBS for ~3 min at 2 gm/ml concentration (w/v). The homogenized tissue lysate were centrifused at 5000 rpm and the supernatant were diluted appropriately. A 50 µl of the supernatant was plated on TSB plates. From the bacterial counts obtained, total CFU/ wound were calculated by multiplying the counts with dilution factor and normalizing with respect to the weight of the tissue.

For some experiments, bacteria load in wounds as a function of time was determined by surface swabbing method [97] as it is known that the surface counts of wounds show good correlation with the counts obtained from the tissue homogenates. For this each wound was rinsed by placing a sterile glass tube (15 mm in diameter) in an inverted position on the back of mouse in such a manner that the total crust of the wound was tightly enclosed . Then 100 µl of PBS were added to the glass test tube, the contents were mixed 10 times with a pipette to remove the infecting organisms from the surface of the wounds. Then each wound was swabbed with a cotton swab

for 5 times. The cotton swabs were placed in 0.5 ml PBS and vortexed for ~30 seconds. The contents obtained from the surface rinsing and swabbing were mixed, appropriately diluted and plated. Colonies were counted and expressed as total bacterial counts per wounds.

## 2.5 Preparation of tissue lysate and western blotting

Animals were euthanized at determined time points by cervical dislocation. Wounds along with ~ 2 mm normal skin were excised and the tissues were snap frozen in liquid nitrogen. The tissues were then transferred to -80$^{o}$ C and used for assays within 3 days. For preparing tissue homogenates samples were thawed on a cool glass plate. Approximately 150 mg of tissue was suspended in Tris (20 mM) Hcl buffer (pH 7.4), maintaining the ratio of tissue to buffer as (1: 5) (w/v). Buffer contained 150 mM Nacl, 1 mM EDTA and a cocktail of protease inhibitors (Cat No INHIB1-1 KT Sigma Aldrich,USA). The concentration of the inhibitors in buffer were as follows, 400 nM aprotinin, 0.5 mM AEBSF,50 µM antipain, 2 mM benzamidine HCl, 40 µM Bestatin, 10 µM E-64, 0.5 mM N-ethylmaeimide, 50 µM leupeptin,0.5 mM pepstatin. The tissues were homogenized with a dounce homogenizer at the speed of 5000 rpm and then incubated for 20 min at 4$^{o}$C. To the homogenate, 1 % Triton-X 100 (v/v) was mixed and the suspension was then sonicated at 20 kHz for four cycles of 10 s each with gap of 10 s. The lysate thus obtained was then incubated on ice for 30 min following which it was centrifuged (10000 rpm at 4$^{o}$C) for 10 min. The clear supernatant was collected and divided into aliquots and transferred to -80$^{o}$C. The aliquots were thawed and used for western blotting within a week or two. An aliquot

of the supernatant was used for protein estimation according to the bicinchoninic acid method.

Sample proteins (~50 µg) were separated by SDS-PAGE. Electrophoresis was carried out at 10 mA constant current (56 V) per 0.75-mm gel till the dye front reached the bottom of the separating gel (15 min). Then the current was increased to 20 mA (90 V) per gel, till the loading dye reached the bottom of the resolving gel (45 min). Sample proteins separated by SDS-PAGE were transferred to nitrocellulose membranes (Hoefer, Inc., USA) using a semidry blotter (Hoefer, Inc., USA) set at constant current (0.8 A/$cm^2$) for 1-1.5 h. Membrane were blocked in 5% non-fat dried milk, 0.1% (v/v) Tween 20 in PBS for 1 h at room temperature on an orbital shaker and then rinsed using two changes of PBS/0.05% Tween-20 (PBS/Tw), for 5-10 min per wash at room temperature. The membranes were then incubated overnight at 4$^oC$ with polyclonal antibodies (0.5 µg/ml) specific for murine MMP-8 (sc-8848), MMP-9 (sc-6840), obtained from Santa Cruz Biotechnology Inc (Santa Cruz, CA, USA). The membranes were washed thrice for 5 min with PBS/0.05% Tween-20 (~ 4ml/$cm^2$) at room temperature. Each membrane was then incubated with the corresponding secondary horseradish-peroxidase-conjugated antibodies diluted 1:4000 in 5% non-fat dry milk for 1.5 h at room temperature, washed 4-6 times with PBS/Tw for ~5 min per wash, at room temperature. Then the membranes were incubated for 1 min at room temperature with the chemiluminescence detection substrate (0.125 ml/$cm^2$) provided along with the kit (RPN 2135, Amersham Biosciences, GE Health Care Life Sciences, US). Chemiluminescence imaging of the blot was carried out with a cooled CCD camera attached to a chemiluminescence imaging system (Chemi-HR-16, Syngene, UK).The images were captured and processed using software (GENESNAP,

Syngene, UK). Densitometric band analysis was carried out using GENETOOL software (Syngene, UK).

## 2.6 ELISA measurements for cytokines

In experiments involving ELISA for measurement on different biomarkers (of inflammation and angiogenesis), the powdered tissues were mixed with lysis buffer provided along with the individual ELISA kit and kept on ice for 30 min. The lysates were sonicated (section 2.6) by keeping on ice and then centrifuged (5000 rpm, 10 min, 4$^{o}$C). The sample supernatant of each group was mixed (1:1, v/v) with a sample diluent buffer and incubated in the capture antibody coated micro wells provided with the kit, for 18 h at 4$^{0}$C. The assay was carried out according to the protocol described in the kit and absorbance was recorded using a microplate reader.The absorbance were normalized with protein concentration.

## 2.7 Hydroxyproline assay for collagen remodeling

Hydroxyproline assay was carried out according to the protocol described in [98]. Wound tissues were mixed gently with 6N HCl (25 mg/ml final concentration). The hydrolysate was then lyophilized. The lyophilized powders were suspended in 200 µl distilled water. This solution was neutralized by adding 10 µl of 10 N NaOH to adjust pH upto 7.3. From this solution, 50 µl was taken and was mixed with 450 µl of chloramine-T , mixed gently, and the oxidation was allowed to proceed for 25 min at room temperature. Then 500 µl of Ehrlich's reagent was added to each sample, mixed gently, and the chromophore was allowed to develop by incubating the

samples at 65 °C for 20 min. Absorbance of each sample was read at 550 nm using a spectrophotometer .

## 2.8 Histology and Masson's trichrome staining

The tissues were fixed in 10 % neutral buffered formalin for 24h, following which all the tissue sections were processed using standard histological procedure. The deparafinized sections were stained with Masson's trichrome staining. The slides were examined under a microscope to determine tissue changes such as inflammation, reepithelialization, arrangement of collagen fibres, and presence of blood micro vessels.

The trichrome stained slides were viewed under a microscope at 400 X magnification. In each microscopic view the main histologic outcomes measured included the amount of acute and chronic inflammatory infiltrates, collagen deposition, reepithelialization [99]. Trichrome stain, in addition to the collagen specific staining, consists of other dyes which can stain different cells and other components such as; (i) inflammatory cell with multilobed nuclei ( as dark purple) , (ii) epithelial cells as red/purple (iii) erythrocytes – yellow (or red), (iv) cytoplasm, fibrin, muscle – red. Hence, it can be used for studying presence of inflammatory cells, reepithelialization, neovascularization as well as crust/necrotic layer. Further, compared to hematoxylene & eosin staining protocol, the contrast between different types of cells appears to be better in case of trichrome staining. Indeed, this staining method has been used previously for studying reepithelialization and neovascularization.

Using the Abramov's scoring system [100], we assessed cell inflammatory infiltration. The scoring was done independently by three scores and assigned a score of 0–3. For acute and chronic inflammatory infiltrates, grading was done as: 0 (none), 1 (scant < 10% of cells ), 2 (moderate , between 25 % to 50 % of total cells), 3 (abundant, more than 50 % of total microscopic view). Three independent persons performed the histological examination and applied the scoring system in a blinded fashion. For each slide, 4-5 microscopic views were considered and for each sample experiment atleast 3 slides were scored. The scores obtained from atleast three experiments were averaged and represented as mean inflammation score.

# 3. Photodynamic effects of free and poly lysine conjugated chlorin p6 on Gram positive, negative bacteria


## Abstract

In this chapter, we present the phototoxicity of cp6, and its poly-L-lysine conjugate pl-cp6 on methicillin resistant *Staphylococcus aureus* (MRSA), *Pseudomonas aeruginosa* and HaCaT, a keratinocyte cell line, used as a model system for host cells. Results show that photobactericidal efficacy of pl-cp6 is higher than that of cp6. Also, for these bacteria, photokilling efficacy of pl-cp6 is independent of growth phase, a desirable feature because in wound milieu bacteria may be in different phases. Furthermore, at given PS concentration, and light fluence resulting in 2-3 log survival loss in bacteria, sub lethal (20 -50 %) of survival loss was observed in HaCaT cells .

## 3.1 Introduction

Antimicrobial photodynamic therapy (APDT) is a promising therapeutic modality for the inactivation of antibiotic resistant bacteria causing infections of wounds [52, 53 , 64, 101, 102]. This approach is based on interaction of PS and visible light of appropriate wavelength to generate ROS which damage biomolecules and kill the target cells [53, 54, 64, 103]. The advantages of APDT over conventional antimicrobials is that the treatment is limited to light-irradiated regions of the drug-treated area [53,54,64] and as singlet oxygen and free radicals generated in the photochemical reactions react with almost every cellular component, it is highly unlikely for bacteria to develop resistance. Nevertheless, a disadvantage of many of the PS used for APDT is that these act on a single class of bacteria and do not have the desired broad spectrum activity. While Gram positive bacteria are photosensitive to both anionic and cationic photosensitizers, Gram negative bacteria are less susceptible to photoinactivation by anionic drugs due to the structural complexity of cell envelope [53, 54, 64].

The important parameters that an ideal PS for APDT should have include (i) high ROS quantum yield, (ii) cationic charge as well as amphiphilic nature to ensure higher accumulation at the polyanionic microbial cell surfaces and (iii) a strong absorbance in the red region to minimize the energy deposition in tissue [64]. Cationic phenothiaziniums, like methylene blue (MB) and toluidine blue (TB) have been the most widely investigated photosensitive drugs currently being investigated for APDT. However, these have relatively lower triplet yield (0.39), hydrophilic nature, and

efflux pump dependent uptake into bacterial cells [70, 71]. In fact the photodynamic efficacy of the commonly used cationic PS (TB, MB) is also low for Gram negative bacteria compared to Gram positive bacteria [103, 70]. Therefore, there is interest in exploring other PS which can address these issues. Chlorophyll derivatives like chlorin p6 (cp6) are particularly attractive because these have good triplet yield (~0.8), amphiphilic nature and strong absorbance in the red (660 nm) region [72]. Since cp6 is anionic [72], its conjugation with cationic peptide poly-L-lysin (pl-cp6) is expected to enhance the targeting of the cp6 to bacterial cells [104-106].

In this chapter, we report the results of our investigations on the photobactericidal effect of cp6 and pl-cp6 on MRSA and *P.aeruginosa,* which are frequently responsible for infections of wounds. In addition, result of the studies carried out to assess cytotoxicity induced by cp6 and pl-cp6 mediated APDT on HaCaT, a keratinocyte cell line, used as a model system for host cells, has also been reported.

## 3.2 Materials and methods

### 3.2.1 *Bacterial strains*

The two organisms used in this study were, a MRSA strain procured from ATCC (ATCC 43300); and *P. aeruginosa* stain procured from IMTECH (MTCC 3541, Chandigarh, India). Both the bacteria were maintained by routinely subculturing on tryptone soya agar (TS) (Himedia, Mumbai, India). For experiments, a colony was inoculated into tryptone soya broth (TSB) and was grown aerobically for 18 h at 37°C using a shaker incubator. Cells were then harvested by centrifugation (10,000 rpm, 5min) and resuspended in sterile PBS. Exponential phase cells were obtained by

growing overnight culture in fresh medium to an optical density (OD) of 0.4 and 0.5 at 600 nm corresponding to ~$10^8$ cells/ml for MRSA and PAO respectively.

### 3.2.2 *Preparation of polylysin-cp6 conjugate*

Cp6 was prepared following the procedure described by Hoober et al [89] and the conjugate of cp6 with polylysin was prepared by carbodiimide coupling method described in [107] with slight modifications. This has been elaborated in chapter 2.

### 3.2.3 *p-nitrosodimethylaniline photobleaching and Nitro blue tetrazolium reduction assay*

Detection of singlet oxygen generation from cp6 or pl-cp6 was achieved by irradiation in the presence of imidazole and RNO (p-nitrosodimethylaniline) [108]. Production of singlet oxygen leads to reaction with imidazole to form a peroxide intermediate, which subsequently reacts with RNO to cause photobleaching and decrease in absorbance. A total reaction volume of 1000 µl was prepared containing 15 µM RNO, 8 mM imidazole, and 2 µM cp6 or pl-cp6 in phosphate buffer (10 mM phosphate, pH 7.4). Photoirradiation of different groups (2, 4 and 8 min) was carried out using the parameters as described in table 2.1, same as that used for bacterial killing experiments. During irradiation, the reaction mixture was stirred. At the end of irradiation, the reaction mixtures were drawn out and photobleaching of RNO was detected by measuring absorbance at 450 nm using a spectrophotometer. The RNO photobleaching observed in samples exposed to different light fluence was expressed as decrease in OD with respect to the unirradiated control.

Detection of superoxide generation was carried out by photoexcitation of both cp6 and pl-cp6 in the presence of NADH and nitroblue tetrazolium (NBT). A total reaction volume of 1 ml was prepared containing 2 μM cp6 or plc-cp6, 10 mM NADH, and 80 μM NBT [109]. Illumination was carried out in the same manner as RNO photobleaching experiements. Reduction of NBT resulting in the production of a formazan was detected by absorbance at 600 nm using a spectrophotometer. The NBT reduction observed in samples exposed to different light was expressed as increase in OD with respect to unirradiated control.

### 3.2.4 *Uptake of cp6 and pl-cp6 by bacteria*

Suspensions of bacteria (~$10^6$ CFU/ ml) in PBS were incubated in dark at 37$^o$C with with different sensitizer concentrations (1–10 μM) for 15 min. The cultures were centrifuged (3000 g for 15 min) and then resuspended with PBS. The cell pellets, obtained by centrifugation (3000 g for 15 min) and three washing steps, were dissolved in 2 ml of 0.1 M NaOH-2% sodium dodecyl sulfate(SDS) for 24 h at 4$^o$C and then sonicated for 30 min. The fluorescence of dissolved pellets was measured using spectrofluorimeter. The excitation wavelength was set at 400 nm and the emission spectra of the solution were recorded in the wavelength spanning 580 to 700 nm. Calibration curves were made from a stock of the PS dissolved in NaOH-SDS and used for determination of PS concentration in the suspension. Uptake values were obtained by normalizing the concentration of PS with the protein content (mg) of bacteria.

### 3.2.5 *Photoxicity study in MRSA and P.aeruginosa*

*MRSA* (containing ~ 1 × $10^8$ cells/ml) and *P. aeruginosa* (containing ~ 1 × $10^7$ cells/ml) in sterile PBS, were incubated with different concentrations of PS which ranged from 1.0-8.0μM for cp6 or 0.1-5.0 μM for pl-cp6 for 15 min in the dark. 1ml of PS treated and untreated cell suspensions were placed into 12 well microplates. Wells containing sample were then exposed to red light (660 nm ± 25 nm) fluence of ~2-50 J/$cm^2$ , delivered from a broadband light source (LC122-A, Lumacare, Ci-Tec,USA) using a fiber optic probe (diameter 1 cm). Untreated control samples were neither treated with PS nor exposed to light. Following exposure to light, 100 μl aliquot was removed from each well and added to 900 μl PBS. Serial dilutions were made, and 50 μl aliquot (in duplicate) from each dilution was plated on to TS agar, and grown overnight at 37°C. Surviving bacterial colonies were counted. The surviving fractions ($N/N_0$) of cells were determined by counting the number of colony-forming units (CFU) formed per ml in treated samples (N) and untreated sample ($N_0$).

### 3.2.6 *Cytotoxicity assay of HaCaT cell line*

HaCaT cell line was obtained from NCCS, Pune. The cells were routinely maintained and sub cultured in DMEM: F12 (1:1) medium with 10 % Fetal Bovine Serum. The cells were grown in 5 % $CO_2$ at 37$^o$C. For studies on cp6 and pl-cp6 mediated PDT, ~$10^5$cells were plated into each well of a 12 well plate, grown till mid exponential

phase and then incubated with different concentrations (0.1 – 10 μM) of cp6 and pl-cp6 for 15 min. Cells were then washed twice with DMEM:F12 medium without FBS and replenished with DMEM: F12 (1:1) medium containing 10 % FBS. Cells were then exposed to 660 ± 25 nm light (~100 mW/cm$^2$) for different durations to achieve fluence of ~10- 50 J/cm$^2$. Cytotoxicity in HaCaT cells was assessed by MTT assay. The absorbance of the formazon formed in the untreated ($A_0$) and photodynamically treated samples (A), at 565 nm, was used to calculate fraction of surviving cells ($A/A_0$) absorbances in the .

### 3.2.7 *Data analysis*

All experiments were performed at least thrice. Values expressed are mean ± SEM. The difference between two means was assessed for significance by two-tailed Student's t test, assuming equal or unequal variances of the standard deviations. A value of $p < 0.05$ was considered significant.

## 3.3 Result

### 3.3.1 *Characterization of conjugate*

The absorption spectra of cp6 and pl-cp6 in 0.1 M NaOH–1% (w/v) methanol are shown in figure 3.1. The spectrum of free cp6 shows a strong absorption peak at 404 nm (Soret band), a weaker absorption peak at 654 nm. The spectrum of conjugated cp6 showed higher absorption at 280 nm .

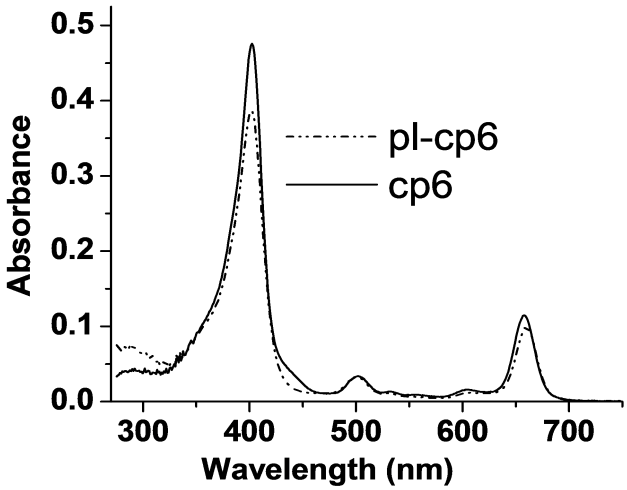


**Figure 3.1** Absorption spectra of cp6 (solid line) and pl-cp6 (dotted line) in 0.1 M NaOH–1% sodium dodecyl sulphate. In the peptide conjugated cp6 wavelength peak was red shifted to 656 nm.

### 3.3.2 *RNO photobleaching and NBT reduction*

We then investigated whether the photophysical properties of cp6 had been altered after conjugation reactions. The photochemical assays involving singlet oxygen mediated oxidation of RNO in the presence of histidine and superoxide mediated reduction of NBT in the presence of NADH were carried out address this question. The results presented in figure 3.2 (A and B) show RNO photobleaching (fig 3.2 A) and NBT reduction (fig 3.2 B) caused by cp6 and pl-cp6 mediated photosensitization.

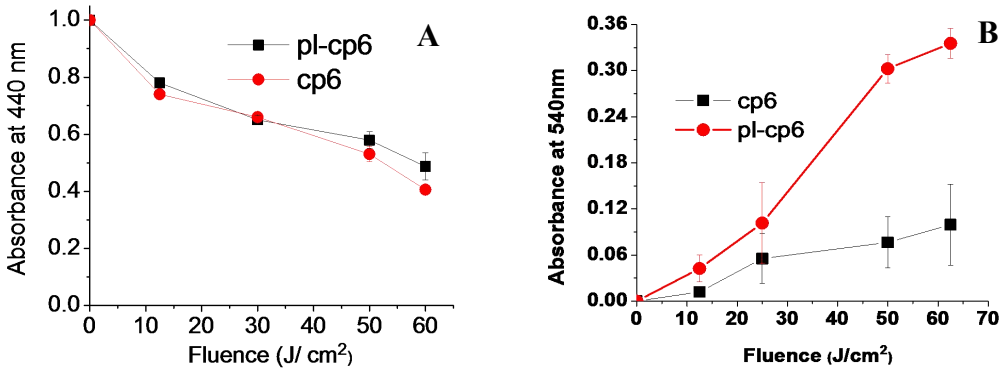


**Figure 3.2** RNO photobleaching (A) and NBT reduction assay (B) for measuring singlet oxygen and superoxide anion in cp6 and pl-cp6 in PBS. The assays were carried out using protocols described in section 3.2.

The results show that for the given concentration (1 µM) of both cp6 and pl-cp6, at all the light fluence used, photochemical singlet oxygen production was similar. However, the photochemical superoxide anion generation in case of pl-cp6 mediated photosensitization was higher.

### 3.3.3 *Uptake of cp6 and pl-cp6 in MRSA and P.aeruginosa*

The drug dose dependent uptake of unconjugated and poly-l-lysine conjugated cp6 by *MRSA* and *P.aeruginosa* was studied by measuring fluorescence of bound drugs extracted from bacteria after incubation with drugs in dark for 15 min (fig . 3.3 A and B). The results show that rate of uptake of cp6 and pl-cp6 was higher in MRSA when incubated at lower concentrations of PS as compared to *P.aeruginosa*. At high concentrations, rate of uptake of both cp6 and pl-cp6 changed negligibly for MRSA indicating saturation of binding sites. Cp6 accumulation by MRSA incubated with 1 µM pl-cp6 was comparable with bacteria incubated with 8 µM of cp6. As compared

to MRSA, uptake of cp6 was lesser in *P.aeruginosa*. Nevertheless, the concentration of pl-cp6 bound to *P.aeruginosa* was about two fold higher than the concentration of cp6 at all the concentrations with the difference in uptake being more pronounced at higher concentrations.

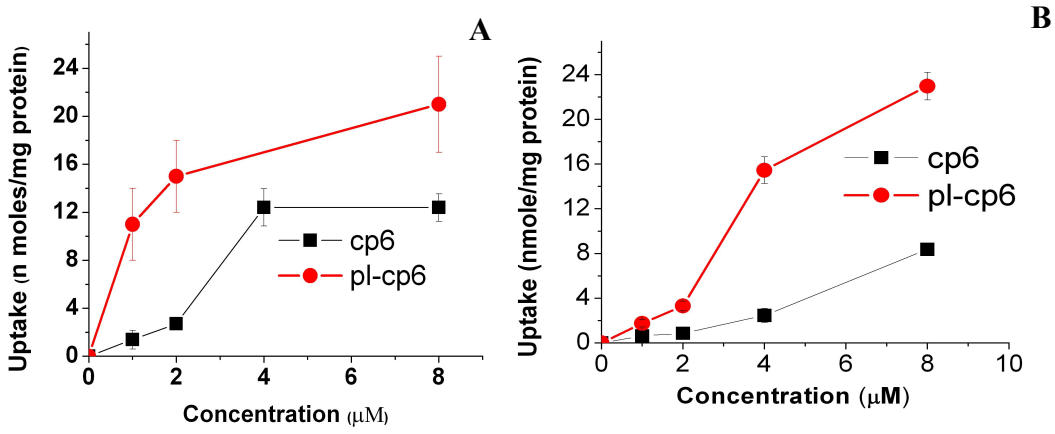


**Figure 3.3** Uptake of cp6 and pl-cp6 by *MRSA* (3.3.A) and *P.aeruginosa* (3.3.B) incubated with different concentrations of cp6 and pl-cp6 in dark. Values represent mean ± SD.

## 3.3.4 *Lethal photosensitization of MRSA and P.aeruginosa by cp6 and pl-cp6 mediated APDT*

### 3.3.4.1 Lethal photosensitization of MRSA

In figure 3.4 (A and B) we show the dependence of the phototoxicity induced by free and conjugated cp6 on MRSA as a function of concentration and light fluence, respectively. For cp6 concentration range studied (1-8 μM), no dark toxicity was observed. The phototoxicity was not significant when MRSA was irradiated with red

light at a fluence of ~ 25 J/cm$^2$ in presence of 1 μM cp6. However, survival reduced by ~ 0.9 log and ~ 2.3 log in MRSA incubated with 4 and 8 μM cp6, respectively, on being exposed to the same light fluence. In contrast, even at 1 μM of pl-cp6, significant dark toxicity (~1.0 log) was observed and survival reduced by ~4 log following irradiation at light fluence of ~25 J/cm$^2$ as compared to the survival observed in the untreated bacteria. In figure 3.4 B, we show the effect of light fluence on MRSA treated with free cp6 and pl-cp6. In MRSA treated with 8 μM of cp6, surviving fraction reduced by ~1.3, ~2.4, and ~2.6 log at light fluence of ~12.5, ~25 and ~50 J/cm$^2$ respectively as compared to unirradiated bacteria treated with cp6. In contrast, a concentration of 1.0 μM of pl-cp6 was sufficient to reduce the bacterial counts by ~1.3 log, ~3.4 log and ~3.9 log when irradiated at light fluence ~12.5, ~25 and ~50 J/cm$^2$, respectively.

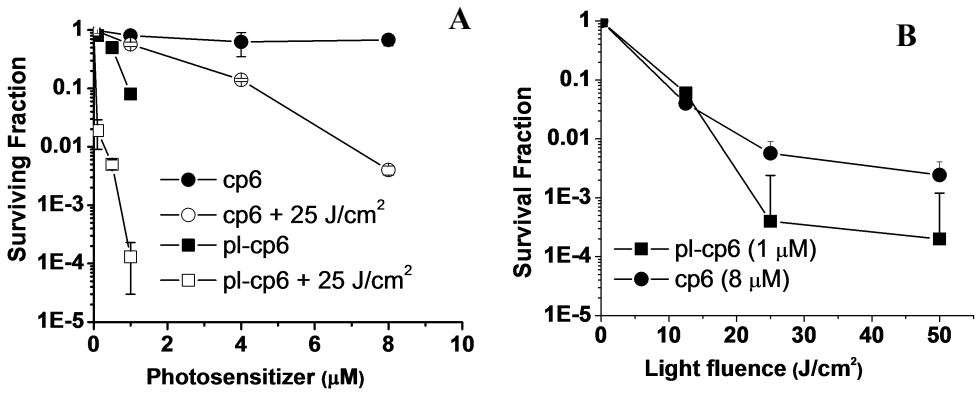


**Figure 3.4** Photodynamic inactivation of MRSA with cp6 and pl-cp6. (A) Surviving fraction of MRSA treated with cp6 and pl-cp6 at the indicated concentrations for 15 min in the dark and then exposed to ~ 25 J/cm$^2$ red light. (B) Surviving fraction of MRSA treated with cp6 or pl-cp6 for 15 min in the dark and exposed to various fluences of light as indicated.

### 3.3.4.2 Lethal photosensitization of *P.aeruginosa*

In figure 3.5.A we show the surviving fraction of *P.aeruginosa* incubated with different concentrations of cp6 and pl-cp6 with and without irradiation. While cp6 did not exhibit phototoxicity in these bacteria in the concentration range (1-8 μM), for pl-cp6, at concentration of 2.5 μM , survival of *P. aeruginosa* reduced by ~ 70 % even in absence of light. Incubation of cells with 2.5 and 5 μM of pl-cp6 followed by exposure to light fluence of ~ 25 J/cm$^2$ reduced the cell survival by 3.5 log and 5 log, respectively. Figure 3.5 B shows the surviving fraction of *P.aeruginosa* incubated with 2.5 μM of pl-cp6 and exposed to different light fluence. Survival reduced by ~4 log at a light fluence of ~ 25 J/cm$^2$ as compared to bacteria treated with drug alone. Beyond this light fluence, no significant change in phototoxicity was observed.

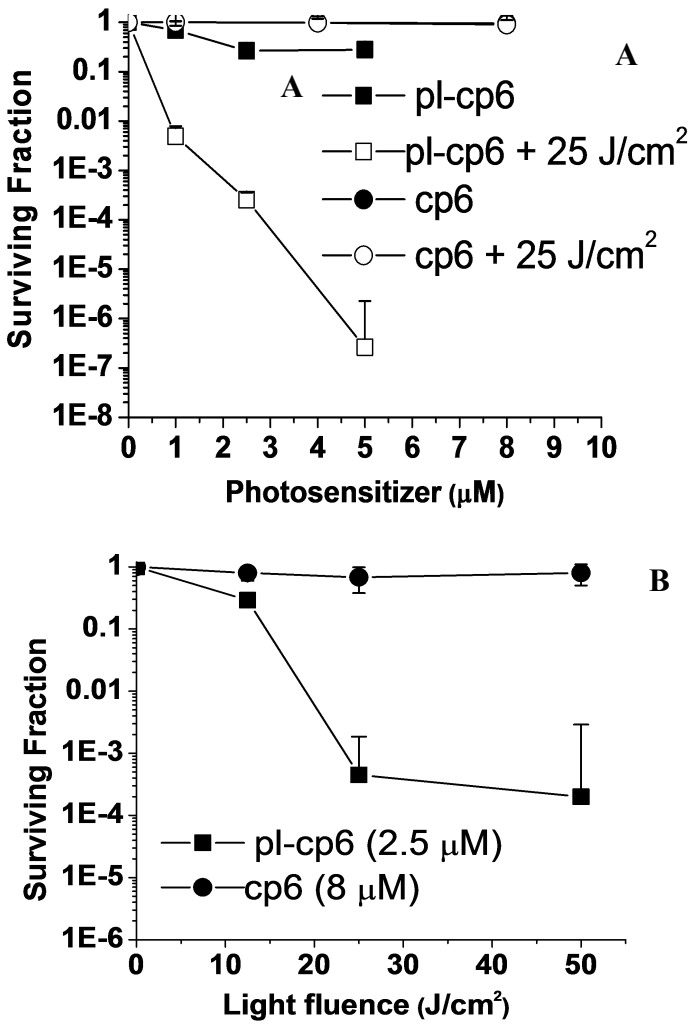


**Figure 3.5** Photodynamic treatment of *P.aeruginosa* with cp6 and pl-cp6. (A) Surviving fraction of *P.aeruginosa* treated with cp6 and pl-cp6 at the indicated concentrations for 15 min in the dark and then exposed to red light fluence ~ 25 J/cm$^2$. (B) Surviving fraction of *P.aeruginosa* treated with cp6 (8 μM) or pl-cp6 (2.5 μM) for 15 min in the dark and exposed to different light fluence as indicated.

### 3.3.4.3 Effect of bacteria growth phase on cp6 and pl-cp6 mediated phototoxicity

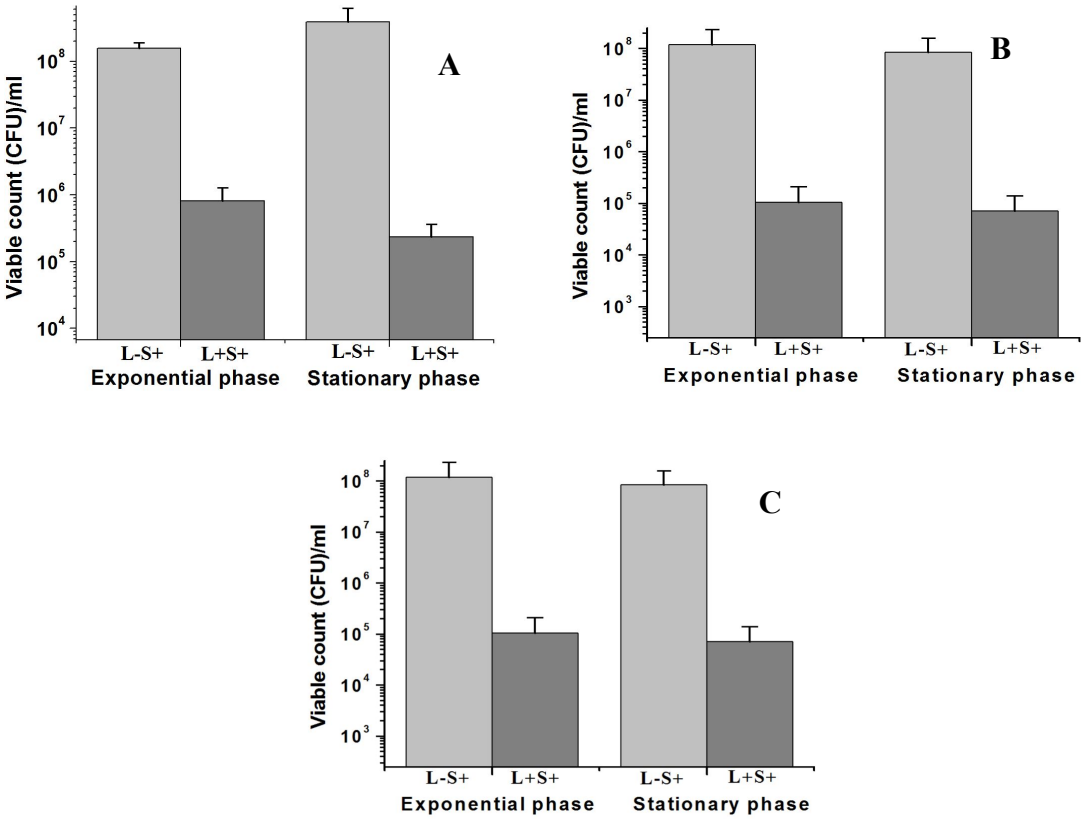


**Figure 3.6** Effect of growth phase on the photosensitivity of : (A); MRSA to cp6 (8 μM), (B); MRSA to pl-cp6 (1 μM), and C) *P.aeruginosa* to pl-cp6 (2.5 μM). Exponential and stationary phase cells were incubated with PS at the indicated concentrations for 15min. Cells were either kept in the dark [grey bars, (L-S+)] or exposed to ~50 J/cm$^2$ red light fluence [black bars, L+S+)]. L = Light. S = Sensitizer.

In figure 3.6 we present the results on phototoxicity of cp6 and pl-cp6 on MRSA and *P.aeruginosa* in stationary and exponential growth phases. For MRSA, viability of exponential and stationary phase bacteria treated with 8 μM cp6 was comparable. Phototoxicity of free cp6 (8 μM) following irradiation at light fluence ~ 50 J/cm$^2$ was

also not significantly different ($p>0.05$) for stationary and exponential phases (fig. 3.6 A). Similarly, no growth phase dependent change in viability was observed in bacteria treated with 1 μM of pl-cp6 and irradiated with ~ 50 J/cm$^2$ light (fig. 3.6 B).

In *P.aeruginosa* incubated with 2.5 μM pl-cp6, and exposed to red light fluence ~ 50 J/cm$^2$ toxicity was higher in stationary phase cells as compared to exponentially growing cells treated under identical conditions (fig. 3.6 C). Under these conditions while viable count of stationary phase cells reduced by ~4.8 log, for exponential phase cells, it reduced by ~3 log as compared to bacteria treated with pl-cp6 alone. For *P.aeruginosa,* since no phototoxicity was observed with cp6, growth phase dependence effect was not studied.

### 3.3.4.4 Cytotoxicty induced in HaCaT cell line by cp6 and pl-cp6 mediated PDT

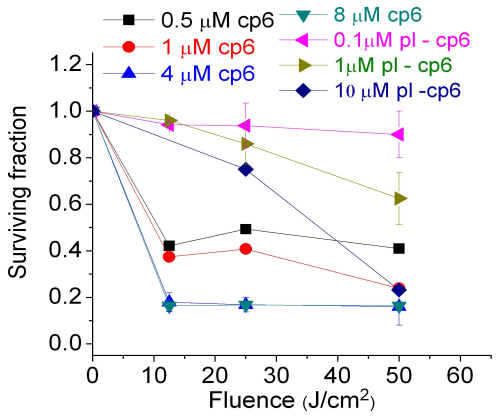


**Figure 3.7** Phototoxicity induced by cp6 and pl-cp6 mediated photosensitization in HaCaT cells. Cells were incubated with drugs for 10 min followed by washing and exposure to red light.

The results in figure 3.7 show the cytotoxicity induced cp6 and pl-cp6 mediated PDT in HaCaT cells. As can be inferred from the figure that for the drug concentration of 1

μM for cp6, pl-cp6 and a light fluence of ~25 J/cm$^2$ while there is > 2 log survival loss in MRSA or PAO, the survival loss in HaCaT is < 50 %. Furthermore, compared to the cytotoxicity induced in HaCaT cells by free cp6 and light fluence ~ 25 J/cm$^2$, the cytotoxicity induced by pl-cp6 and light (~ 25 J/cm$^2$ ) is much lesser .

## 3.4 Discussion:

In this study, photobactericidal potential of free cp6 and poly-lysine conjugated cp6 on MRSA and *P. aeruginosa,* the two common wound-infecting bacteria has been compared. While free cp6 shows significant phototoxicity to MRSA, *P. aeruginosa* was photosusceptible only to pl-cp6. Even for MRSA, pl-cp6 was more effective in killing than cp6. For example, eight times lower concentration of conjugated cp6 (1.0 μM) than free cp6 co uld induce comparable (~98%) cell killing when irradiated at similar light fluence (~ 12.5 J/cm$^2$). The greater photodynamic potency of pl-cp6 may be due to the enhanced binding of the cationic and amphiphilic PS to bacteria [110] which upon photo irradiation induces higher level of damage to the bacteria. Free cp6, though smaller in size, has anionic charge which reduces its overall uptake and hence the phototoxicity.

In our study we also observed that the uptake of the cp6 from poly-lysine conjugate was higher as compared to free cp6 in both Gram positive and Gram negative bacteria. This is believed to be due to the more efficient binding of the positively charged pl-cp6 to the outer membrane of PAO as well as to the phosphate groups of the wall teichoic acids of MRSA, which have negative charge [105]. Due to the porous nature [63] of the peptidoglycan wall in Gram positive bacteria, uptake of cp6 and pl-cp6

occurs faster and leads to accumulation of higher concentrations of the drug as compared to *P.aeruginosa*. For *P.aeruginosa,* which has larger size as compared to MRSA, higher quantity of drug is required to attain saturation. In addition, mechanism of uptake in *P.aeruginosa* may also differ from MRSA. In Gram negative bacteria, poly lysine may bind first to anionic sites of LPS and weaken the interactions of constituents in the outer membrane and due to which the permeability of cp6 to inner membrane and cytoplasm is enhanced [105,110]. The lesser accumulation of anionic free cp6 observed in Gram positive and Gram negative bacteria is because of the negative charge on the outer wall/envelope. This observation is in agreement with data reported previously for conjugates of poly lysine with chlorin e6 for different Gram positive and Gram negative bacteria by Sukos et al [105]. They reported almost two to four times higher uptake of ce6 poly lysine conjugate as compared to unconjugated ce6 by *Actinomycetes viscosus* a, Gram positive bacterium found in subgingival plaques.

After studying the uptake in MRSA *and P.aeruginosa* we then investigated the relative photobactericidal efficacy of the cp6 and pl-cp6. *P. aeruginosa* was observed to be refractory to photodynamic treatment with cp6. However, as the results presented in figures 3.5 A and B show, pl-cp6 mediated photosensitization induces substantial killing in *P.aeruginosa.* This is expected, because the polycationic nature of pl-cp6 allows it to bind more effectively and displace the divalent cations from the LPS,PG molecules in the outer membrane, increase outer membrane permeability, thus allowing the cationic peptide PS conjugate access to intracellular targets [111]. This process, known as self-promoted uptake, is exemplified by the bactericidal mechanisms of cationic peptides including naturally occurring cationic antimicrobial

peptides such as defensins, cecropin, and gramicidin [112]. The photokilling efficacy of pl-cp6 for *P.aeruginosa* was slightly lower than that observed in case of MRSA. For example, for achieving ~99.9% cell killing in *P. aeruginosa*, under similar light irradiation conditions, ~ 2.5 times higher concentration of pl-cp6 was required than the concentration used for MRSA. This may be expected due to the lesser permeability for the penetration of PS into the Gram negative *P. aeruginosa* because of the presence of the outer membrane [113,107]. It is known that Gram positive bacterial cell wall displays higher degree of porosity. Macromolecules with molecular weight of 30,000–60,000 Da (glycopeptides, polysaccharides) can readily diffuse into the inner plasma membrane. In contrast, Gram negative bacteria contain an additional highly organized outer membrane in the cell wall and also their envelope contains lesser amount of PGs than the Gram positive bacteria [64]. Such a highly organized system inhibits the penetration of several compounds, even hydrophilic molecules of MW 600–700 Da, which can otherwise diffuse through the porin channels [63].

This study shows that, for MRSA, phototoxicity induced by cp6 and pl-cp6 is not strongly dependent of growth phase (fig. 3.6 A, B). Various factors such as slime production, charge and hydrophobicity of slime and expression of surface receptors may lead to the dependence of photosensitivity on growth phase [114,104]. Earlier studies on phototoxicity carried out in wild type *S.aureus* (SA113 ($PS/A^+$ $slime^+$) and *S. epidermidis* (M187sn3 ($PS/A^+$ $slime^+$) and their isogenic mutants deficient in slime production have shown that extracellular slime could be one of the important factors for the growth phase dependent phototoxicity of cationic and anionic photosensitizers. It has been shown that *S.aureus* (SA113 ($PS/A^+$ $slime^+$) in exponential phase is more photosensitive to free ce6 mediated PDT than the bacteria in the stationary phase

which can be attributed to trapping of the anionic PS within the slime produced during stationary phase and thereby inhibits the binding of drugs to bacterial components. The same study also reported that poly lysine conjugated ce6 being cationic and more hydrophilic than free ce6 induces comparable phototoxicity to *S. aureus* (SA113 ($PS/A^+$ $slime^+$) in exponential and stationary phases which was presumed to be due to the binding of drug to bacteria rather than slime. In our study, no growth phase dependent photosensitivity was observed with both free cp6 and pl-cp6. This may be because the MRSA used in our study is not a slime forming bacteria, so, it is probable that the uptake of free as well as conjugated PS was similar in MRSA growing in both the stationary as well as exponential phases, which in turn contributed to the observed lack of differences in phototoxicity. These results are consistent with results reported previously [115], in which it is shown that killing induced by AlPcS2 mediated photosensitization is not dependent on growth phase of MRSA.

The results presented in figure 3.6.C imply that in contrast to MRSA, *P.aeruginosa* is more photosensitive to pl-cp6 mediated photosensitization in the stationary phase than in the exponential phase. Since this strain of *P.aeruginosa* produces more extracellular polysaccharide (alginate) in stationary phase [116], the increased sensitivity of the exponential phase may not be related only to extracellular polysaccharide production. However, the growth phase dependent changes in hydrophobicity and surface charge of the Gram negative bacterial outer membrane may cause differences in uptake/accumulation of PS [117, 118]. It has been reported that more phosphate groups are exposed in the outer membrane of stationary phase Gram negative bacteria than that in early growth phase [117]. Therefore, it is possible

that poly cationic drug uptake in stationary phase cells is higher and also the PS is located in more sensitive sites which may have led to higher phototoxicity on exposure to light than phototoxicity in the bacteria of exponential phase.

The results presented in figure 3.7 suggest that pl-cp6 mediated APDT induced far less toxicity in a keratinocyte cell line compared to bacteria. The reason for this observation could be the combination of the polycationic nature, amphiphilicity and increased size due to conjugation. The selectivity of a cationic peptide binding to bacterial membrane arises because of anionic nature, higher negative transmembrane potential (-130 to -150 mV) via a vis the zwitterionic nature, lower transmembrane potential (-90 mV to -110 mV) of mammalian cell membranes [67]. Also, the cationic peptides have higher affinity to the phosphatidylglycerols (PG) which are predominantly present in bacterial outer envelope while in mammalian cells the PGs are more sequestered in the inner leaflet of the cell membrane. While the cationic charge ensures accumulation of the cationic PS at polyanionic microbial cell surfaces, the combination of hydrophobic and hydrophilic substituents results in an intramolecular polarity axis which will facilitate the PS straddle the interface of the hydrophilic head groups and the fatty acyl chains of membrane phospholipids. This is also observed in case of many naturally occurring antimicrobial amphipathic peptides that assume a helical structure with the cationic charges on one side of the helix and hydrophobic amino acid residues on the opposite side. The results presented in fig 3.7 also show that the survival loss induced in HaCaT cells by pl-cp6 mediated APDT is lesser compared to that induced by cp6. It may be noted here that both singlet oxygen and superoxide generation by cp6 was not affected because of conjugation, (fig 3.2.) and in fact there is higher uptake of the drug when bacteria are incubated with the

conjugate. So the lesser phototoxicity of pl-cp6 in the keratinocytes is most likely because of its lesser uptake. This may have occurred because of the increase in molecular weight (few kDa) caused by the conjugation of the PS to polylysin (~ 22 kDa). It is known that pl-cp6 uptake into cancer cells occur largely via the relatively slower endocytosis process [68]. Whereas, cp6 being anionic and smaller is taken up through diffusion [119], which is a faster process compared to endocytosis. Therefore, when applied to wounds, while pl-cp6 will bind faster to bacteria, cp6 would bind to a lesser degree to the bacteria and taken up more rapidly by host cells like keratinocytes. Further, when illumination is performed at short intervals (min) after PS application PDT induced damage to host tissue will be minimized in case of pl-cp6, whereas, in case of cp6, light illumination will cause higher host tissue damage, together with the reduced photobactericidal effect, leading to bacterial regrowth. In fact this has been shown in a study of soft tissue infection treated with ce6 and its poly lysin conjugate, wherein pl-ce6 proved to be more effective in killing bacteria without causing host tissue damage, while the free ce6 induced more host tissue damage [120].

## 3.5 Summary

In summary, singlet oxygen and superoxide generation capability of pl-cp6 is not adversely affected compared to cp6. The photobactericidal efficacy of pl-cp6 is higher than that of free cp6 and is independent of growth phase of bacteria. Further, in HaCaT cell line, only sublethal phototoxicity is induced by pl-cp6 mediated PDT at drug concentration and light fluence which caused 2 log survival loss in bacteria.

# 4. Effect of antimicrobial photodynamic treatment on bacteria cell envelope


## Abstract

In this chapter, we present the results of the studies carried out by us on the mechanism of bacterial cell damage induced by APDT mediated by the different photosensitisers; cp6, pl-cp6 and a standard phenothiazinium PS, toluidine blue O (TBO). Results show that while APDT mediated by both TBO and pl-cp6 resulted in a significant reduction in the mean cell height, flattening of Gram negative bacteria (*P.aeruginosa and E.coli*) suggesting damage to the bacterial membrane and reduction of cell volume due to the loss of cytoplasmic materials, in Gram positive bacteria (*S.aureus)* significant differences were observed in the morphological changes subsequent to APDT mediated by TBO and pl-cp6. While the major effect of TBO mediated APDT was breakage in the contact between the cell wall and the membrane, pl-cp6 mediated APDT resulted in damage primarily to the outer peptidoglycan layer.



*Some aspects of the results presented in this chapter have appeared in J. Photochem. Photobiol. B 96, 9–16 (2009) .*

## 4.1 Introduction

Photodynamic inactivation of bacteria depends upon the nature of photosensitizing drug as well as its interaction with the bacterial cell envelope [63]. Several studies have shown that photobactericidal efficacy of PS are different for Gram positive and Gram negative bacteria [69,121]. This has been attributed to the differences in the structure and the composition of the cell wall of bacteria. Further, for a particular species of bacteria, the nature of cell envelop damage caused by different PS may vary significantly according to hydrophobicity and size of the PS. For example, amphiphilic PS are expected to be better partitioned in the bacterial cell membrane [67, 110]. Also, a smaller PS is likely to diffuse to inner layers through porins, the larger PS (> 1000 Da) are more likely to initially localize at the outer layer because of the permeability barrier imposed by the outer membrane in Gram negative bacteria. Since the interaction of PS with the cell envelop plays a critical role in the initiation of photoinactivation process, direct observation of morphological changes on the cell surface induced by the photodynamic treatment provides useful information for understanding the mechanism of action of different PS in different types of bacteria. Scanning and transmission electron microscopies (TEM) are the most widely used techniques for elucidating the morphological alterations in bacteria [122, 123]. Ultrastructural alterations like formation of blebs, holes on cell surface and appearance of electroluscent areas in cytoplasm of photodynamically treated bacteria have been observed. Based upon these observations mechanism of action of different PS have been proposed. However, the electron microscopic techniques are tedious

and require elaborate sample preparation which may alter the dimensions of the cellular structures [124].

Of late, it has been recognized that atomic force microscopy (AFM), because of its high resolution and less complicated sample preparation procedures can be an attractive way to investigate the surface morphology of biological specimens [124-132]. For example, AFM has been used recently for elucidating the mechanism involved in membranolytic effects of different antimicrobial peptides in *E. coli* [130-134], for studying the cell surface alterations induced by membrane permeabilizers [133] and antibiotics in bacteria [134]. In these studies distinct morphological changes ranging from formation of holes in the membrane to cell lysis could be observed by AFM in bacteria following treatment with different antimicrobial agents.

In this chapter, we present the results of the studies carried out by us on the mechanism of bacterial cell damage induced by APDT mediated by the different PS; cp6, pl-cp6 and a standard phenothiazinium, TBO using AFM, absorbance spectrophotometry and fluorescence microscopy.TBO was chosen because this PS has been very widely examined for APDT [69,121, 135-137] as it binds to different structural components of both Gram positive and Gram negative bacteria. For instance, while in Gram positive bacteria TBO binds to the teichuronic acid residues of the outer wall [122,123], in Gram negative bacteria it predominantly binds to the LPS present in the outer cell envelope [64, 69,121]. Therefore, it is expected that that cationic TBO may induce different kinds of morphological alterations in Gram positive and Gram negative bacteria. Poly-L-lysin conjugate of cp6, is cationic, amphiphilic, and has larger molecular weight because of the attached peptide. Hence,

it may be expected that the kind of topological alterations induced by pl-cp6 mediated APDT would be different from that induced by TBO .

## 4.2 Materials and Methods

### 4.2.1 *Photosensitizers*

TBO (80% purity), was procured from Himedia (Mumbai, India) and used as such. A stock solution (1.5 mM) of TBO was prepared by dissolving appropriate quantity of the dye in sterile distilled water. Solution was filter sterilized and stored at 4$^{o}$C in the dark for not more than a week before use.

Cp6 was prepared following the procedure described in [89] and pl-cp6 was prepared by carbodiimide coupling method described in the material and method section 2.2.

### 4.2.2 *Bacterial cell culture*

*S. aureus* (MTCC 740, ATCC 9144) was procured from Himedia. *P. aeruginosa* (MTCC 3541) was procured from Institute of Microbial Technology, (Chandigarh, India). *E. coli* DH5α was a gift from Dr. S. Tole (TIFR, Mumbai, India). All the bacteria were routinely grown overnight in Lauria Broth (Himedia, Mumbai, India) under aerobic conditions at 37$^{o}$C using a shaker incubator. For experiments designed to study the membranolytic actions of TBO, both the bacteria were grown to the exponential phase corresponding to an optical density (OD) 0.4 at 660 nm. At this OD, the colony forming units (CFU) per ml was ~0.3 x $10^7$ for *E.coli* and ~ 0.7 x $10^7$ for *S.aureus*. For *P.aeruginosa,* OD of 0.5 (~0.7 x $10^7$) was taken. The cultures were

centrifuged (7000 g, 5 min, 4$^{o}$C) and the cell pellets were resuspended in PBS. The cell suspensions of bacteria were divided into two aliquots. To one of these aliquots of bacteria, a suitable volume of the stock solution of PS (TBO, cp6 and pl-cp6) was added to achieve the required dye concentration. To the other aliquot, used as control, PBS was added to make its total volume equal to that of the PS treated sample. Both the PS treated and untreated cultures were incubated at 37$^{o}$ C for different durations in the dark.

### 4.2.3 *Photodynamic treatment of bacterial cell suspension*

MRSA and *P. aeruginosa* suspended in sterile PBS, were incubated with different amount of PS; 1.0-8.0 µM cp6 or 2.5 µM pl-cp6, for 15 min in dark. 200 µl of PS treated and untreated cell suspension was placed into 96 well microplates. Wells containing sample were then exposed to 660 nm (± 25 nm) light fluence ~1-50 J/cm$^2$. Controls were neither treated with PS nor exposed to light. The photoirradiation parameters for these studies are mentioned in table no 2.1 of chapter 2.

For assessment of photobactericidal efficacy of TBO, bacterial cell suspension was treated with TBO (25 µM) for 60 min and transferred to a cuvette of path length 1 cm. Dye treated bacterial cell suspension was irradiated for different durations with Helium-Neon laser (632.8 nm). Laser beam was expanded to a spot of 1 cm diameter for uniform irradiation of the entire cell suspension. The power output of the laser at the sample plane, as measured by a power meter (LASERMATE, Coherent Inc,USA), was 14 mW. The intensity of laser light at the plane of the cells was ~18 mW/cm$^2$. The cell suspensions were irradiated for different durations to achieve the light

fluence of ~1–40 J/cm $^{2}$. During irradiation, the cell suspensions were stirred and temperature was maintained at 37$^{o}$ C.

### 4.2.4 *AFM imaging of bacterial cell suspension subjected to photosensitization*

#### 4.2.4.1 Sample preparation

For AFM analysis, bacterial samples were prepared following the protocol described by Robichon et al [127]. Briefly, 4-5 μl (~2.5 x 10 $^{5}$ CFU/ml) of photodynamically treated and untreated cells were spread on a clean glass coverslip and air dried at room temperature in the dark for 10 min. It has been reported that bacteria remain alive when dried in ambient conditions [125]. Though AFM imaging can be performed in liquid, the image resolution is unsatisfactory because of the noise arising due to the poor adhesion of bacteria to the substratum and the motility of their floating appendices [127]. We have used air dried samples for AFM imaging as this mode of imaging is generally used for evaluating the changes in morphology of bacteria caused by antibacterial agents [125].

#### 4.2.4.2 AFM imaging

Surface topography of photodynamically treated and untreated (control) bacteria were imaged using a multimode scanning probe microscope (NT-MDT, SOLVER-PRO, Russia). AFM measurements were carried out in a non contact mode using silicon cantilever tips having radius of curvature of ~10 nm and a spring constant of 5.5 N/m at resonance frequency of 190 KHz under ambient conditions. From the topographic

images of both treated and untreated cells, mean length and width of individual cells were measured using the imaging software (SOLVER-PRO, Russia). Measurements on mean cell height (MCH) were carried out from the 3-dimensional (3-D) reconstructed images using the same software. In each sample (control as well as treated), an average of 100 cells were imaged to ascertain the effect of photodynamic treatment on cell surface morphology. Analysis was carried out in triplicate samples for each light fluence.

### 4.2.5 *Absorbance measurements of cellular contents released after photosensitization of bacteria*

Leakage of cytoplasmic contents is an indication of damage to the bacterial cytoplasmic membrane [138]. Absorbance at 260 nm was used to estimate the amount of intracellular contents leaked from bacteria subjected to different light fluences of photosensitization. For these experiments, 1.2 ml of bacterial suspension was irradiated at fluences of ~1, 2 and 4 J/cm$^2$. The samples were centrifuged at 5000 pm for 10 min and then filtered to remove bacteria [138]. The supernatants were then diluted appropriately and OD at 260 nm ($OD_{260}$) was measured. The % increase in $OD_{260}$ of the photodynamically treated samples with respect to the dark control as a function of light fluence was calculated. In order to monitor the kinetics of release of intracellular contents, cell suspensions of both the bacteria were transferred to 37$^o$C following photoirradiation. Aliquots (400 μl) were drawn out immediately (0 min) and at 60, 120 min post irradiation time points. After filtering cells, $OD_{260}$ of the supernatants were measured. The % change in $OD_{260}$ at 60 and 120 min post

irradiation time was calculated with respect to the $OD_{260}$ of the sample measured at 0 min.

### 4.2.6 *Fluorescence microscopic imaging of Propidium Iodide uptake in bacteria*

Cell membrane integrity of photodynamically treated bacteria was also assessed by monitoring the uptake of the fluorescent probe, PI (Sigma, USA). It is a membrane impermeant nuclear stain and is used as an indicator for determining the cell membrane integrity [139]. For determining the intracellular PI uptake, cell suspensions of the dark control and photodynamically treated bacterial samples were centrifuged (1700 g, 2 min,) and the pellets were resuspended in PBS. The cell suspensions were incubated with PI (5 μg / ml) at 37$^{o}$ C for 10 min in the dark. Cells were centrifuged at 5000 rpm and the pellet was washed twice in PBS following staining to remove the unbound PI. An aliquot of these suspensions was placed on a coverslip and observed under an inverted fluorescence microscope (Zeiss, Axiovert 135, Germany) using 100 X oil immersion objective (1000 X magnification). The PI stained cells were viewed using 546 nm excitation and 620 nm emission filters. Both phase contrast and fluorescece images were recorded using a cooled CCD camera (DC 350 F, Leica Microsystems Imaging, Cambridge, UK).

### 4.2.7 *Data analysis*

Data from at least 3 experiments were used to calculate the mean and the SD. Student's t-test was used to determine the significance of the difference between two means. Level of significance was set at $p < 0.05$.

## 4.3 Results

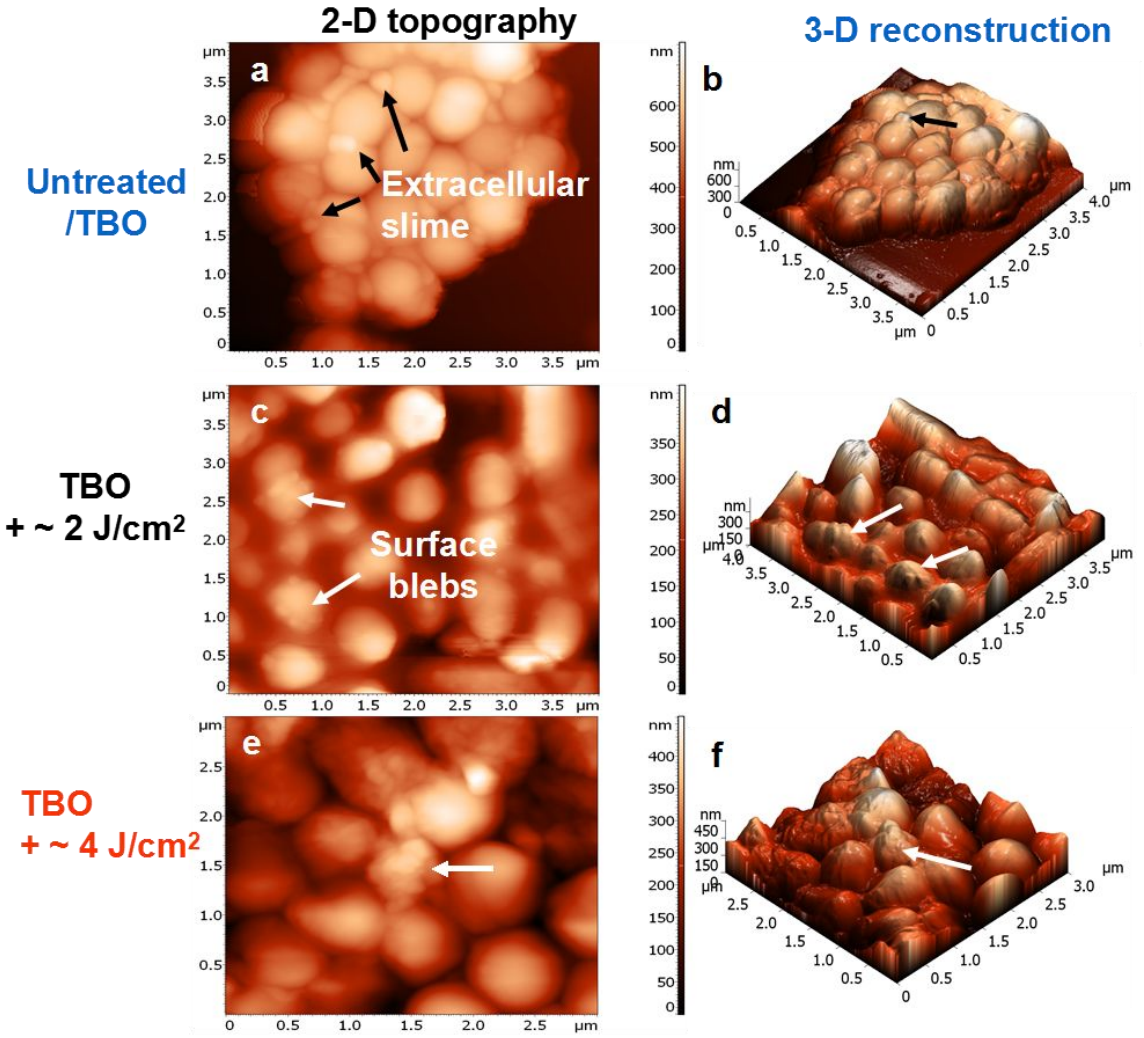


**Figure 4.1** AFM 2-D topography (left panel) and the corresponding 3-D reconstructions (right panel) images of *S. aureus* cells treated with 25 µM TBO alone (a and b, scan area: 4 µm x 4 µm) and irradiated with light fluence of ~2 (c and d, scan area: 4 µm x 4 µm ) and ~ 4 J /cm$^2$ (e and f, scan area: 3 µm x 3µm). Height scale in figs b, d, f is 0-500 nm. Arrow (white): blebs.

### 4.3.1 *Morphological alterations induced by TBO mediated APDT in S.aureus*

In figure 4. 1, the 2-D and the corresponding 3-D reconstruction images of *S. aureus* treated with TBO (25 μM) in the dark and after irradiation with laser light (632.8 nm) causing ~ 70 % ($LD_{70}$, ~2 J/cm$^2$) and ~ 2 log survival loss (~4 J/cm$^2$), are shown. Images of the cells treated with TBO in the dark revealed cocci in clusters which is typical morphology of *S. aureus* (fig. 4.1, a and b). The surface of these bacteria was smooth in texture (fig. 4.1 a). However, cells have indistinct borders indicating the presence of extra cellular slime. This has been confirmed by crystal violet assay (data not shown). These images were similar to the bacteria that were neither treated with TBO nor light (untreated control). Mean diameter and MCH measured from AFM images were 700 ± 80 nm and 350 ± 50 nm, respectively. In contrast, the morphology of the irradiated cells displayed significant perturbations (fig. 4.1, c-f). The surfaces of the some of the TBO treated cells exposed to light fluence of ~ 2 J/cm$^2$ ($LD_{70}$) were rough and showed 2-3 blebs measuring ~ 100 nm each. The slime surrounding bacteria was also less obvious in the photodynamically treated samples. For TBO treated bacteria subjected to higher light fluence (~4 J/cm$^2$), majority of cells showed morphological changes(fig. 4.1, e and f). Also, the cell surface roughness and number of blebs (~5-7 per cell) increased . However, as compared to untreated controls, no significant change in cell width were observed in irradiated cells.

### 4.3.2 *Morphological alterations induced by TBO mediated APDT in E.coli*

The 2-D and 3-D reconstructed AFM images of *E. coli* treated with TBO (25 μM) in the dark showed characteristic rod shaped structure (fig. 4. 2.; a and b). The average length, width and height of the bacteria, calculated from the 2-D and 3-D images were 1900 ± 40 nm, 900 ± 50 nm and 400 ± 20 nm, respectively. In addition, several indentations of the dimensions ~ 40 nm, characteristic of the surface roughness, were observed . TBO treatment did not cause any change in the dimensions as compared to the bacteria not treated with either PS or light (untreated control, data not shown). The size of bacteria determined in our study is in agreement with the other reports [127, 128]. In figure 4.2 (c-f), the 2-D images and the corresponding 3-D reconstructions of *E. coli* irradiated with light fluence responsible for ~ 70 % (~10 J/cm$^2$) and ~ 2 log (~40 J/cm$^2$) survival loss, are shown. Though exposure to ~10 J/cm$^2$ did not induce any obvious change in shape, surface roughness was observed to increase (fig. 4.2. c and d). A significant reduction (four times) in the MCH was noted as compared to the cells treated with TBO in the dark.

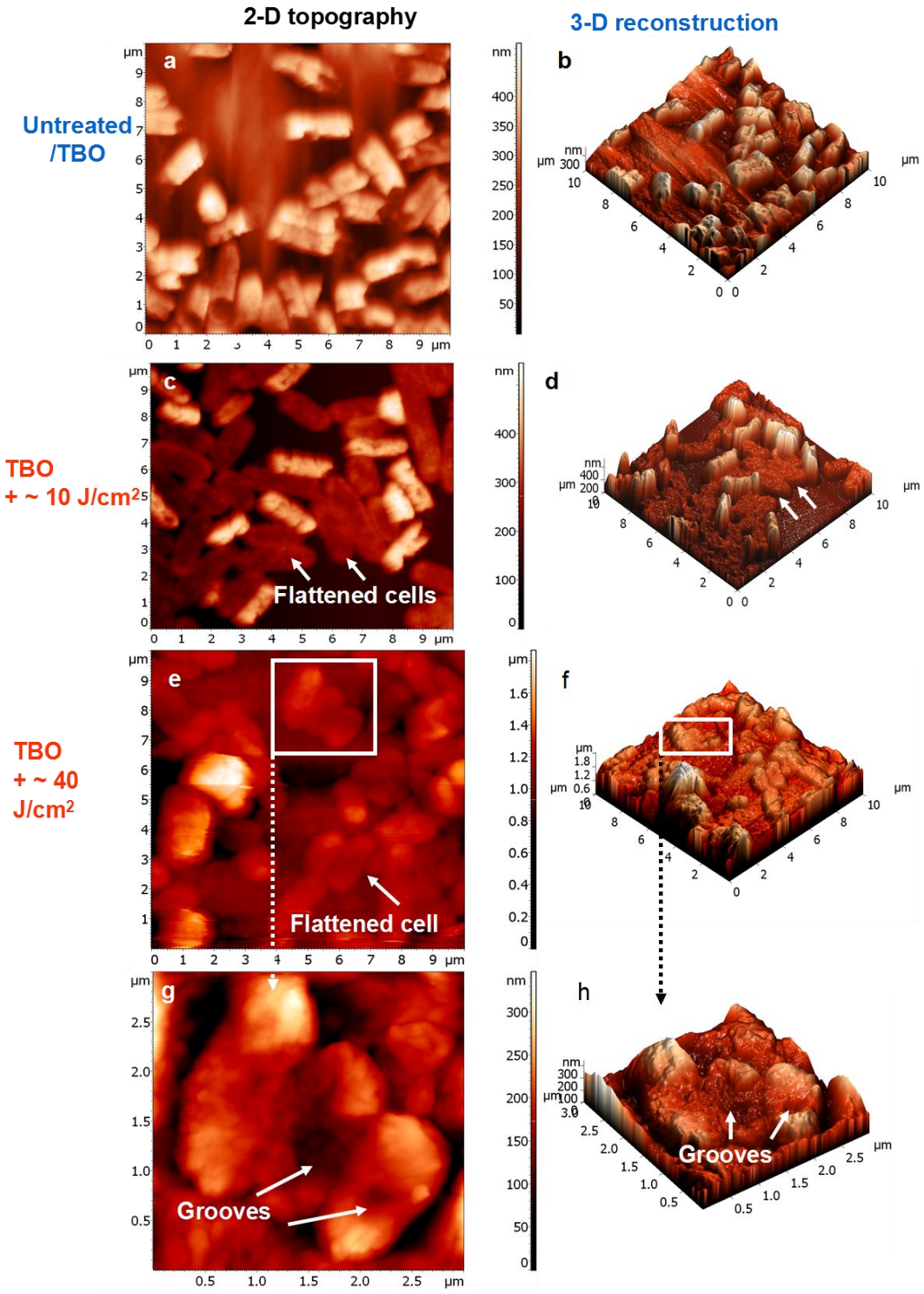


**Figure 4.2** AFM 2-D topography (left panel) and the corresponding 3-D reconstructions (right panel) images of *E. coli* cells treated with 25 µM TBO alone (a and b) and irradiated with light fluence of 10 (c and d ) and ~ 40 J/cm$^2$ ( e - h ).

Figures a-f, Scan area: 10 µm x 10 µm. Figures g and h: Scan area: 3 µm x 3 µm. Damaged cells and cell debri are represented by solid and dashed arrows, respectively. Height scale in figs b,d,,f, h is 0-500 nm.

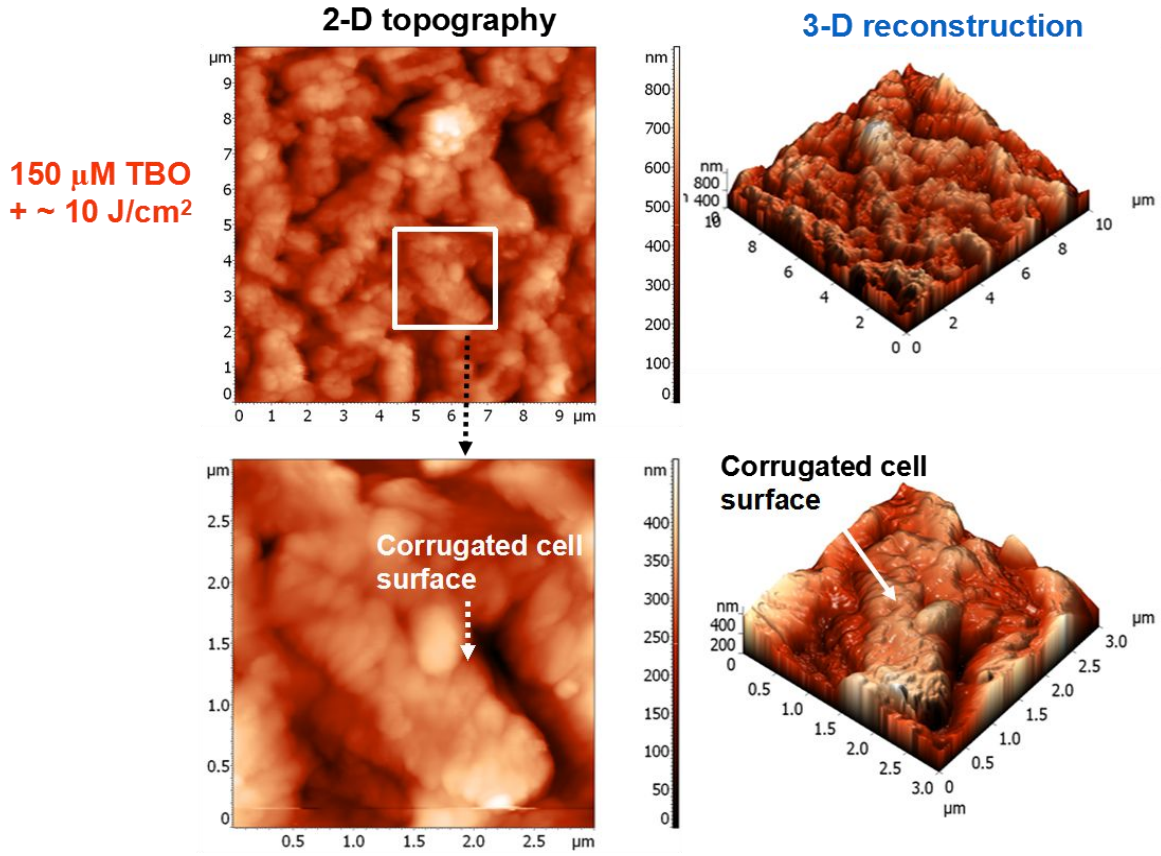


**Figure 4.3** AFM 2-D topography (left panel) and the corresponding 3-D reconstructions (right panel) images of *E. coli* cells treated with 150 µM TBO and irradiated with light fluence of ~ 10 J/cm$^2$ (a & b; Scan area: 10 µm x 10 µm). The marked area in fig. b is magnified and shown in c & d (Scan area: 3 µm x 3 µm). Height scale in fig.b,d is 0-500 nm.

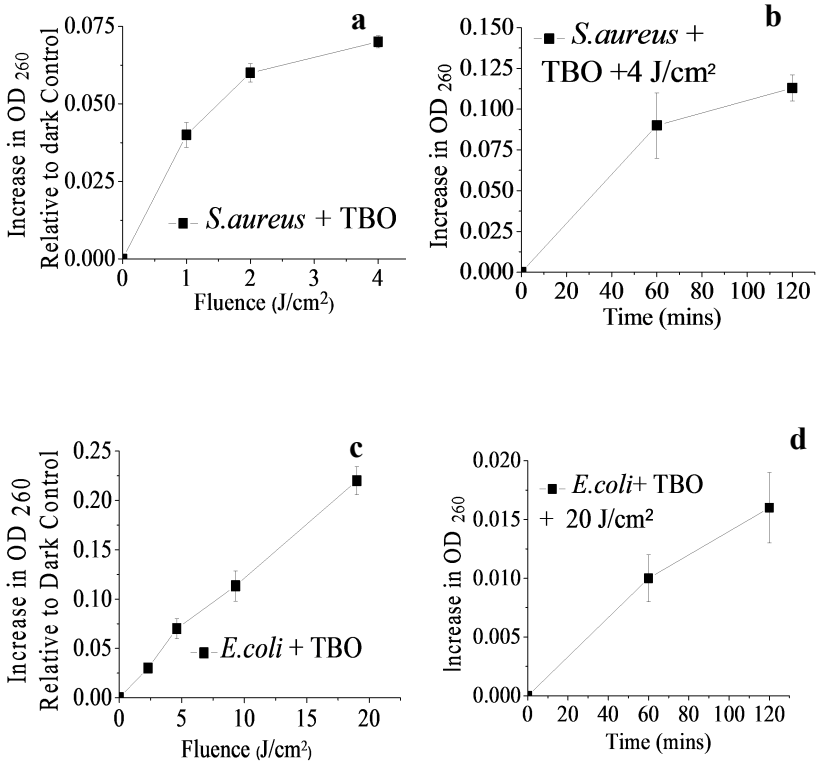


**Figure 4.4** Measured OD at 260 nm for cellular materials released from *S.aureus* (a and b) and *E. coli* (c and d) subjected to photodynamic treatment, as a function of light fluence (a and c ) and post irradiation time (b and d ). Data points and the error bars represent mean and SD of three experiments, respectively.

At higher light fluence (~40 J/cm$^2$) surface of almost all the cells were highly ridged and large depressions (~ 200 nm) were observed in some cells (e and h). An overall reduction in size (length) was also noticed in some cells. For cells treated with 150 μM of TBO and then exposed to ~10 J/cm$^2$ light, there were much larger alterations in the morphology (fig. 4.3; a and b) and the cells appeared completely distorted with deeper grooves and highly corrugated cell surfaces. There was also considerable reduction in cell height (fig. 4.3; c and d).

### 4.3.3 *Intracellular contents release from S.aureus and E.coli subjected to TBO mediated APDT*

In order to understand whether the morphological alterations observed in AFM images were due to the membrane damage, we measured the leakage of cytoplasmic contents by measuring the OD at 260 nm. In *S. aureus* (fig. 4.4; a and b), the leakage of intracellular contents increased with increase in both the light fluence and the post irradiation time. At light fluence corresponding to ~ 70 % and ~ 2-log reduction in viability, the $OD_{260}$ of the supernatant of irradiated cells measured at 0 min, increased by ~ 20 % and ~ 30 %, respectively, as compared to the unirradiated controls. Further, the leakage of the 260 nm absorbing material from *S. aureus* cell suspension subjected to light fluence responsible for ~ 2 log reduction in viability, increased with increase in post irradiation time and reached ~ 40 % at 60 mins beyond which the leakage appeared to slow down (fig. 4.4;b).

In *E. coli* irradiated at light fluence corresponding to ~ 70 % and ~2 log reduction in viability,as compared to unirradiated cells, $OD_{260}$ measured at 0 min increased by ~ 40 % and ~ 60 %, respectively, (fig. 4.4; c). Also, leakage of the cellular material was higher in magnitude than that observed in *S. aureus*. Distinct difference was also observed in the kinetics of 260 nm absorbing cellular contents release with respect to *S. aureus* (fig. 4.4;d). The maximum release of cellular material was observed immediately after irradiation. At later time points (120 mins) only a slight increase (15- 20 %) was observed.

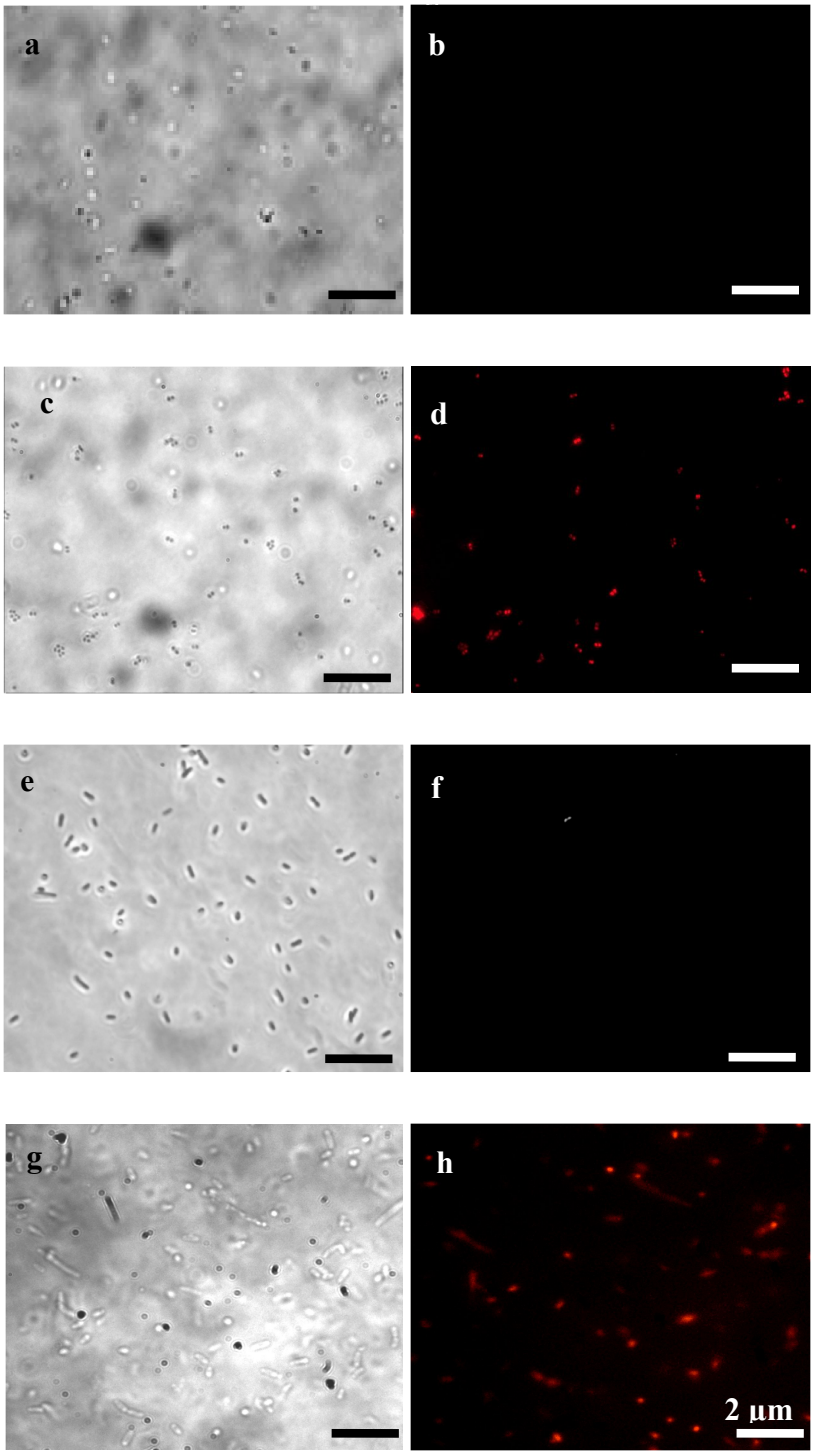


**Figure 4.5** PI uptake in *S. aureus* and *E. coli*. Bright field (left panel) and fluorescence (right panel) micrographs of (a & b) *S. aureus*, (e & f) *E. coli* treated with TBO in the dark and (c and d) *S. aureus*, (g and h) *E. coli* irradiated with the light fluence corresponding to $LD_{70}$. Scale bar: 2 µm.

### 4.3.4 *PI uptake in bacteria subjected to TBO mediated photosensitization*

In figure 4.5 we present the phase contrast (left panel) and fluorescent microscopic images (right panel) of *S. aureus* (fig 4.5; a-d) and *E. coli* (fig 4.5; e-h) treated with TBO in the dark (fig 4.5; a,b and e,f) and after exposure to light fluence of ~2 J/cm$^2$ (fig 4.5; c, d and g,h) and ~10 J/cm$^2$, respectively are presented. Bright fluorescence due to PI uptake was observed in TBO treated *S. aureus* (fig. 4.5; c and d) and *E. coli* (fig. 4.5; g and h) exposed to light. These results suggest loss of the permeability of the inner cell membrane in case of both *S .aureus* and *E. Coli*.

### 4.3.5 *Morphological alterations induced by cp6 and pl-cp6 mediated APDT in MRSA*

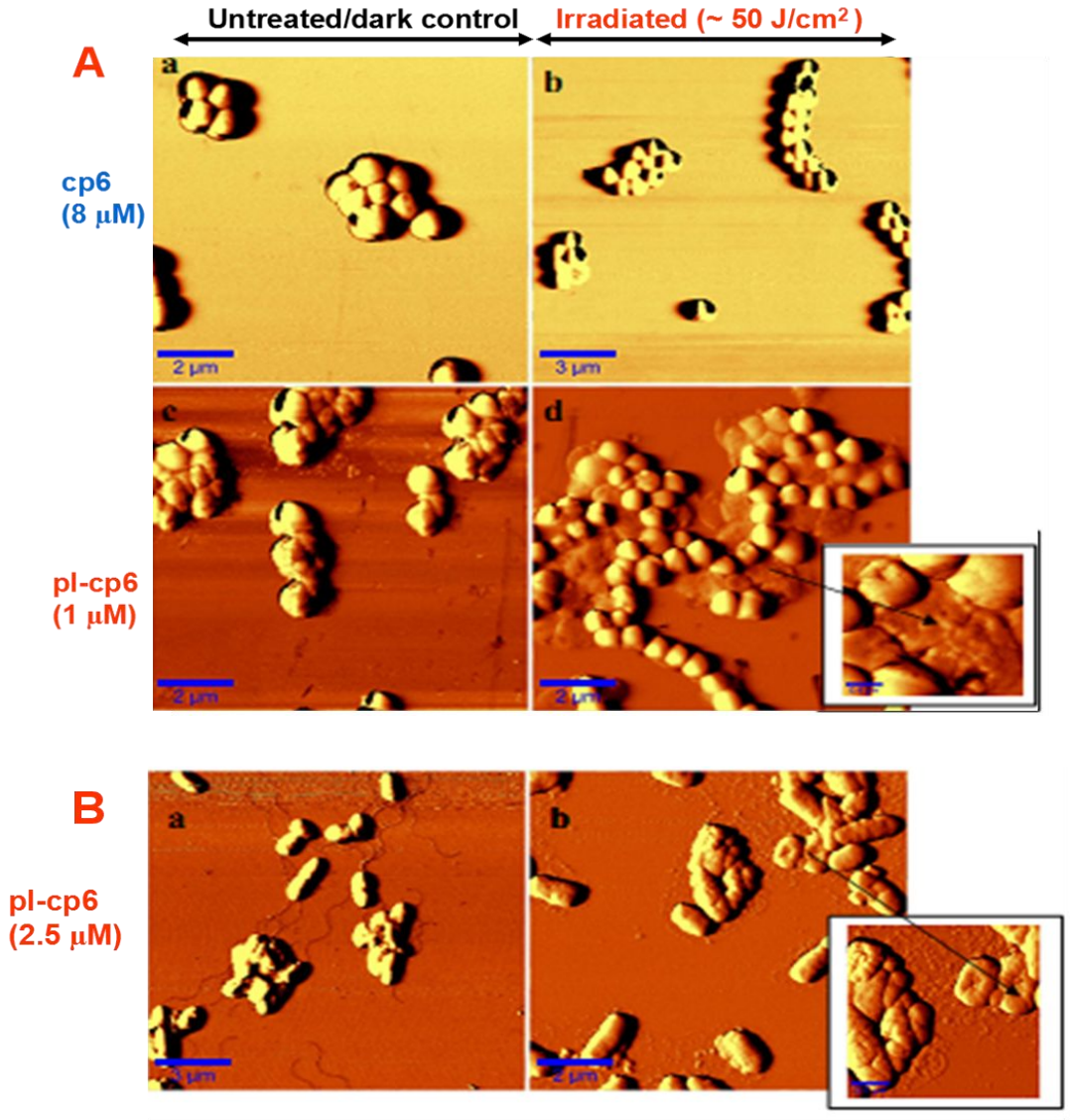


**Figure 4.6** Morphological alterations induced on bacterial surface envelope by cp6 and pl-cp6 mediated lethal APDT. 4.6 A) AFM images of MRSA treated with cp6 (8 µM), a) unirradiated (dark), b) after exposure to light fluence ~50 J/cm$^2$, (c) MRSA treated with pl-cp6 (1 µM), a) unirradiated, b) after exposure to light fluence ~ 50 J/cm$^2$. 4.6 B) *P. aeruginosa* treated with pl-cp6 (2.5 µM), a) unirradiated, b) after exposure to light fluence of ~ 50 J/cm$^2$. Magnified images of damaged cells are shown in the inset.

It may be noted that for AFM studies on morphological alterations induced by cp6 and pl-cp6 also, the PS concentration and light fluence required for ~ 2 log survival loss was used. Figure 4.6 shows the AFM images of MRSA treated with cp6 (8.0 μM) or pl-cp6 (1.0 μM) in the dark and irradiated subsequently with red light. Images of the cells treated with cp6 in the dark showed cocci in clusters with smooth surface which is a typical morphology of *S. aureus* (fig. 4.6 A; a). These images were similar to the bacteria that were neither treated with PS nor light (untreated control). Bacteria treated with cp6 did not undergo significant change in morphology upon irradiation (fig 4.6 A;b). On the other hand, pl-cp6 treated bacteria even in absence of light showed corrugated morphology (fig. 4.6 A ; c). Some of the bacteria showed rough surface with lobes suggesting damage to cell envelops. Mean height measured from AFM images of these bacteria were 430 ± 15 nm. This was slightly lower than the untreated controls (450 ± 10 nm). Morphology of the bacteria treated with pl-cp6 and exposed to light, however, displayed significant changes (fig. 4.6 A ;d). Most of the irradiated cells were flat with mean height of 190 ± 20 nm and rough surface (inset). Some of the cells showed distinct indentations. These results suggest that the cell wall, particularly the peptidoglycan layer, the principal mechanical support, was severely damaged by PDT.

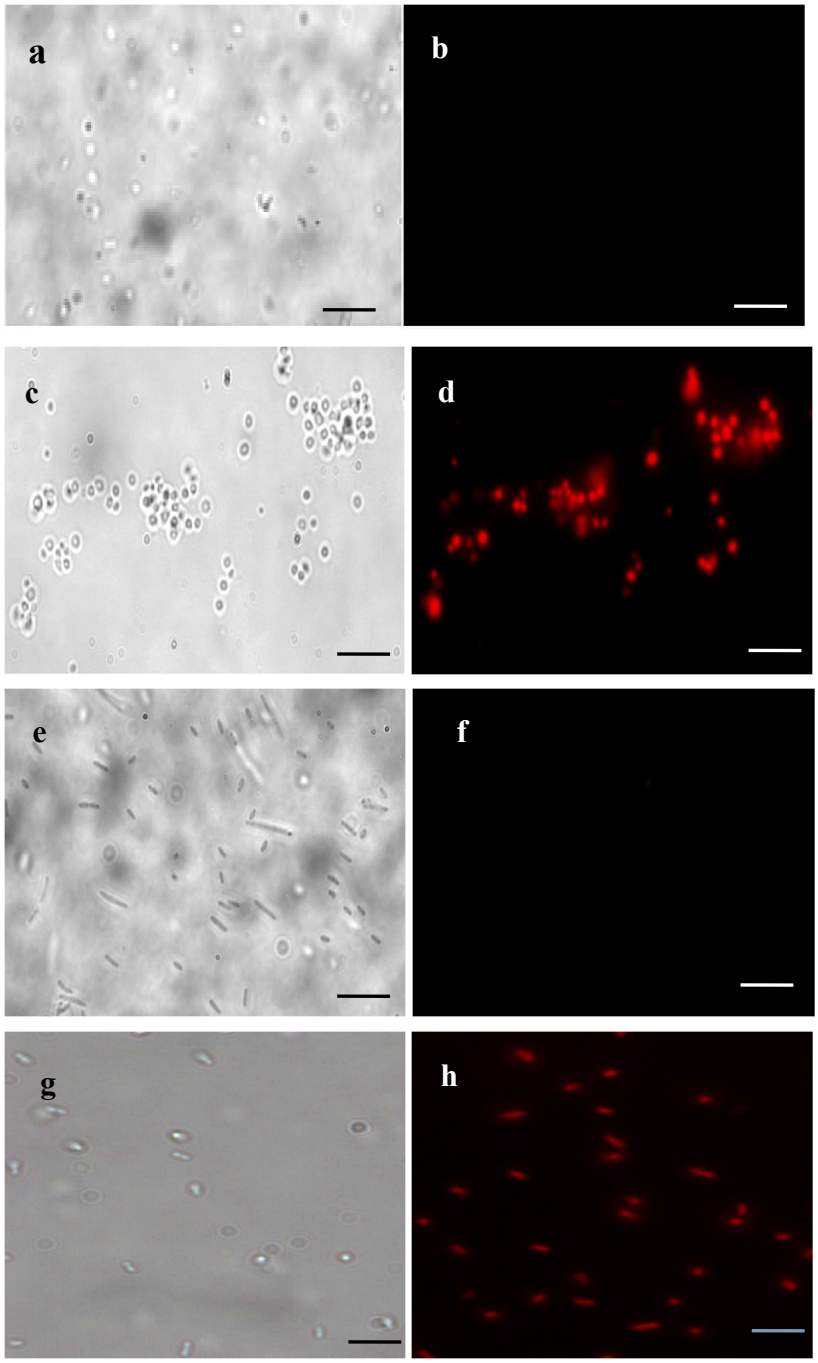


**Figure 4.7** PI uptake in *MRSA* and *P. aeruginosa* subjected to pl-cp6 mediated APDT. Bright field (left panel) and fluorescence (right panel) micrographs of (a & b) MRSA (e & f), *P. aeruginosa* treated with pl-cp6 in the dark and (c & d) *MRSA*(g & h), *P.aeruginosa* irradiated with the light fluence ~50 J/cm$^2$. Scale bar: 2 μm.

### 4.3.6 *Morphological alterations induced by cp6 and pl-cp6 mediated photosensitization in P.aeruginosa*

Figure 4.6. B shows the AFM images of *P.aeruginosa* with and without pl-cp6 mediated photosensitization. The untreated bacteria ( no pl-cp6, no light) showed rod shape cell with monotrichous flagella, relatively smooth surface, and length of 1950 ±134 nm and height of ~ 220 nm. Bacteria treated with 2.5 μM pl-cp6 in the dark, showed no change in height but a decreased length (1600 ± 64 nm). In contrast, surface of the pl-cp6 treated and irradiated bacteria were highly corrugated, and in many cells significant reduction ($p < 0.05$) in length (1300 ± 54 nm), MCH (180 ± 14 nm, inset) and destruction of the flagella were observed. In addition, some fluid and cellular debris could be observed around the damaged cells indicating severe damage to outer membrane, inner membrane and release of intracellular contents (fig 4.6 B; b).

### 4.3.7 *PI uptake induced by pl-cp6 mediated photosensitization in MRSA and P.aeruginosa*

In figure 4.7. the phase contrast and fluorescence images of *MRSA* ( fig 4.7; a-d), *P.aeruginosa* (fig 4.7; e-h) treated with pl-cp6 in the dark (fig 4.7; a,b and e,f) and after exposure to light fluence of ~25 J/cm$^2$ ( fig 4.7; c, d), ~50 J/cm$^2$ are presented. Bright fluorescence due to PI uptake was observed in TBO treated *MRSA* (fig. 4.7; c,d) and *P. aeruginosa* (fig. 4.7; g,h) exposed to light. These results suggest loss of integrity of the inner cell membrane of both *MRSA* and *P.aeruginosa.*

## 4.4 Discussion

The objective of this study was to investigate the mechanism of membranolytic effects of cp6, pl-cp6 and TBO induced photodynamic effects in Gram positive (*S. aureus*) and Gram negative (*P. aeruginosa*, *E. coli)* bacteria. The data obtained from AFM on TBO mediated photosensitization induced morphological alterations in photosensitized bacteria were correlated with absorbance measurements of released intracellular contents and fluorescence microscopic imaging of PI uptake, respectively.

AFM results presented in figure. 4.1 show that photodynamic treatment with TBO induces substantial alterations in the cell surface of *S. aureus.* Increase in cell surface roughness and disappearance of slime suggest damage to the cell wall. This is consistent with the fact that TBO being cationic, readily binds to the negatively charged teichuronic acid residues present on the cell wall [63]. However, due to its smaller size (~300 Da), TBO may diffuse to the inner layers of the peptidoglycan via porins, which upon illumination would generate damage in the inner layers of peptidoglycan layer. In fact, bleb formation following photodynamic treatment suggested breakage in the contact between cell wall and membrane [140] which may be due to the damage induced in the membrane components. Further, the increased leakage of cellular contents with increase in light fluence together with a significant PI uptake (fig. 4.5; c,d) observed in this study corroborate loss of membrane integrity and suggest this may be the primary cause for the loss of bacteria cell survival. However, since irradiation is carried out in presence of TBO it is also possible that, in addition to causing damage to membrane components, TBO could also penetrate into the cytoplasm causing damage to other cytoplasmic components such as DNA [136].

The results presented in figure 4.2 and 4.3 show that the morphological alterations in *E. coli* caused by TBO induced photodynamic action are quite different from that of *S. aureus*. At low photosensitization fluence (Fig 4.2; c,d) the increased roughness of cell surfaces and flattening observed may arise due to structural perturbations in the outer membrane components and damage to inner membrane. This is consistent with the fact that LPS is the predominant constituent of the outer membrane of Gram negative bacteria and because of its highly anionic nature (due to presence of covalently bound phosphate groups, acidic sugars, and fatty acyl groups) TBO binds to LPS readily [64, 69,121]. Light fluence dependent loss of virulence of LPS in *E.coli* following photodynamic treatment with TBO has been reported previously and is believed to be due to structural alterations in this endotoxin [57]. Further, the damage to outer membrane would lead to enhanced localization of photosensitizer molecules to the inner membrane, causing damage of the inner membrane constituents upon irradiation. Indeed, at higher light fluence deep grooves (~200 nm) observed on the surfaces of *E. coli* suggest the total destruction of cell envelope including the inner membrane. This would lead to leakage of the intracellular contents [141] and concomitant cell flattening as observed in the AFM images .This also correlates with the light fluence dependent increase in leakage of 260 nm absorbing cellular contents observed in this study. The extensive cell surface blebbing and distorted cell shape observed in photodynamically treated cells at higher concentration of TBO is indication of the increased damage to outer envelope and is in agreement with the TEM results of Wong *et al.* [142] on *Vibrio vulnificus,* a Gram-negative bacterium, subjected to photodynamic treatment with TBO.

Our results presented in this study also show that fluid loss is more conspicuous and takes place at a faster rate in *E. coli* (fig. 4.4 b), as compared to *S. aureus* (fig. 4.4.a) exposed to TBO and light. This may be because in *E .coli* the peptidoglycan layer (2 to 3 nm) is much thinner than the multilayered peptidoglycan layer (20 to 80 nm) present in the cell wall of Gram positive bacteria. Therefore, in Gram negative bacteria damaged peptidoyglycan and cell membrane can no longer provide the mechanical rigidity leading to cell flattening which would facilitate faster leakage of the intracellular contents. This correlates with the cell membrane damage studied by PI uptake (fig. 4.5.) and the concomitant flattening observed in the AFM images of *E. coli.* Further, our results on the slower release of intracellular contents from Gram positive bacteria are consistent with the results of Romanova *et al.* [143] wherein it was shown that, after photoirradiation with TBO/methylene blue leakage of intracellular ATP was much slower in Gram positive bacteria, *Listeria monocytogenes* as compared to the *E. coli.*

The results shown in figures 4.1-4.5 suggest that the morphological alterations induced by TBO mediated APDT have a good correlation with fluorescence microscopy data on PI uptake and absorbance spectroscopy data on intracellular contents release. Having established this, we then characterized morphological alterations induced by cp6 and pl-cp6 mediated APDT using AFM. We first studied the morphological alterations induced in MRSA. AFM results presented in figure. 4.6. A (a-d) show that photodynamic treatment with cp6 and pl-cp6 induces different alterations in the cell surface of MRSA. In MRSA exposed to only cp6 while no change in surface roughness is observed there is increase in cell surface roughness and loss of mucoid appearance in MRSA following treatment with 1.0 μM pl-cp6,

suggesting pl-cp6 induced damage to outer surface which would explain the dark toxicity observed at this concentration (fig 3.3, chapter 3). Rough cell surface and indentations observed in some bacteria treated with 1.0 μM pl-cp6 and ~50 J/cm$^2$ (fig 4. 6 A; c) is due to damage of cell wall and resulting exposure of the cell membrane beneath it. Flattening of cells and reduction in cell height observed in many bacteria may be the result of leakage of cellular material due to damage of cytoplasmic membrane. These features are somewhat different than the morphological alterations observed by us in the antibiotic sensitive strain of *S.aureus* subjected to photodynamic treatment with TBO previously (fig 4.1). This indicates that pl-cp6 preferentially binds to the peptidoglycan wall causing extensive damage to the cell wall. Since the thicker peptidoglycan wall provides support, damage to the wall resulted in the cell membrane damage (fig 4.7 c,d), flattening of cells (fig 4.6 A, d) and explains the observed loss of cell survival. This observation is consistent with earlier report on transmission electron microscopic observation of cavities in the cytoplasm of bacteria treated with pl-ce6 and red light that is presumably caused by combination of damage to cytoplasm and DNA [123]. Absence of noticeable changes in morphology of MRSA following photodynamic treatment with cp6 even at 8 μM concentration suggests that outer cell peptidoglycan wall is not the target of photodamage (fig 4.6. A; b). This might be explained on the basis of the anionic charge of cp6 which will not permit much of cp6 molecules to bind to the anionic surface of the bacterial wall. Also, the relatively more hydrophobicity of cp6 can also be a factor for its lesser uptake via the hydrophilic pores of wall. It may be still possible that being smaller in size, some cp6 can diffuse through the porous wall but it will be probably localized

more in the inner regions than the outer wall. Hence upon irradiation, the morphological changes are not vivid.

The results presented in figure 4.6 B shows that the morphological alterations observed in *P.aeruginosa* due to pl-cp6 induced photodynamic action are quite different from that of MRSA. There is increased surface corrugation in pl-cp6 treated bacteria (no light) suggesting the polymer bound cp6 incorporates into the components of outer membrane. This is well in accordance with action of many antibacterial cationic peptides and is supported by the fact that polycationic molecule can displace divalent cations from LPS in the outer membrane [112]. This binding may weaken the interactions of the LPS constituents and increase the permeability of the drugs to cytoplasmic membrane [111]. It is known that molecules possessing; (i) protonatable biscationic groups separated by ~14 $A^o$ , facilitate interactions with the adjacent phosphate moieties on the lipid A component of LPS and (ii) a long chain of aliphatic hydrocarbon to promote hydrophobic interactions [144] can bind and neutralize LPS. Consistently, several endotoxin-binding proteins show presence of Lys/Arg cationic clusters [145]. In addition to the cationic motif which is the principal determinant for the binding, presence of an heteroaromatic ring, such as the Trp indol group, is also known to contribute to the preferential LPS binding [144]. Therefore, the pl-cp6 having both the aliphatic polylysin moiety and heterocyclic tetrapyrrole rings, will probably possess a preferential binding ability to the LPS present on Gram negative bacteria. In fact, the crumpled cell surface and the indentations observed on the cell surface observed in AFM images of *P. aeruginosa* following APDT suggest outer membrane damage leading to exposure of inner cell membrane. Debris observed surrounding the bacteria and reduction in height confirms the leakage of cytoplasmic

contents due to damage to inner cytoplasmic membrane. Similar morphological alterations have been observed in our studies on *E.coli* following photodynamic treatment with cationic dye TBO and *P.aeruginosa* treated with sushi peptide [132]. Further, it may be argued that because the damage caused by the pl-cp6 mediated APDT occurs primarily to the cell envelope (fig. 4.2, 4.3 and 4.5), the lethality is largely unaffected by the growth phase of the bacteria (fig. 3.5). This is also a desirable feature for inactivation of bacteria in wound milieu wherein the bacteria may remain in different growth phases.

## 4.5 Summary

AFM images of *S .aureus* and *E. coli* subjected to photodynamic treatment in presence of TBO show marked differences in the nature of the topographical alterations. While in *S. aureus,* photodynamic treatment with TBO resulted in surface bleb formation, in *E. coli* formation of grooves, leakage of cytoplasmic fluids and the concomitant cell flattening were more evident. These results indicate that the membranolytic effects of TBO induced photodynamic treatment are different in Gram positive and Gram negative bacteria. Further, in *S.aureus,* significant differences were observed in the morphological changes subsequent to APDT mediated by TBO and pl-cp6. While the major effect of TBO mediated APDT was breakage in the contact between the cell wall and the membrane, pl-cp6 mediated APDT resulted in damage primarily to the outer peptidoglycan layer. These results suggest that for pl-cp6 mediated APDT the outer membrane is the primary target. The study also

demonstrates that AFM imaging allows both qualitative and quantitative nanometer scale topographical information of the different kinds of alterations induced by different PS on bacterial membrane.

# *5.* Effect of APDT on healing of wounds infected with *P. aeruginosa*


## Abstract

In this chapter, we present the results of the studies carried out to investigate the effect of pl-cp6 mediated topical APDT on the healing of *P. aeruginosa* infected wounds in mice.Apart from monitoring the bacterial load, the levels of proinflammatory cytokines like IL-6, TNF-α were measured to quantitate the effect of APDT on the inflammatory response. The results show that 96 h post APDT, bacteria load, IL-6 and TNF-α level in the infected wounds were reduced by ~1.5 log, ~6 times and ~ 4 times, respectively. The resulting decrease in hyperinflammatory response in wounds may also be contributing to the observed faster healing.



*Some aspects of the results presented in this chapter have appeared in Lasers Med. Sci. 28, 465-471 (2013).*

## 5.1 Introduction

Infections of wound are major health care associated problems worldwide because these not only delay wound healing and lead to longer hospital stays but also increase mortality [146-149]. Among the different nosocomial pathogens, *Pseudomonas aeruginosa* is a common opportunistic Gram negative bacterium [33]. This bacterium produces several extracellular virulent factors [149] like pyocyanin [34], proteases [35,36], quorum sensing inducers [37] and LPS [38-40] which can cause hyperinflammatory response, delayed collagen remodeling, bloodstream invasion, and dissemination. In addition, *P.aeruginosa* can easily form biofilms on ulcers. This pathogen has the abilities to colonize and infect the burn as well as post operative wounds [150], often resulting in fatal infections in immunocompromised hosts [151] and chronic infections [152]. For instance, *P.aeruginosa* is detected in ~50 % of chronic refractory wounds. Considering the global rise in acquired antibiotic resistance and intrinsic resistance of this bacterium [33] to many antibiotics, there is a need to develop alternate antimicrobial approaches for treatment of wound infections caused by this pathogen [153].

Results of our *in vitro* studies presented in chapters 3 and 4 suggest that pl-cp6 mediated APDT inactivates *P.aeruginosa*. Therefore, it may be expected that that pl-cp6 mediated APDT can be a good alternative for treatment of *P.aeruginosa* infections of wounds. In this respect, *in vitro* studies carried out elsewhere have also shown that APDT can inactivate bacterial virulent factors [56, 57] which are known stimulators of proinflammatory cytokines. It is also known that PDT can induce release of proinflammatory mediators as well as matrix metalloproteinases in tumors

[154]. Therefore, in bacteria infected wounds, which already has a hyperinflammatory condition, APDT is expected have profound influence . We have investigated the effect of topical APDT mediated by pl–cp6, on levels of proinflammatory cytokines IL-6 and TNF-α in excisional wounds of mice infected with *P. aeruginosa* and its influence on wound healing.

## 5.2 Materials and Methods:

### 5.2.1 *Bacteria*

The bacteria used in this study were *P.aeruginosa* PAO (MTCC 3541) procured from IMTECH Chandigarh, India. This organism is virulent and produces several virulent factors [56]. The bacteria were maintained by sub culturing in tryptone soya agar (TSA, Himedia, Mumbai, India) routinely. For experiments, a colony was inoculated into TSA and was grown aerobically for 18h at 37$^{o}$C using a shaker incubator. Optical density of the overnight culture was measured at 600 nm and diluted according to required concentration.

### 5.2.2 *Photodynamic treatment of P.aeruginosa infected wounds*

#### 5.2.2.1 Excisional wound model and establishment of infection

Female Swiss albino mice (28–30 g, 6-8 weeks old) were used for all experiments. All animals were housed in individual cages under constant temperature (20 ± 2 $^{0}$C) with a 12-h light /dark cycle, and had free access to food and water. All procedures involving animals were approved by the Institutional Animal Ethical Committee in

accordance with the institutional guidelines on animal care. Leukopenia in these mice was developed by injecting cyclophosphamide intraperitoneally, as described in [96]. To ascertain leukopenia, 5-10 µl of blood was withdrawn from the tail vein, blood was diluted in acidified (acetic acid) crystal violet and total number of leukocytes were counted according to the protocol described in [94] and has been elaborated in section 2.3.1.2, chapter 2. On the 4$^{th}$ day post cyclophosphamide injection, ~80 % reduction in total leukocytes was observed and excisional wounds were then created in these animals.

The procedures for wound creation and infection have been elaborated in section 2.4. of the chapter 2. All the mice in which a single excisional wound was created on the lower back, were divided into following groups as follows: (1) uninfected wound (control), (2) infected untreated control (infected but neither treated with pl-cp6 conjugate nor light), (3) dark control (wounds infected with bacteria and treated with pl-cp6 in dark), (4) APDT group (wounds infected with bacteria, treated with l-cp6 and red light). In addition to these four groups, to compare the efficacy of APDT on bacteria load and healing of wounds with standard antibacterial treatment, in some of the animals the infected wounds were treated with 20 µl of 0.5 % $AgNO_3$ at 24 h post infection. The concentration of $AgNO_3$ (0.5 %) chosen has shown good bactericidal effect for infected wounds in clinical as well as pre clinical studies [155].

### 5.2.2.2 Standardization of pl-cp6, light fluence for *in vivo* APDT

Cp6 was prepared following the procedure described previously [89]. Conjugation to poly-L-lysin was carried out according to protocol described in chapter 2. In order to

standardize pl-cp6 concentration required for inactivation of bacteria growing in wounds, photobactericidal efficacy of different concentrations of pl-cp6 was tested on a lawn of *P. aeruginosa* grown on agar plates as described in Caminos et al. [157]. Bacterial suspension containing $10^7$ CFU/ml was spread on agar. After 30 min, 5 µl of pl–cp6 of different concentrations was placed on a pre-designated position. The drug-treated surface of the agar was exposed to light after allowing the solvent to evaporate. For testing dark toxicity of drug, the same volume of a specified concentration of pl–cp6 (dark control) was placed beside the irradiated region. The plates were incubated overnight at 37°C in the dark. The zone of inhibition of the bacterial growth due to drug and light treatment was measured.

### 5.2.2.3 Photoirradiation

To investigate the efficacy of pl-cp6 mediated APDT for inactivation of *P.aeruginosa* growing in wounds, pl-cp6 (200 µM in 25 µl) was applied topically to the infected wounds at 18 h post bacteria application. After 30 min of pl-cp6 application, wounds of the mice in the APDT group were illuminated with red light fluence of ~ 60 and 120 J/cm$^2$(table 2.1.). All the experimental procedures following incubation of wounds with pl-cp6 were carried out under subdued light.

### 5.2.2.4 Assessment of bacterial load

Bacterial counts in wounds were determined using the tissue surface rinsing and swabbing protocol described in [97]. Bacteria number determined by this method is reported to have good correlation with CFU assay of wound homogenates.

#### 5.2.2.5 Preparation of tissue extract and cytokine analysis by ELISA

Animals were euthanized at determined time points by cervical dislocation. Wounds comprising the scab and granulation tissue were excised, snap-frozen in liquid nitrogen, weighed, and transferred to − 80°C. Frozen tissues were powdered with help of a mortar-pestle, and homogenized according to the protocol described in chapter 2 and also in the ref [158]. Inflammatory cytokines [IL-6,TNF-α] level in wound tissues of different treatment groups were measured using a Mouse Inflammatory Cytokines and Chemokines Multi analyte™ ELISA Array Kit (Cat No MEM 004A, SA Biosciences Corp, Frederick, Md). The assay was carried out according to the instructions given in the assay protocol of the kit. Detection was carried out in a mircoplate ELISA reader by reading absorbance at 450 nm within 30 min of stopping the reaction with a wavelength correction at 570 nm. The results were expressed as absorbance (O.D.) values [159] per milligram protein. Protein concentration was estimated by Bicinchoninic acid (BCA) assay [160].

### 5.2.3 *Assessment of healing response*

To assess the effect of PDT on wound closure, the dimensions of wounds (width and length) were measured on different days after wounding by vernier calipers and the wound area was calculated. A time (days) dependent relative change in the area of each wound with respect to the initial wound area (on day 0) was determined in different groups to assess the effect of treatments.

In order to study the histological changes in response to infection and APDT, wound tissues of the different groups of mice were excised on day 14 p.w. The tissues were fixed in 10 % neutral buffered formalin for 24 h, processed using standard histological procedures. The deparafinized sections were stained with Masson's trichrome staining. The slides were examined under a microscope to determine tissue changes such as inflammation, reepithelialization, arrangement of collagen fibres, and presence of blood micro vessels. The criteria used to score each histological parameter have been described in [99].

### 5.2.4 *Assay for virulent factors of P.aeruginosa*

The effect of photoirradiation on virulent factors present in the supernatant of *P. aeruginosa* cell suspension was studied following the protocol described in [56,57]. Briefly, 100 µl of culture supernatant of bacteria grown overnight was incubated with 200 µM pl–cp6 for 30 min in the dark in a 24-well plate and then exposed to a light fluence of ~60 J/cm$^2$. In both control and treated samples, extracellular protease activity was measured. Optical density values were normalized with respect to proteins present in the sample and expressed as percent change with respect to dark control.

### 5.2.5 *Statistical analysis*

All the experiments were repeated at least thrice and data were presented as mean ± S EM. For assessment of treatment effects, comparisons between the means of different

groups were carried out by one-way ANOVA. Values of $p < 0.05$ were considered as statistically significant.

## 5.3 Results

### 5.3.1 *Photodynamic inactivation of P. aeruginosa on agar*

Photodynamic activity of pl–cp6 was tested under *in vitro* conditions by irradiating an area of bacterial lawn on agar surface which was pretreated with pl–cp6. No dark toxicity was observed with drug concentration up to 200 μM pl–cp6. Light induced inhibition of bacterial growth on agar plates treated with 200 μM pl–cp6 and ~60 J/ $cm^2$ light fluence is shown in figure 5.1. This result suggested that pl– cp6 and ~ 60 $J/cm^2$ is effective for inactivation of surface bound bacteria.

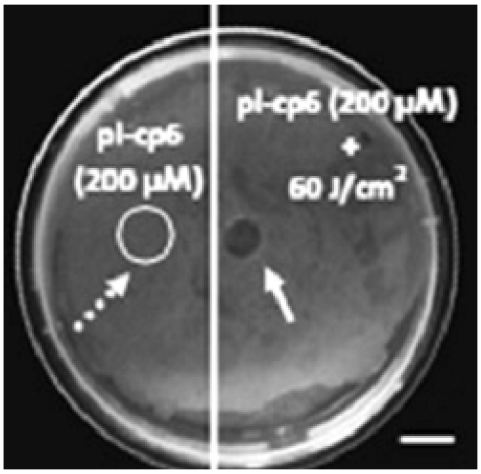


**Figure 5.1** Photodynamic inactivation of *P. aeruginosa* grown on agar plates. Scale bar, 5 mm.

### 5.3.2 *Establishment of infections of wounds with P. aeruginosa and photodynamic treatment*

For initiating infection in wounds of mice, *P. aeruginosa* suspension containing ~$10^7$ CFU (20 µl) was applied on wounds. This resulted in a recovery of >2 × $10^7$ CFU per wound after 24 h and the wounds had more yellowish regions and purulent discharge compared to uninfected wounds. These features confirmed the development of infection. However, no significant death occurred due to infection. This indicated that the infection was not fatal in the normal mice model used. In cyclophosphamide treated mice, however, ~80 % mortality was observed. Change in bacterial counts in untreated control (no pl-cp6, no light), dark control (pl-cp6, no light), and photodynamically treated (pl-cp6 and light exposure) wounds of normal mice as a function of time is shown in figure 5.2.

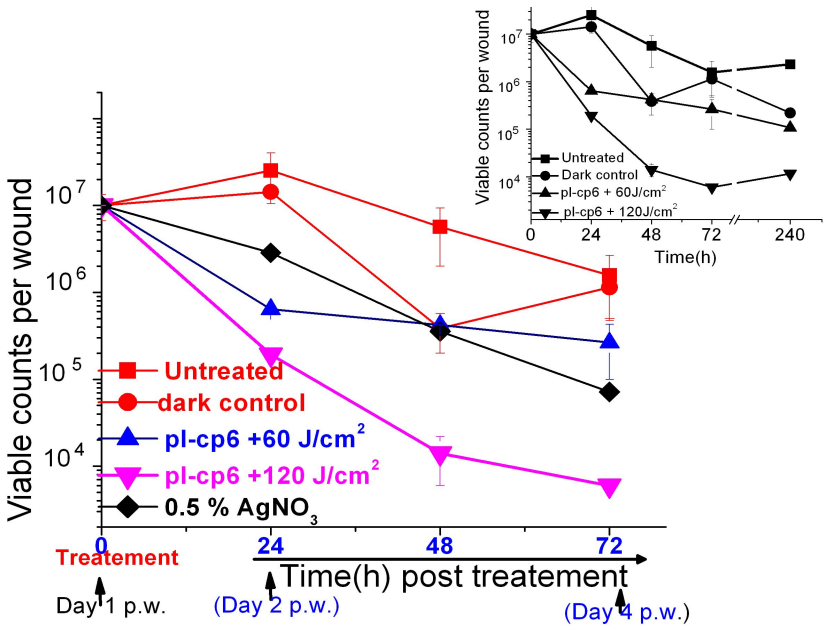


**Figure 5.2** Effect of APDT on bacterial counts in wounds as function of time in different groups. *P.aeruginosa* (~$10^7$ CFU) was applied on wound. APDT and $AgNO_3$

(0.5 %) was given on 24 h post APDT (day 2 p.w). Bacterial counts were determined at 24 , 48, 72 and 240 h post treatment time (inset) as described in section 2.5. The results represent mean ± SE; n = 6, except for the $AgNO_3$ group (n = 4).

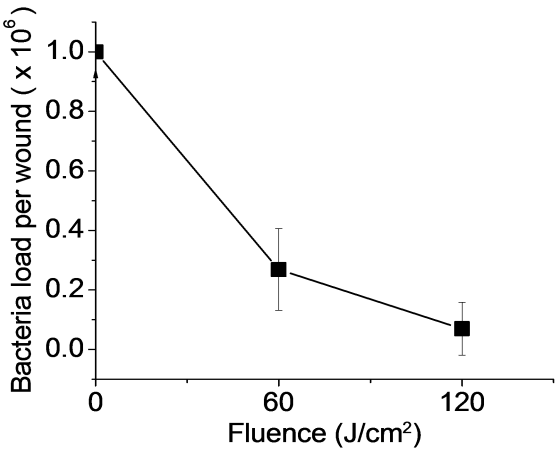


**Figure 5.3** Effect of light fluence on *P.aeruginosa* in wounds of immunocompromised mice. Infection in the immunocompromised models were developed by topically applying ~$10^6$ CFU *P.aeruginosa* to wounds. After 6 h, wounds were subjected to APDT. The results represent mean ± SEM; n=6.

In the untreated and dark control wounds, at 24 h post APDT the bacterial counts increased by ~ 30 % compared to initial inocula (~$10^7$) and then decreased at 72 h. In wounds irradiated with light fluence at ~ 60 J/$cm^2$ or ~ 120 J/$cm^2$ bacterial counts reduced by ~1.5 log or ~ 2.5 log respectively at 72 h. Increase in bacterial counts was observed in untreated, only pl-cp6 and photodynamically treated wounds at 240 h (fig. 5.2., inset). Nevertheless, the counts in the PDT group were significantly lower than that of untreated and dark control wounds, but comparable to that of $AgNO_3$ treated wounds.

In leukopenic mice, irradiation of wounds with APDT at fluence of ~60 J/cm$^2$ led to ~90 % reduction in bacterial counts. Increasing the light fluence to ~ 120 J/cm$^2$ reduced the bacterial count by ~ 1.5 log (fig 5.3) and improved the survival of mice. For example, while ~10 % of the mice in which the infected wounds were left untreated or treated with pl-cp6 alone survived beyond 48 h, only ~ 80% of the mice in which the infected wounds were photodynamically treated survived.

### 5.3.3 *Effect of APDT on healing of P. aeruginosa infected wounds*

Wound healing in treated and untreated mice was monitored only in immunocompetent mice as the leukopenic mice which received no treatment, did not survive beyond 48 h. Change in wound area with respect to original wound dimension in different groups as function of post treatment time is shown in figure 5.4.A. Compared to untreated or only pl-cp6 treated infected wounds, dimension of the photodynamically treated wounds decreased faster. The difference in wound area between photodynamically treated and untreated wounds was significant ($p<0.05$) upto day 10 p.w. Effect of APDT on closure of infected wounds is shown in figure 5.4.B. The untreated infected wounds healed by day 21 p.w. At the same time, the uninfected wounds and photodynamically treated infected wounds healed 4-5 days faster than the infected wounds which did not receive APDT. In the infected wounds treated with $AgNO_3$ the healing occurred marginally faster ($p > 0.05$) than the untreated or pl-cp6 treated wounds, but slower ($p < 0.05$) than that of photodynamically treated wounds (fig. 5.4. B).

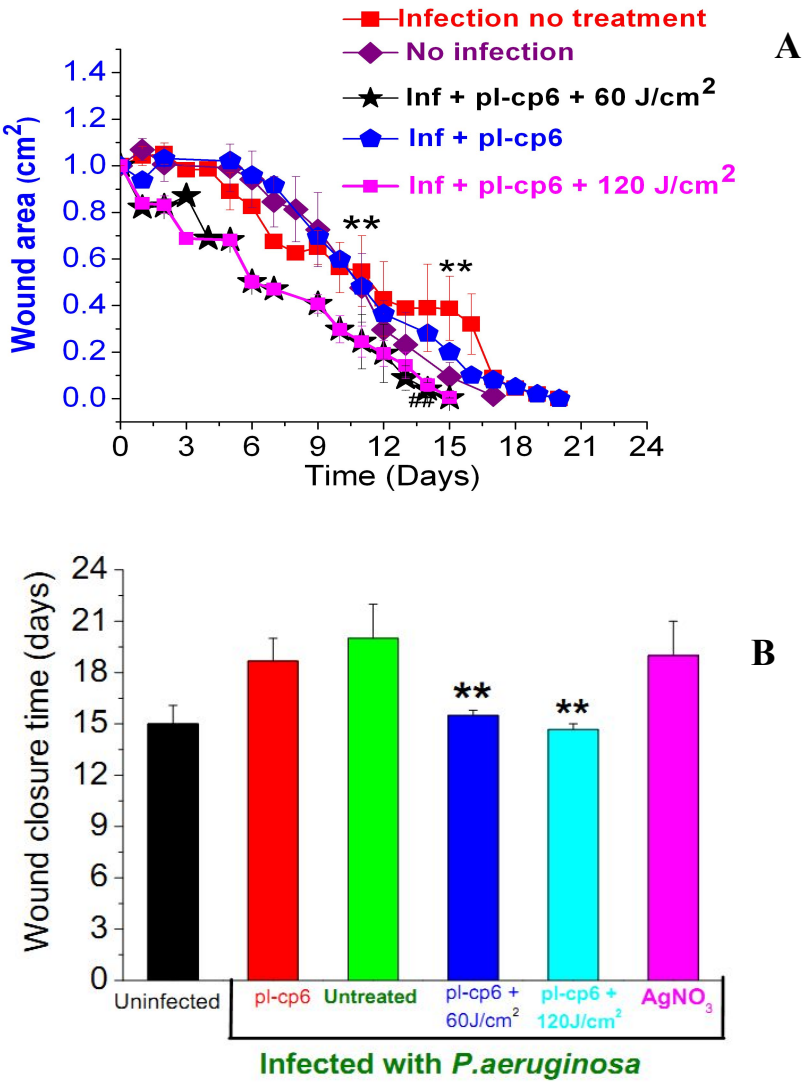


Figure 5.4 Wound area reduction (A) and wound closure (B) in different groups. It may be noted that the wound area reduction for $AgNO_3$ group is almost similar to that of untreated and pl-cp6 treated groups. Hence, the data for $AgNO_3$ group have not been included in figure 5.4 A. The results and error bars represent mean and SE, respectively, for n = 5. **: $p < 0.05$ comparison of means between the untreated and photodynamically treated wounds (one way ANONA).

### 5.3.4 *Effect of APDT on level of proinflammatory cytokines (interleukin-6 and TNF-α) in wounds infected with P.aeruginosa*

Increase in dermal inflammatory cytokines IL-6 and TNF-α has been reported in *P. aeruginosa* infected wounds [161,162]. PDT also has been shown to upregulate inflammatory cytokines expression [154,163]. Therefore, level of IL-6 and TNF-α proteins in wounds was investigated in an attempt to clarify whether PDT would aggravate the already hyperinflammatory environment of infected wounds. IL-6 and TNF- α levels in wound tissue were measured at early (day 2 p.w.) and late (day 5 p.w.) inflammatory phase of wound healing in uninfected, untreated infected, and pl–cp6 treated infected wounds exposed to a light fluence of ~ 60 J/cm $^2$ (fig. 5.5 ). A significant increase in expression of IL-6 ( ~1.9 times) and TNF- α (~3 times) proteins was noted in infected wounds as compared to uninfected wounds ($p < 0.05$). At 96 h post APDT (day 5 p.w.), compared to day 2 p.w., the levels of these two cytokines in infected wounds increased further although the bacterial counts decreased by ~40 % ( fig 5.2).

In contrast to untreated wounds, photodynamic treatment led to down-regulation of IL- 6 and TNF- α protein at both 24 h (day 2 p.w.) and 96 h (day 5 p.w.) post APDT. Interestingly, in photodynamically treated infected wounds, levels of IL-6 and TNF- α were four to five times lower as compared to untreated infected wounds at 96 h time point although there was no significant difference in bacterial counts in these groups (fig. 5.2 , inset).

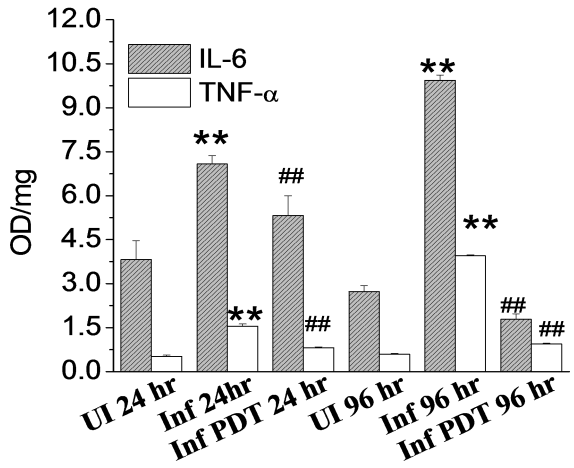


**Figure 5.5** Proinflammatory cytokines expression in treated and untreated infected wounds on 24 h (day 2 p.w.) and 96 h (day 5 p.w. ) post APDT. UI : uninfected wounds, Inf : infected untreated wounds, Inf PDT: infected wounds treated with pl–cp6 and ~60 J/cm$^2$ light fluence. ** p <0.05; Inf vs UI, ## p <0.05 Inf PDT vs Inf. The results are expressed as mean ± SE of three different experiments.

### 5.3.5 *Histopathological analysis*

The histomicrographs and the histological attributes for diffrent wounds of treated and untreated wounds excised on day 14 p.w., are shown in figure 5.6. and table 5.1, respectively.

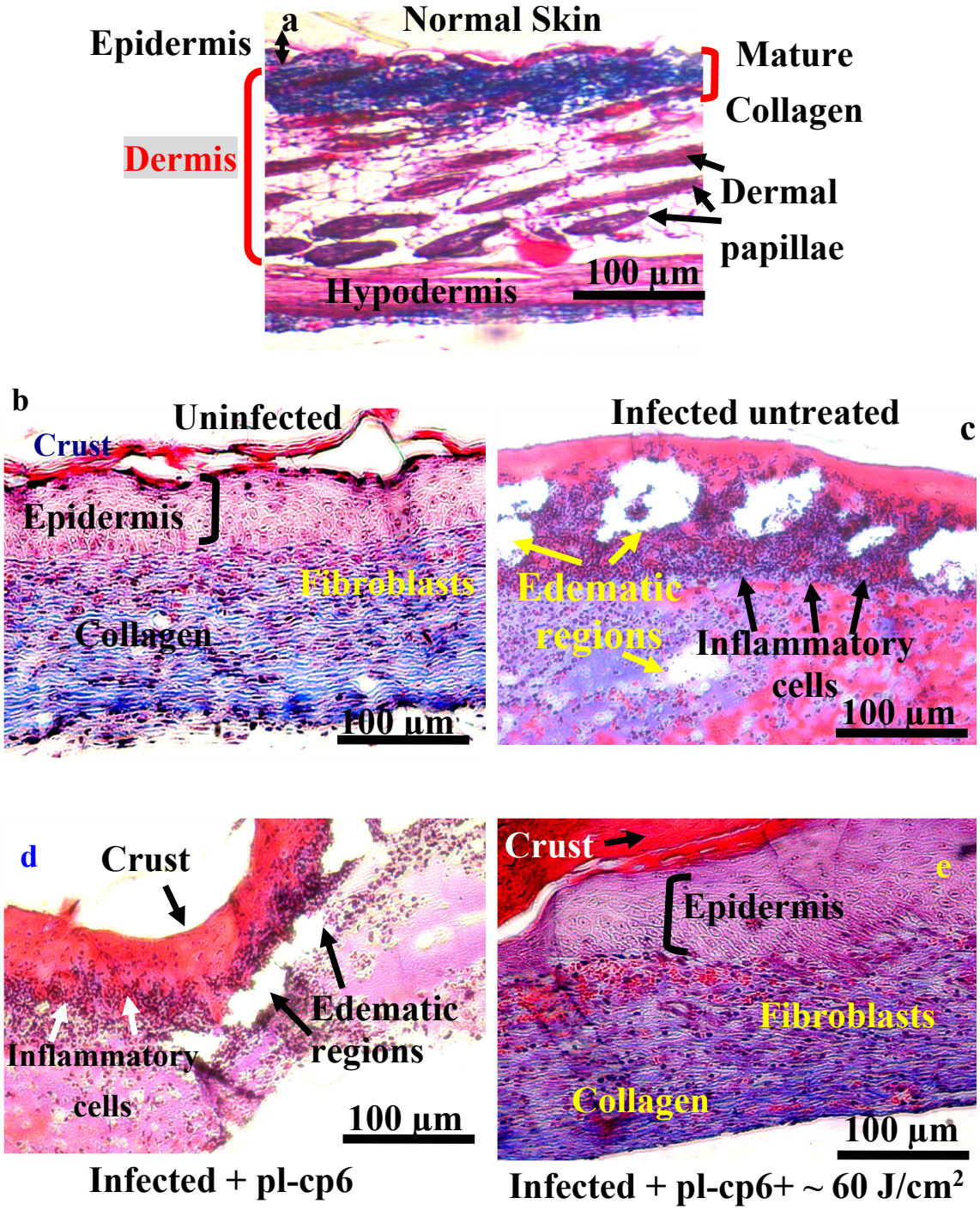


**Figure 5.6** Masson's trichrome stained sections (200 X magnification) of normal skin (a), uninfected wound (b), infected wounds (c), infected wounds treated with pl- cp6 (200 µM) (d), infected wounds treated with pl-cp6 (200 µM) and light (~60 J/cm$^2$) (e). Collagen layer : blue.Fibroblasts : spindle shaped cells. Inflammatory cells : dark stained, multilobed nuclei. Crust : red. Scale bar in each image : 100 µm.

| Criteria | Uninfected | Infected untreated | Infected + pl-cp6 | Infected + pl-cp6 + ~60 J/cm$^2$ |
|---|---|---|---|---|
| **Inflammation** | Discrete | Intense | Intense | Discrete |
| **Reepithelialization** | Present Covering > 90 % of the wound with regular thickness | Incomplete Covering < 25 % of the wound with irregular thickness | Incomplete Covering < 25 % of the wound with irregular thickness | Covering > 90 % of the wound with regular thickness |
| **Epidermis Thickness (µm)** | 40 ± 1 (Continuous) | Discontinuous | 20 ± 2.5 (Discontinuous) | 75 ±10** (Continuous) |
| **Neoangiogenesis** | Numbers less than that of untreated infected wounds | Newly formed blood vessels with number greater than that seen on healthy skin | Large blood microsections upto 150 µm. | Numbers less than that of untreated infected wounds |
| **Collagen fibers** | Parallel to wound surface. Dense. | Disorganized. Sparsely deposited. | Disorganized Sparsely deposited. | Parallel to wound surface. Dense |

**Table 5.1** Histomorphometric analysis of photodynamically treated and untreated wounds. The photomicrographs of wound samples of day 14 p.w. were used for analysis. The results are representative of three different measurements. **: $p < 0.05$; for comparison of means of Inf Vs Inf-PDT group (ANOVA).

Histology of normal skin shows orderly arranged collagen, hair follicle and fat cells (fig 5.6.a). Uninfected wounds showed complete reepithelialization with little inflammatory region, discrete blood cells and lack of any dead (necrotic) tissue (fig. 5.6. b, table 5.1). However, dermal papillae and fat cells were absent. On the other hand the untreated infected wounds (fig. 5.6. c) and infected wounds treated with the

conjugated drug alone (fig. 5.6. d) showed histological features indicative of incomplete healing (table 5.1). The photodynamically treated wounds exhibited complete reepithelialization, little inflammatory regions (fig. 5.6. e). The tissue architecture below the continuous epidermis layer was compact and rich with parallel collagen fibers (table 5.1).

## 5.4 Discussion

The results presented in this chapter shows potential of pl-cp6 mediated APDT for inactivation of *P.aeruginosa* in wounds. The results show that in the wounds of both immunocompetent and immunocompromised mice infected with *P.aeruginosa* and treated with pl-cp6 there is light fluence dependent reduction in the bacterial load . Inactivation of bacteria is expected to be achieved due to enhanced binding of the PS (cp6) due to its conjugation with poly-L-lysine and subsequent destruction of cellular components on irradiation. APDT, however, did not induce apparent erythema or edema in wounds. Lack of adverse effect in the photodynamically treated wounds show that APDT is selective to bacterial components and is consistent with the results of our studies presented in figure 3.6 and earlier studies of other groups wherein it has been shown that concentration of PS and light fluence resulting in significant survival loss of bacteria in infected tissue spares the host tissue [120]. Our results on APDT induced destruction of bacteria are also comparable with the magnitude of *P.aeruginosa* inactivation reported in a previous study [156], wherein similar magnitude of reduction in bacterial counts of wounds infected with invasive strain of bioluminescent *P. aeruginosa* following treatment with 200 μM conjugated ce6 and

~240 J/cm$^2$ light fluence was observed. However, in these studies, photodynamic treatment of wounds were carried out soon after application of bacteria. In present study, for assessing efficacy of APDT, we used an established infection wound model in mice. The post treatment time dependent decrease in bacterial count observed in photodynamically treated wounds of mice suggests that PDT is effective for not only killing the bacteria but may also inactivate the virulent factors of *P. aeruginosa* which otherwise would have affected the microbicidal functions of immune cells. Indeed, inactivation of the virulent factors of *P. aeruginosa* subjected to PDT has been reported under *in vitro* condition [56-58].

Our study in *P.aeruginosa* infected wounds also showed that wound healing was delayed in untreated wounds when compared with photodynamically treated wounds. One of the reasons for this could be the release of the virulent factors of *P. aeruginosa* which are potent inducers of inflammation. This difference in wound healing may be attributed to interference of toxins with the healing processes. Previous studies have shown a significant increase in IL-6 and TNF-α level in wounds treated with purified exotoxin A [164]. Extracellular protease [165] and quorum sensing molecules [166] produced by *P. aeruginosa* have also been shown to induce hyperinflammatory response.The virulent factors secreted from *P. aeruginosa*, have been reported to delay wound repair by inducing premature cellular senescence and altering actin skeleton [167]. *P. aerugionsa* exotoxin; exoenzyme S induces disruption of actin microfilaments [168], immune cell apoptosis [169] and the endotoxin lipopolysaccharide causes endothelial cell injury [170, 171]. High TNF-α level is known to inhibit angiogenesis [172] and promote tissue degradation through higher MMP production [13, 173, 174]. Similarly, elevated IL-6 production has also been

shown to predispose the host to subsequent immunosuppression, depressed cellular immunity, and sepsis [175]. Therefore, it seems likely that the bacterial infection sustains a higher level of TNF-α and IL-6, causing higher inflammation which would in turn result in increased proteolytic cleavage of growth factors, tissue degradation as well as decreased blood microvessel growth at initial wound healing phases.

In contrast to untreated infected wounds, photodynamic treatment led to down regulation of IL-6 and TNF-α protein at both 24 and 96 h time points. Interestingly, in photodynamically treated infected wounds, levels of IL-6 and TNF- α were four to five times lower as compared to untreated infected wounds at 96 h post APDT although there was no significant difference in bacterial counts in these groups (fig. 5.2 , inset). This indicated that APDT leads to inactivation of bacterial virulent factors which may influence the inflammatory response in wound. To test this hypothesis, we measured the protease activity in *P. aeruginosa* cell supernatants after treating with pl–cp6 and exposing to a light fluence of ~60 J /cm$^2$. PDT at this light fluence led to ~50 % decrease in protease activity. These results also agree with the anti virulent effect of APDT demonstrated previously in cell free endo and exotoxins [56-58].

It is known that only reduction in bacterial load without bringing down the inflammation is not sufficient to induce favorable wound healing response [176,177]. In fact, it has been reported that the use of bacteriolysis-inducing antibiotic agents generate counterproductive results like sepsis [42] or may lead to delayed healing because of the release of cell components like LPS [40, 55]. In our study, we observed that though the $AgNO_3$ treated wounds showed a similar decrease in bacterial counts as that caused by APDT fluence of ~60 J/cm$^2$ on day 3 , the wound

closure in $AgNO_3$ treated wounds occurred in a lesser time scale compared to that observed in photodynamically treated wounds. This may be because $AgNO_3$ is not known to directly inactivate the bacterial virulent factors. In fact, it has been observed that $AgNO_3$ may not cause any change or even induce an increased MMPs levels of infected wounds [155]. Considering the role played by the overexpressed MMPs in chronic wound development, it is clear that APDT has better wound healing promoting effect in the infected wounds. Our results also showed that that apart from killing bacteria APDT led to inactivation of proteases which could have attenuated the hyperinflammatory response of infected wounds. In fact, while the untreated infected wounds show presence of a heavy inflammatory infiltrate, incomplete reepithelialization and disorganized collagen in (fig 5.6. c) on day 14 p.w, there is faster regeneration of epidermis and collagen remodeling phase in infected wounds subjected to APDT, confirming shortening of inflammatory phase in the infected wounds due to APDT. These features suggest that wound repair is faster due to a shortened inflammatory phase and correlates well with the decreased IL-6 and TNF-α and the results of previous studies which show that  that wound repair is promoted due to inhibition of TNF-α [178]. To the best of our knowledge, this is the first study which shows APDT induced attenuation of hyperinflammatory response in bacteria infected wounds, which may have contributed in improved healing by expediting the ensuing processes, for instance, the collagen remodeling.

## 5.5 Summary

In this chapter we demonstrated that photodynamic treatment of *P.aeruginosa* infected wound with pl–cp6 not only reduced the bacteria load but also reduced the levels of IL-6 and TNF-α. Since overexpression of proinflammatory cytokines such as TNF-α is implicated in delayed growth factor production and angiogenesis, the results indicate that APDT, at least in part, improved healing by reducing the hyperinflammatory conditions and increasing growth factor production of *P. aeruginosa* infected wounds in mice.

# 6. Effect of topical antimicrobial photodynamic treatment on collagen remodeling of bacteria infected wounds of mice


## Abstract

In this chapter, we present the results of the studies carried out to investigate the effect of pl-cp6 mediated topical APDT on collagen remodeling response of methicillin resistant *Staphylococcus aureus* (MRSA) and *P. aeruginosa* infected wounds. Collagen remodeling was monitored by measurements on tissue retardance using Polarization sensitive optical coherence tomography hydroxyproline content and matrix metalloproteases (MMPs) level in wounds. The results show compared to the untreated infected wounds or treated with pl-cp6 alone, in the infected wounds treated with pl-cp6 and light, the hydroxyproline content and retardance were higher by a factor of ~3 and ~2 respectively but MMP- 8, 9 levels were lower, suggesting APDT induced promotion of collagen remodeling of wounds.



***Some aspects of the results presented in chapter 6 are published in Photomed. Laser Surg. 32, 23-29 (2014).***

## 6.1 Introduction

In wounds, invasion of host tissues by bacterial pathogens can initiate destruction of structural proteins including collagens. This is caused by either the direct collagenolytic action of bacterial proteases [35] or bacterial protease induced activation of latent host collagenases [26,179] like MMPs [180] which contribute to delayed wound healing. Bacterial endotoxins are also known to inhibit development of wound tensile strength [181]. Therefore, inactivation of bacteria and the bacterial proteases [56-58] is expected to reduce inflammation and restore collagen remodeling in wounds. Indeed, in our earlier study reported in the chapter 5, we show that topical APDT in *P.aeruginosa* infected wounds, reduced the hyperinflammatory response [182] on day 4 p.w.. Since, MMP level in wounds peak during this time point and also the over expression of proinflammatory cytokines are often the cause behind overexpression of MMPs, the results presented in chapter 5 suggested that one way by which the PDT induced decease in IL-6 and TNF-α contribute to faster healing is by bringing down the levels of MMPs in wounds. At the same time, it is known that ROS may lead to the activation of MMPs, either through reaction with the thiol groups in catalytic domains of the MMPs or may even cause destruction of tissue inhibitors of MMPs [183,184].

One approach used commonly for monitoring collagen remodeling is hydroxyproline assay [185]. A limitation of this approach is that it provides an estimation of collagen content and does not indicate collagen cross linkage which is required for wound closure and recovery of tissue tensile strength. Histology followed by Masson's trichrome staining is also another approach used to study collagen deposition in

wounds during healing. However, histology provides semi quantitative information on collagen remodeling and because of its invasiveness leads to random sampling.

Collagen is birefringent and its ordering contributes to tissue birefringence. This can be quantified using Polarization sensitive optical coherence tomography (PSOCT), a real-time, non invasive cross-sectional imaging tool. Both OCT [186] and PSOCT [187-189] have been utilized for visualization of morphological changes, in wound healing particularly collagen remodeling. In a previous study, using PSOCT, we were able to quantify the decrease in collagen remodeling in bacteria infected superficial wounds by measuring birefringence of wounds [190]. In this chapter, we report the results on the effect of pl-cp6 mediated APDT on collagen restoration in murine excisional wounds infected with MRSA and *P.aeruginosa,* studied using PSOCT. These results have been validated by trichrome staining of histological sections, hydroxyproline assay and immunoblotting of MMP-8, 9.

## 6.2 Material and Method

### 6.2.1 *Bacteria*

The bacteria used in this study were *P.aeruginosa* PAO (MTCC 3541, Chandigarh, India) and MRSA (ATCC 43300, Himedia India). Both bacteria were maintained routinely by sub culturing in TSA (Himedia, Mumbai, India). For experiments, a colony of the bacteria was inoculated into TSA and was grown aerobically for 18h at 37$^{o}$C using a shaker incubator. For infecting wounds, optical density of the exponential culture of bacteria was measured at 600 nm and diluted to obtain required concentration.

### 6.2.2 *Establishment of wound infection and photodynamic treatment of wounds*

A total of 60 female Swiss albino mice (weight ~25g, 8 weeks) were used for all experiments. All animals were housed in individual cages under constant temperature (20 ± 4 $^0$C) with a 12-h light /dark cycle, and had free access to food and water. In anesthetized mice, excisional wounds of ~1.2 x 0.8 cm (length x width) were created on the dorsal skin. Infection of the wounds was initiated by applying ~ $10^8$ CFU MRSA or ~ $10^7$ CFU *P.aeruginosa* growing in exponential phase. Mice with wounds were divided into following groups: (1) uninfected wound, (2) Infected (with either MRSA or PAO) untreated wounds, (3) Infected dark control (treated with only pl-cp6), (4) Infected PDT group (treated with pl-cp6 and light). Photoirradiation was carried out using the the irradiation parameters descibed in table 2.3 to achieve light fluence ~ 60 and 120 J/cm$^2$. The Institutional Ethical Committee, in accordance with the institutional guidelines on animal care approved all procedures involving animals.

### 6.2.3 *PSOCT imaging of wounds*

Figure 6.1 shows a schematic of the PSOCT setup used for imaging of the wounds. OCT (back scattered intensity) image is obtained by summing the squares of amplitude of the orthogonal polarization components. The PSOCT (phase retardance) images are displayed as spatial maps of optical phase retardation obtained by computing the arctangent of the ratio of $I_H$ and $I_V$ [189]. The axial and lateral resolutions of the setup are ~11 and ~17 μm, respectively. The image acquisition time was about 2 min for an image comprising of 200 x 1000 pixels. In each wound, ~ 6-8

different regions were scanned. A-scan registration was performed to minimize the motion artifacts arising due to breathing of anesthetized mice. The measured phase retardation as function of depth was averaged over ten consecutive lateral positions (spaced by ~17 μm). From this the phase retardation per unit length was calculated by a linear fitting of these data. Each imaging measurement was repeated thrice.

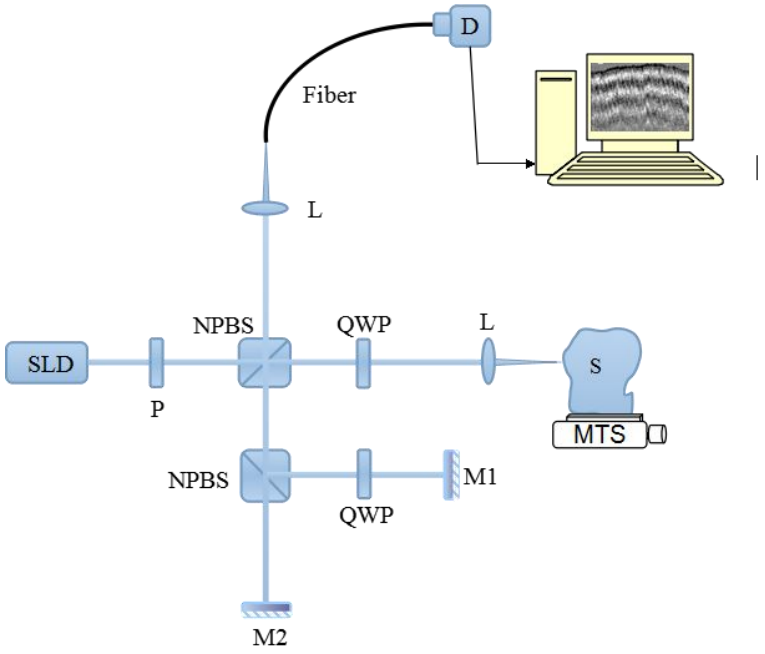


**Figure 6.1** PS OCT set up used for imaging. P= polarizer; L= lens; M= mirror; NPBS= nonpolarizing beam splitter; QWP= quarter wave plate; DAQ= data acquisition board. SLD = Superluminescent diode. MTS = Manual translation stage.

### 6.2.4 *Histopathological analysis*

On day 18 p.w., mice were euthanized by cervical dislocation. A ~1 x 0.8 cm portion of dorsal skin including the wound region was excised. The tissues were fixed in 10 % neutral buffered formalin for 24 h and processed using standard histological

procedure. The deparafinized sections were stained with Masson's trichrome stain and examined under a microscope to observe reepithelialization and arrangement of collagen fibers.

### 6.2.5 *Hydroxyproline assay*

Mice were euthanized on day 18 p.w. and a ~1 x 0.8 cm portion of dorsal skin including the wound region in the middle was excised, weighed, frozen in liquid nitrogen and stored at -80˚C till use. Hydroxyproline assay was carried out according to the protocol described in [98] and has been elaborated in chapter 2. The values were expressed as milligram (mg) hydroxyproline per gram (gm) tissue weight.

### 6.2.6 *Western Immunoblot analysis and densitometry*

On day 5 p.w., mice were euthanized and wounds (scab and granulation tisue) were excised. The supernatant of wound homogenates, prepared according to the protocol described in chapter 2 was used for western blotting and protein estimation. Protein samples (~50 μg), separated by SDS-PAGE were electroblotted to nitrocellulose membrane. The membranes were incubated with anti-MMP-8 (sc-8848), MMP-9 (sc-6840) antibodies (Santacruz biotech, USA) followed by incubation with HRP-conjugated secondary Ab. Blots were developed using protocol described in an ECL kit (RPN 2135, Amersham Biosciences, GE Health Care Life Sciences, USA). Chemiluminescence images were captured with an imaging system (Chemi-HR-16, Syngene, UK) and processed using GENESNAP software (Syngene, UK). Densitometry was carried out using software GENETOOL (Syngene, UK). Glyceral

dehyde-3-phosphate dehydrogenase (GAPDH) was used as a loading control. Blot intensities of MMPs were divided with that of the GAPDH. To quantify treatment effect, intensities of the blots of uninfected wounds were divided with that of other groups.

### 6.2.7 *Statistics*

The results were represented as mean ± SD of three independent measurements performed in at least six animals. The statistical significance of the difference between means was assessed by one way ANOVA. $P < 0.05$ was considered statistically significant.

## 6.3 Results

### 6.3.1 *Effect of APDT on collagen remodeling of MRSA infected wounds.*

In figure 6.2 we show representative OCT, PSOCT and histological images of uninfected (fig. 6.2, a-f) and MRSA infected wounds (fig. 6.2, g-l). In uninfected wounds, on day 7 p.w. (fig. 6.2 a), the back scattering images show a highly scattering wound crust on the wound surface, below which, the newly formed epithelial layer is observed. The patches of scattering regions observed below this new epithelium layer (star mark, fig. 6.2 a) near the wound margin, indicate the early granulation tissue. The corresponding retardation image (fig. 6.2 b) of the wound bed shows a relatively week polarization contrast [15]. At this time point, phase retardance ~0.03 degree/μm) of wounds is much lower than that of normal skin (~0.2 degree/μm). On day 14 p.w.

(fig. 6.2 c) and day 18 p.w. (fig. 6.2 e), the crust is completely absent and the back-scattered intensity of wounds is increased considerably. The birefringence images, on day 14 p.w. (fig. 6. 2 d) and day 18 p.w. (fig. 6.2 f), also show increased retardation compared with that of day 7 p.w.. The phase retardance of wounds on day 14 and 18 p.w. are ~0.05 and ~0.07 degree/ μm, respectively, indicating restoration of connective tissue.

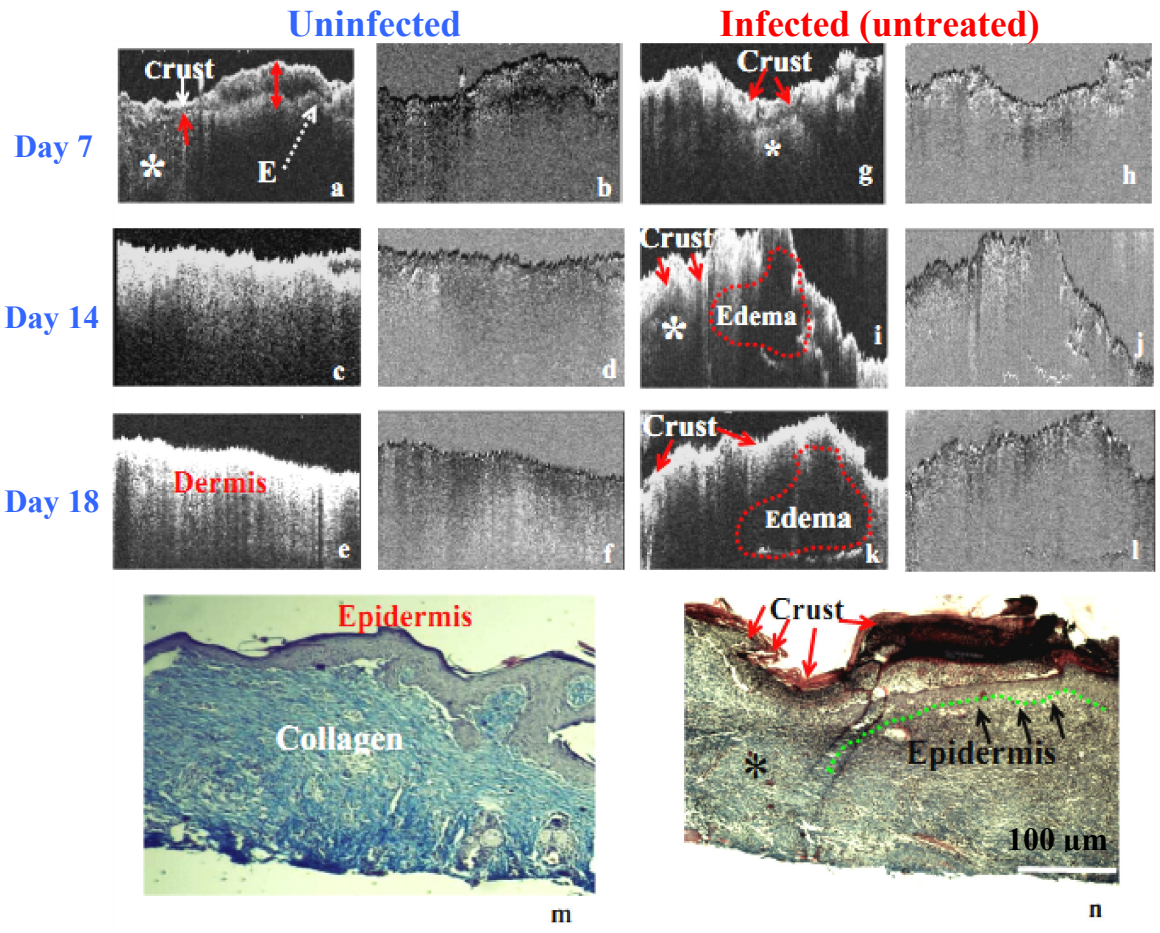


**Figure 6.2** Time-dependent structural changes in uninfected (a-f) and MRSA infected (g-l) excisional wounds of mice. Panels (a, c, e, g, i, k) and (b, d, f, h, j, l): backscattered (OCT) and phase retardation (PSOCT) images. Image dimension: 1.5 mm (H) x 3 mm (L). Oppositely facing arrows and double arrow show the crust and

gap between crucnew epithelium layer (E). Lowermost panel: Trichrome stained histological sections of uninfected (m) and infected (n) wounds, scale bar : 100 µm. *: Granulation tissue (Histology and OCT images).

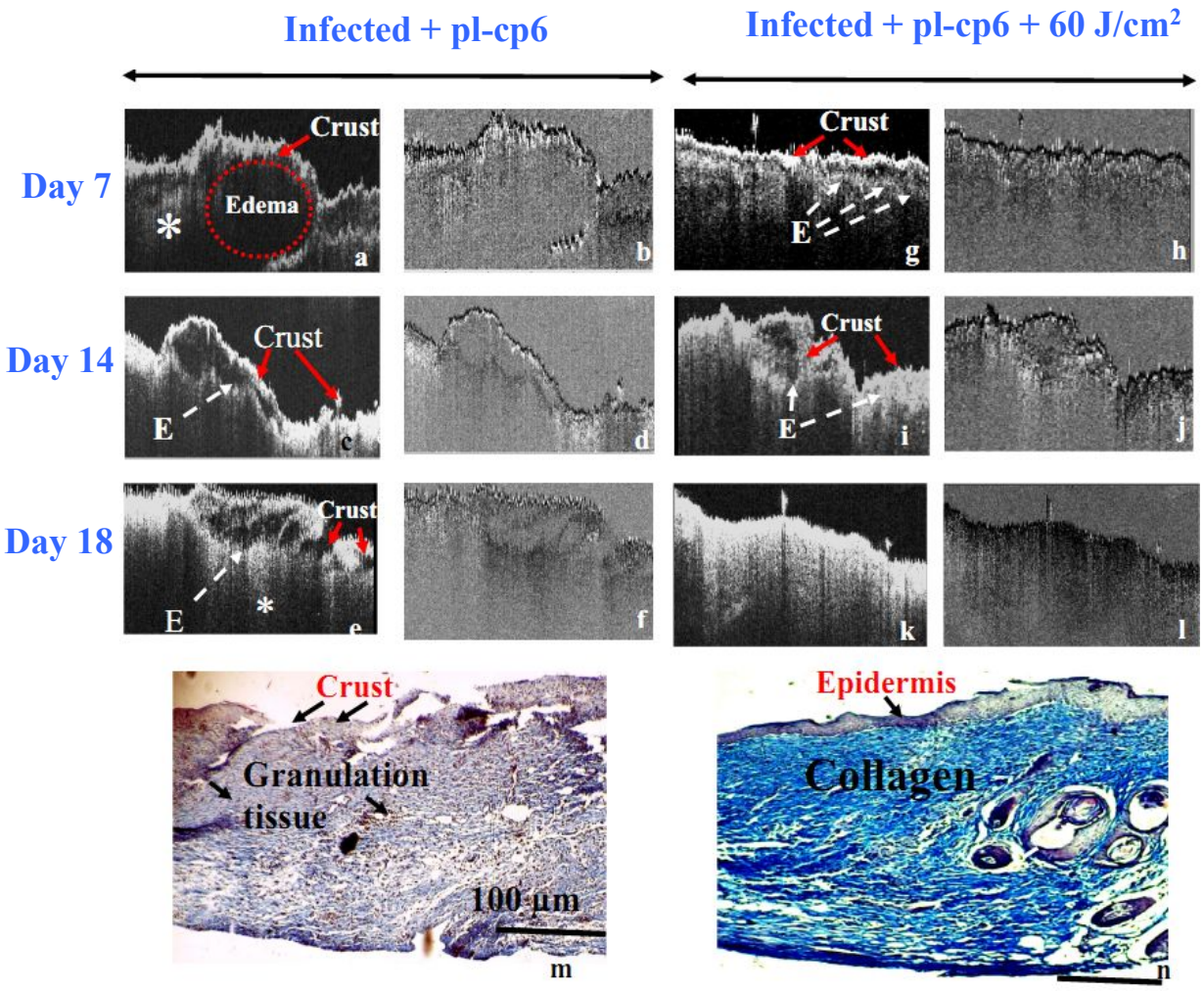


**Figure 6.3** Effect of APDT on collagen remodeling of MRSA infected wounds. Panels (a,c,e, g, i, k) and ( b, d, f, h, j ,l) : backscattered and phase retardation images. Image size in OCT images: 1.5 mm x 3 mm. Lowermost panel : trichrome images of infected wound treated with plcp6 in dark (m) and irradiated with light (n), scale bar: 100 µm. E : New epithelium layer.* : Granulation tissue.

The OCT images of MRSA infected wounds (fig. 6.2 g, i, k) show presence of much thicker crust, prolonged edematic response. Also, considerably less polarization contrast is observed at all the post wounding time points (fig. 6.2 h, j and l). On day 18 p.w.,the phase retardance of infected wounds (~0.032 degree/μm), in comparison to that of uninfected wounds,is significantly lower ( $p < 0.05$). The structural features observed in the OCT images of the uninfected and infected wounds are consistent with that of the histology images. Compared to uninfected wounds (fig. 6.2m), infected wounds (fig. 6.2 n) showed more inflammatory exudates, incomplete epidermis, lesser trichrome staining indicating less ordered collagen.

After confirming the delayed collagen remodeling of wounds due to MRSA infection, we then studied effect of APDT on collagen remodeling response of wounds by using PSOCT.Prior to carrying out this investigation, we carried out preliminary experiments to ascertain whether PDT alone caused any adverse effect on collagen remodeling of wounds. The results of those studies showed that in wounds exposed to APDT induced by pl-cp6 (200 μM) and light fluence of either ~ 60 or ~120 J/cm$^2$ did not have any quantifiable adverse effect on collagen remodeling (data not shown). In addition, in MRSA infected wounds exposed to pl-cp6 and APDT fluence of ~ 60 or ~ 120 J/cm$^2$, immediately after the APDT, the bacterial load of wounds decreased by ~1.2 or ~ 2 log, respectively.Therefore, for studying APDT effect on collagen remodeling of infected wounds we used these two light fluence. Figure 6.3 shows OCT, PSOCT and histological images of wounds of MRSA infected dark control and APDT (~ 60 J/cm$^2$) group. The scattering and phase retardance patterns observed in the OCT images of the infected dark control wounds, on day 7 p.w. (fig. 6.3 a,b), 14 p.w. (fig. 6.3 c,d) and day 18 p.w. (fig. 6.3 e,f) were similar to that of the untreated

infected wound (fig. 6.2 g-l). In contrast, infected wounds subjected to APDT on day 7 (fig. 6.3 g,h), 14 (fig. 6.3 i, j) and day 18 p.w. (fig. 6.3 k,l) show increased backscattering and less edematic regions. The phase retardance of the photodynamically treated wounds on day 14 (~0.045 degree/μm) and day 18 p.w. (~0.06 degree/μm) are significantly higher ($p < 0.05$) than the phase retardance values of both untreated and pl-cp6 (100 μM) treated wounds on day 18 p.w. (~0.032 degree/μm). Consistent with the PSOCT images and the calculated retardance, the histological analysis of infected wounds subjected to APDT show lesser inflammatory cells, completely formed epidermis and denser trichrome staining, compared to MRSA infected dark control (fig. 6.3 m,n) wounds. Infected wounds subjected to higher light fluence (~ 120 J/cm$^2$) show no significant differences in the scattering features, birefringence and trichrome staining pattern (data not shown). It may be noted here that in our previous study on *P.aerugionsa* infected wounds (Fig 5.4 B, chapter 5), we did not observe any light fluence dependent effect on healing .

### 6.3.2 *Effect of APDT on hydroxyproline content of MRSA infected wounds*

In order to confirm the changes in retardance and collagen staining pattern observed in the wounds, hydroxyproline content was estimated in wound tissues on day 18. The results (fig. 6.4) show that in infected wounds subjected to APDT, hydroxyproline contents are ~3 fold higher ($p<0.05$) than that of untreated or dark control wounds. However, the hydroxyproline levels of the wounds subjected to APDT fluence of ~60

or ~120 J/cm$^2$ do not vary significantly ($p > 0.05$). It may be noted here that a lack of light fluence dependent APDT effect on healing was also observed in the PSOCT images of MRSA infected wounds and also in our studies on *P.aeruginosa* infected wounds, presented in chapter 5 (Fig 5.4 B) suggesting that the maximum beneficial response is achieved with the fluence of ~60 J/cm$^2$.

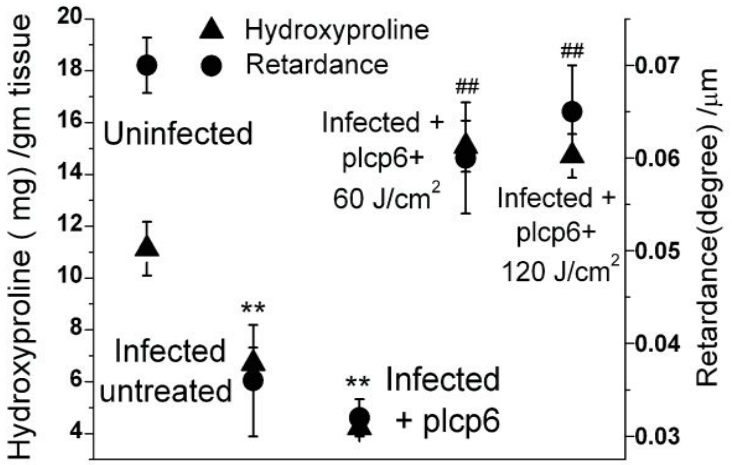


**Figure 6.4** APDT induced changes in hydroxyproline content and calculated phase retardation (mean ± SD) of MRSA infected wounds on day 18. **: $p < 0.05$ compared to uninfected wounds. ## : $p < 0.05$ compared to untreated and pl-cp6 treated.

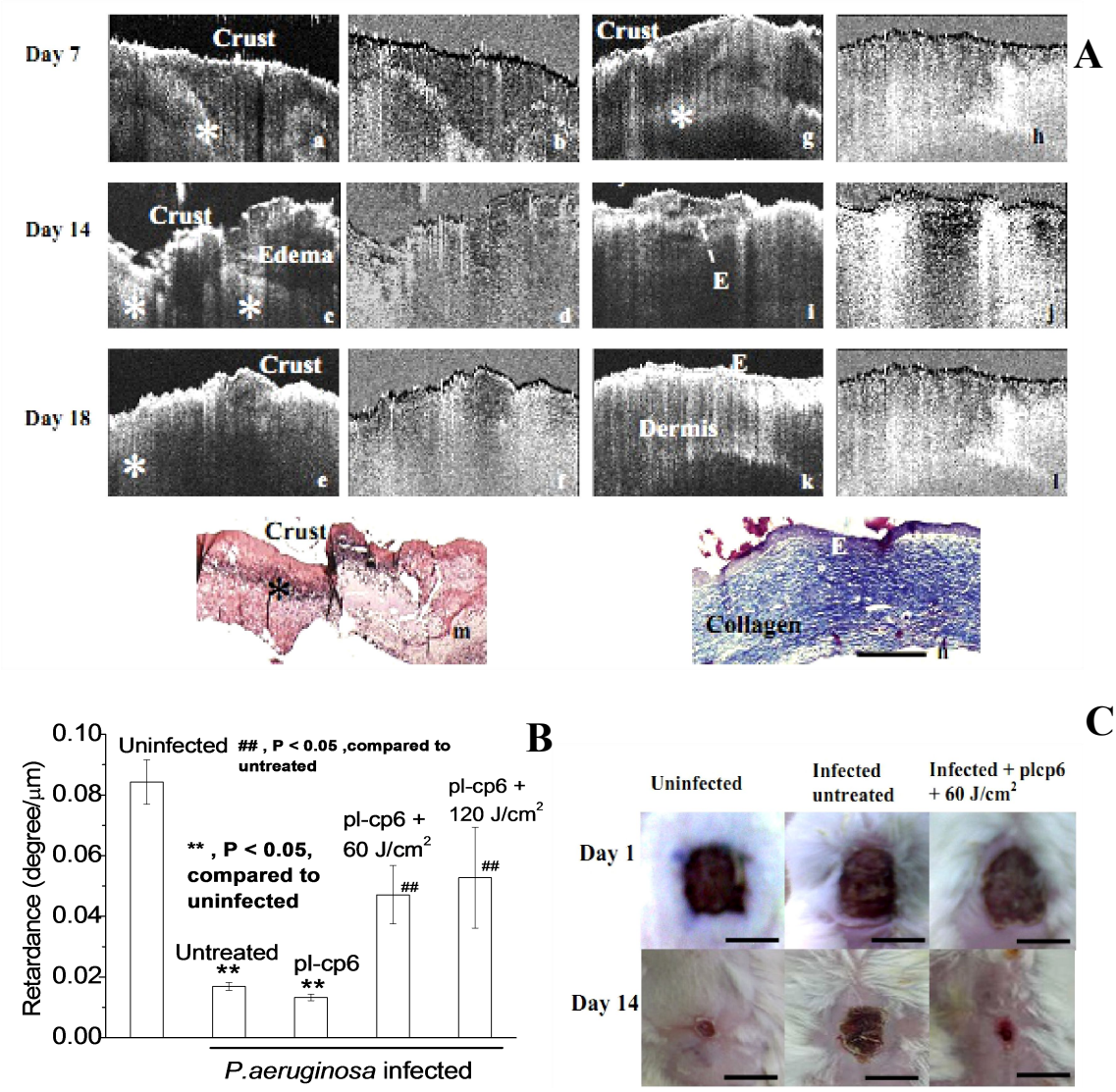


**Figure 6.5** (A) Effect of APDT on collagen remodeling of *P. aeruginosa* infected wounds. Panels (a,c,e, g, i, k) and (b, d, f, h, j, l) : backscattered and phase retardation images. Image size in OCT images: 1.5 mm x 3 mm. *:Granulation tissue.E= Epithelial layer. Lowermost panel: trichrome sections of infected wound treated with plcp6 in dark (m) and irradiated with light (n). E : New epithelium layer. Histological images scale bar 100 µm. (B) Retardance calculated from PSOCT images of wounds day 18 p.w. (C) Photographic images of wounds on day 1 and 14 p.w. Scale bar: 1 cm.

### 6.3.3 *Effect of APDT on collagen remodeling of P. aeruginosa infected wounds*

We then studied whether APDT also influenced the collagen remodeling of *P.aeruginosa* infected wounds. In figure 6.5 (A) OCT, PSOCT, histological images and in fig 6.5 B the calculated retardance of the *P.aeruginosa* infected wounds are shown. Further, in figure 6.5 C we show the photographic images time dependent wound closure. The OCT and PSOCT images of untreated and dark control (pl-cp6 treated) infected wounds are almost similar and showed presence of thick crust, more signal poor regions indicative of infection induced edema and lower retardance on day 7 and 14 (fig. 6.5 A; a-f). On day 18, the phase retardance in untreated and pl-cp6 treated infected wounds were much lower ($p < 0.05$, ANOVA) compared to that of uninfected wound. However, in photodynamically treated wounds (fig. 6.5 A; g-l), reepithelialization occurred much earlier and there was significant increase in the phase retardance (~0.052 degree/μm, figure 6.5. B). Histological analysis of photodynamically treated wounds show lesser inflammatory cells, complete epidermis and more compact dermis compared to infected dark control (fig. 6. 5 A; m, n). The photographs of uninfected and *P.aeruginosa* infected (untreated and photodynamically treated) wounds at day 1 and 14 p.w , showing faster closure in wounds subjected to PDT also confirm the PSOCT and histology data.

### 6.3.4 *Effect of APDT on MMP expression in P.aeruginosa infected wounds*

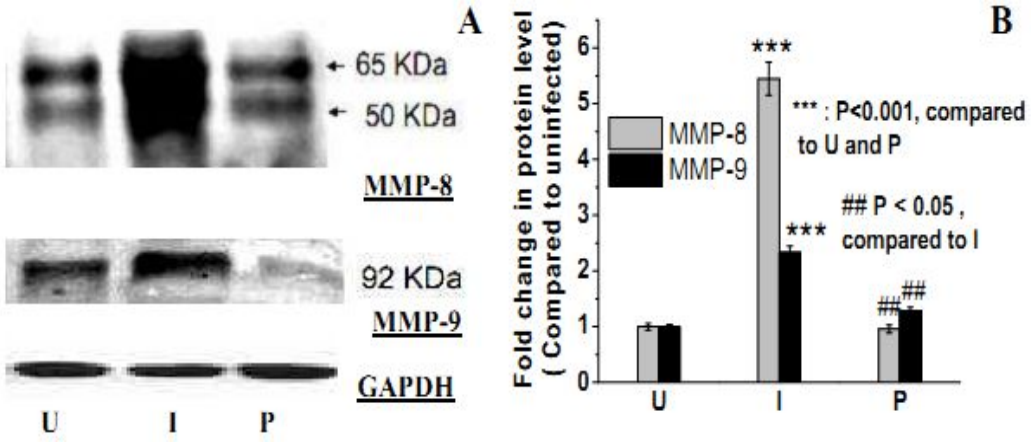


**Figure 6.6** Effect of PDT on MMPs expression in *P.aeruginosa* infected wounds on day 5 p.w.. A; Immunoblots of MMP-8,9 and GAPDH (internal control). B; Densitometric analysis (mean ± SD) of immunoblots from three independent experiments. U; Uninfected, I; Untreated Infected, and P; Infected + pl-cp6 + ~60 J/cm$^2$.

*P. aeruginosa* toxins are known to stimulate over production of MMPs [179] which can cause excessive degradion of the collagen deposited in the granulation matrix. Therefore, we studied MMP expression in *P. aeruginosa* infected wounds. The results (fig. 6.6) show that in the untreated infected wounds of MMP-8, 9 protein levels were overexpressed. In the photodynamically treated wounds, however, MMP levels were reduced considerably ($p < 0.001$).

## 6.4 Discussion

It is known that in bacteria infected wounds, collagen remodeling is compromised because of the collagenolytic enzymes secreted by bacteria [35] and infection induced stimulation excess collagenase [26,179] production by host cells. This affects the collagen fibril arrangement and tensile strength during scar maturation phase of the wound. Therefore, in order to assess the effect of an antibacterial therapeutic intervention in wounds more accurately, monitoring collagen remodeling is necessary.

Our results presented in figures 6.2, 6.3 and 6.5A showed persistence of scattering poor regions and lower retardance in PSOCT images even during 3$^{rd}$ week indicating prolonged edematic and collagen degradation response due to bacteria infection [26,35, 179, 191]. It is known that the toxins produced by *S. aureus* can cause extensive host tissue damage by eliciting either apoptotic response in epithelial cells [192] or hyperinflammatory response [193, 194]. There may also be infection induced increased interstitial matrix metalloprotease MMPs [179, 195] production by inflammatory cells. Similarly, *P. aeruginosa* elastase can cleave directly the collagen type III [35] of the early granulation tissue. In addition, *P. aeruginosa* infection can stimulate local overproduction of proinflammatory mediators such as TNF-α [190] and pro-MMP [180]. TNF-α inhibits of collagen I synthesis [196] and promotes higher MMP production [197]. MMP-8 degrades type-I collagen into gelatins which are substrates for MMP-9 [180]. Excess MMP-9 (fig. 6.6) leads to reduced collagen IV at the leading edge of the epithelial tongue [198]. Therefore, MMP-8, 9 overexpression in infected wounds delays collagen restoration.

The results presented in figures 6.3 and 6.5 A show that collagen remodeling in photodynamically treated MRSA and *P. aeruginosa* infected wounds was faster as compared to wounds treated with pl-cp6 in dark. The faster collagen remodeling in mice wounds was confirmed by hydroxyproline measurement (fig. 6.4), histology and PSOCT measurements (fig. 6.3 and 6.5 A). Increased (~3 fold) retardance, more ordered collagen fibrils, and higher hydroxyproline content (~4 times) in photodynamically treated MRSA infected wounds as compared to untreated infected wounds confirmed the faster collagen remodeling (fig. 6.4). Similarly, significant increase in retardance (fig 6.5.B) and parallel collagen fibers (fig 6.5.A) in *P. aeruginosa* infected wounds following APDT also suggest better scar maturation. The faster recovery in treated wounds may be because of abrogation of hyperinflammatory response and collagen degradation induced by bacterial toxins. Our previous study has shown that APDT mediated by pl-cp6 reduces expression of IL-6 (~ five fold) and TNF-α (~four fold) in *P. aeruginosa* infected wounds. The results presented in this study showed that there is no adverse rise in MMP level in the wounds subjected to PDT fluence of ~60 J/cm$^2$, in fact there is considerable decrease in MMPs (fig. 6.6).

The results of our study show that phase retardance of wounds increases with time. Previous studies have demonstrated that a similar trend also exists for wound tensile strength [185]. Since both wound tensile strength [185] and birefringence [199] reflect collagen arrangement, therefore, PSCOT based retardance can be a good indicator of tissue tensile strength and wound repair. In contrast, hydroxyproline level, beyond certain time point, does not increase alongwith wound tensile strength [185] and in several situations, though the hydroxyproline content of wounds subjected to therapeutic intervention may be same, the tensile strength may differ significantly

[200]. Hence, predicting an outcome based on hydroxyproline level may be erroneous [200].

There were reports that PDT does not influence wound healing or may even cause epidermal necrosis, decrease in tensile strength and delayed healing. These variations might have arisen mainly because of the differences in photosensitizer administration modes (intra peritoneal or intravenous), use of higher light fluence ( > 200 J/cm$^2$) and the random sampling by invasive techniques like histology [83]. Therefore, one of issues that is clarified by our results presented in chapter 6, is that single topical APDT at fluence of ~ 60 J/cm$^2$ accelerates healing in bacteria infected wounds by attenuation of collagen degradation (fig 6.5) of bacteria infected wounds, but, in wounds exposed to the higher fluence of ~120 J/cm$^2$, the healing outcomes such collagen remodeling and hydroxyproline contents does not seem to be further enhanced (fig 6..3 and, fig 6.4). These results are also consistent with our results on wound area reduction and closure time presented in fig 5.4.While the exact reasons for this observation is not clear, this may have arised due to increased damage to host cells such as macrophages and other cells at higher fluence [201]. APDT fluence dependent host inflammatory cell damage, delayed infection resolution and repair of injury has been demonstrated in a study using murine model of MRSA infection induced arthritis wherein it has been shown that, while a fluence too low (~5 or 20 J/cm$^2$) leads to insufficienct bacteria inactivation, high fluence (~120 and 160 J/cm$^2$ ) causes synovial microvessels damage and bacterial regrowth. Further, the light fluence of ~ 50 J/cm$^2$ produces maximum bacteria inactivation and inflammatory cell migration to the infection site [201]. However, a direct extrapolation of conclusions

obtained from the study involving arthritic mice in which an inradermal PS delivery was used, to the possible outcomes in case of APDT (topical) for wounds, may not be accurate. Therefore, to establish a possible link between APDT fluence dependent oxidative stress with healing outcome in wounds more investigations are needed, particularly in diabetic conditions wherein reduced inflammatory cell functions, antioxidant levels are observed.

## 6.5 Summary

Collagen remodeling response, post APDT, in excisional wounds of mice infected with antibiotic resistant and virulent strains of bacteria could be quantified by PSOCT based retardance measurements. The data on retardance, MMP-8,9 expression, hydroxyproline content and histology suggested that topical APDT induced by pl-cp6 and red light expedites collagen restoration in bacteria infected wounds of mice by attenuating collagen degradation. It benefits wound repair in bacteria infected wounds by significantly enhancing epithelial layer migration, hydroxyproline content, and collagen fibril arrangement.

# 7. Effect of topical antimicrobial photodynamic treatment on healing of wounds of diabetic mice infected with methicillin resistant *Staphylococcus aureus*


## Abstract

In this chapter, we present results of the studies carried out to investigate the effect of single or multiple APDT on the healing response of MRSA infected and uninfected wounds of diabetic mice. The parameters monitored include bacteria regrowth, thiobarbituric acid reactive substrates (TBARS), Protein carbonyl (PC) ,GSH, NO and VEGF-A levels in wound tissues. Further, to quantify the effect of APDT on inflammatory cells of wounds, measurements were also made on the level of Myeloperoxidase (MPO) and neutrophil elastase (NE).The results show that APDT enhance healing of wounds in diabetic mice by increasing NO, GSH and VEGF-A levels. Further, there is also increased MPO and NE level in wounds of diabetic mice subjected to APDT which may have additional beneficial response in infection resolution.



***Some aspects of the results presented in chapter 7 have appeared in Lasers Med Sci. 30:1923-9 (2015).***

## 7.1 Introduction

Impaired wound healing is a serious complication for diabetic patients which is caused by several systemic and local abnormalities [19-22]. These abnormalities include compromised immune response like defective phagocytic functions of immune cells, defective angiogenesis [19, 20] and reduced production of NO [7,21,22,202,203], which is important signaling intermediate for diverse cellular responses of wound healing such as cell proliferation, angiogenesis, macrophage function and collagen remodeling [7]. These abnormalities predispose the wounds to higher risk of infections [204]. Infections can become fatal if causative microorganism is resistant to antibiotics. Indeed, infections of wounds caused by MRSA has been reported as one of the leading causes of lower limb amputation and mortality in diabetic patients [ 30-32]. Therefore, alternative therapeutic methods, which can eliminate antibiotic resistant bacteria and improve healing, are essential for management of wounds in diabetic conditions .

Our results on APDT induced beneficial effects like reduction in hyperinflammatory response [182], MMPs but better collagen remodeling [205] response in wounds of normal mice, presented in chapter 5 and 6, suggest that APDT can be a potential alternative for management of wound infections in diabetic subjects. However, an important concern pertaining to the use of APDT for infected wounds in diabetes is control of regrowth of bacteria and avoidance of possible oxidative damage to inflammatory cells [201], as it is known that diabetes causes marked reduction in function of neutrophils [206-208], persistent inflammation [209] and oxidative stress [210], reduction in levels of antioxidants [211]. In addition, some previous studies

have shown that PDT can modulate angiogenesis [212] in tumors. However, for diabetic wounds, this aspect has not received any attention so far. Therefore, in this study we have also investigated effect of pl-cp6 mediated APDT on angiogenesis of wounds of diabetic mice.

In this chapter, we have presented the results of the investigations on (i) effect of APDT on level of oxidants, antioxidants and inflammatory cell sequestration and (ii) the possible APDT induced alterations in NO and angiogenesis in wounds of diabetic mice.

## 7.2 Material and Methods

### 7.2.1 *MRSA growth in suspension and biofilm biomass quantitation.*

The MRSA strain (ATCC 43300) used in this study was maintained routinely by sub culturing in TSA (Himedia, Mumbai, India). For experiments, a colony of the bacteria was inoculated into TSA and was grown aerobically for 18 h at 37$^{o}$C using a shaker incubator. For infecting wounds, optical density of the overnight culture of bacteria was measured at 600 nm and diluted to obtain required concentration.

In order to study the effect of glucose on growth of bacteria, MRSA were incubated with TSA with and without externally added glucose (0, 0.2, 0.4 %) for different duration. At specified time duration, OD measurement and colony forming units assay were carried out. MRSA biofilms were grown on fibrinogen coated surface. For this, 96 well polystyrene plates were coated with fibrinogen by placing 50 µl of 1% fibrinogen for 48 h and air dried. Biofilm biomass quantitation was carried out

according to the protocol described in [60]. Briefly, biofilms formed on the plates were washed twice with PBS. Then, the cells were fixed with 95% ethanol for 10 min and stained with 0.1% crystal violet for 15 min, and after several washings, the wells were air dried. For a quantitative estimation of biofilms, crystal violet was solubilized with 10 % glacial acetic acid and absorbance of the solubilized dye was determined at 590 nm in a microplate reader. Biofillm quantitation was also carried out by MTT assay. Briefly, in the fibrinogen 96 well plate, bacteria were grown for 48 h in TSA containing different glucose concentrations. At 48 h, to each well 150 µl PBS, 50 µl MTT (0.5% in PBS) was added. The plate was incubated at 37° C for 2 h in dark. Post MTT incubation, medium containg MTT was removed and to each well 150 µl of DMSO was added. The color intensity of the soluble formazan formed was determined by using microplate reader at 570 nm with 630 nm as reference.

### 7.2.2 *Induction of diabetes and establishment of infection in wounds*

A total of seventy six Swiss albino mice (male and female weight 30-35 g, 12 weeks) were used for all experiments. The Institutional Animal Ethical Committee (IEAC) in accordance with the institutional guidelines on animal care approved all procedures involving animals. Induction of diabetes, creation of wounds were carried out according to the protocol described in [92, 93] which has been elaborated chapter 2. Presence of biofilm on wounds were studied by Gram staining of the histological sections. Then the bacteria inocula required for development of a chronic infection in diabetic mice were ascertained. The mortality for diabetic and non diabetic mice in which the wounds were infected with $10^{8}$ CFU MRSA, was ~ 70 % and ~15% ,

respectively , on day 5 p.w. Without any treatment, the bacterial load was observed to increase by ~ 0.8 log and ~1.8 log for wounds of non diabetic and diabetic mice on day 3 p.w. Also, even if all the wounds were infected with same number of bacteria, the wounds of diabetic mice showed higher bacteria load (~ 2.5 times) than wounds of non diabetic mice. Therefore, for developing chronic infection, while in each diabetic mice a bacterial inoculum of ~$10^{7}$ CFU MRSA /wound was used, for non diabetic mice a bacterial load of ~$10^{8}$ CFU MRSA /wound was used .

In order to check the reasons for increased bacteria growth in wounds of diabetic mice, experiments on bactericidal action of blood derived from tail vein of both non diabetic and diabetic mice was studied [213]. Blood (200 µl) was collected in vials containing sodium citrate (2.5%) mixed with exponential culture of MRSA in a 2:1 ratio to yield a final concentration of $10^{5}$ CFU/ml for MRSA. The samples were incubated at 37°C on a shaker, and aliquots were removed to determine the bacterial number at 0 and 120 min by plating on TSA. The data were expressed as percent reduction (or increase) from the initial inoculum ($10^{5}$ CFU/ml).

## 7.3 Antibacterial treatment for MRSA infected wounds of diabetic mice

For establishing infection, bacteria were allowed to grow for 48 h in wounds of both normal and diabetic mice. All the mice with wounds were divided into following groups: (1) uninfected wound, (2) infected untreated wounds, (3) infected dark control (infected wounds treated with only pl-cp6), (4) infected APDT group; single (treated with both pl-cp6 and light fluence of 60 or 120 J/$cm^{2}$) and (5) multiple APDT.

Photoirradiation was carried out according to the protocols described in table 2.2. For multiple APDT ,a repeated PDT protocl was used in which wound were treated with pl-cp6 and exposed to red light photoirradiation at 24 h intervals during day 1-3 w.w (figure 2.1). Wound tissues were excised 24 h post PDT (day 3 p.w.),weighed and homogenized in PBS (1 gm tissue in 5 ml PBS). Appropriate dilutions of the supernatant were plated on TSA. CFU per wound was calculated by taking into account the dilution factor, volume of the tissue homogenate and then normalizing with tissue weight [182,205].

In order to compare the effect of multiple APDT with the other wound healing promoting treatments, in some of the diabetic mice, multiple applications of 0.5 % $AgNO_3$ (topical, thrice) [155, 214] were given during day 1-3 p.w or multiple (4 times) intraperitoneal aminoguanidine (AG) treatments were given 6 h prior to wound creation and during day 1-3 p.w. [ 215, 216] .

### 7.3.1 *Oxidative Markers and non enzymatic antioxidants assay of tissues*

Wounds of different groups were excised on day 3 p.w., weighed, snap frozen in liquid nitrogen and stored at -80$^{o}$C till use. All the assays were carried out within a month.

### 7.3.2 *Measurements on Thiobarbituric acid reactive substrate, Protein carbonyl contents of tissues*

Normal skin and wound were homogenized in phosphate buffer (pH 7.4). In the homogenates, the level of TBARS was carried out following method described in [217], with some modifications. Tissue supernatant (0.1 ml) of different groups was mixed with 0.5 ml of 5% (w/v) chilled trichloroacetic acid (TCA) and incubated for 30 min at room temperature following which ~0.5 ml of 0.67% (w/v) Thiobarbituric acid (TBA) was added. The reaction mixture was centrifuged at 1000 g for 15 min. Thereafter, the supernatant was collected and placed in a boiling water bath (95$^{o}$ C) for 10 min. The absorbance of pink color produced in different samples was measured at 535 nm in a spectrophotometer. Protein concentration was measured by BCA assay [160]. The TBARS content was calculated by using the molar extinction coefficient of 1.56 x $10^5$ $M^{-1}$ $cm^{-1}$ and expressed as nmol of TBARS per mg of protein [218].

The protein carbonyls in the tissue homogenates were measured according to the protocol described in [218, 219]. Briefly, 200 µl of the tissue supernatant, in 100 mM phosphate buffer was treated with 2 mM DNPH dissolved in 2N HCl, for 1 h. The TCA- precipitated proteins were washed with a mixture of ethanol-ethy acetate (1:1) to remove free DNPH. The DNPH- coupled carbonylated proteins were then measured spectrophotometrically at 366 nm. The PC concentration was calculated using a molar extinction coefficient of 22 x $10^4$ $M^{-1}cm^{-1}$using 22,000 t and expressed as mM/ mg protein.

### 7.3.3 *GSH level in wound tissue*

GSH level in skin and wounds was estimated by the method of Ellman [220] using a 96-well microplate assay [221]. Supernatants from homogenized tissues were deproteinated by adding 2.5 % TCA and the precipitate was removed by centrifugation (600 g, 10 min). To a 5 µl of the supernatant, 0.5 M sodium-phosphate buffer (pH=8.0) and then 5 mM Ellman's reagent were added. The samples were incubated for 30 min at room temperature followed by the absorbance measurements at 412 nm. The concentration of GSH in the samples was estimated using a standard curve of GSH prepared at concentration ranges of 0–1 mM and expressed as mmol/mg protein [221].

### 7.3.4 *Myeloperoxidase and neutrophil elastase assay*

Myeloperoxidase (MPO) activity in skin and wounds was measured spectrophotometrically by using 3,3', 5,5' -tetramethylbenzidine (TMB) as a substrate according to the protocol described in [222]. Briefly, the wounds were homogenized in 0.1 M phosphate buffer, pH 7.4. The homogenates were then centrifuged at 800 g for 5 min at 4ºC and the supernatants were decanted and stored , for use in neutrophil elastase (NE) assay. The pellets were resuspended in 1 ml 50 mM phosphate buffer containing 0.5% hexadecyltrimethylammonium bromide (HTAB). After three freeze-thaw cycles, the samples were briefly sonicated (20 kHz, 10 s, 4 times with gap of 10 s) on ice and incubated at 60°C for 2 hrs. The samples were centrifuged at 500 × g for 10 min, and the supernatants were transferred to 1.5 ml tubes. Aliquots of samples (50

μL) were placed in 1.5 ml centrifuge tubes with 500 μl assay buffer containing 0.1 M phosphate buffer, pH 5.4, 1% HTAB, 0.43 mg/ml TMB. The reaction was initiated by the addition of 50 μl 15 mM $H_2O_2$. After addition of the substrate, the kinetics of absorbance was measured at wavelength of 630 nm in an ELISA plate reader for 20 min period [223] at 50 second intervals. The slope of the linear portion of the OD graph denotes the change in OD per min (milli OD per min) . Using this slope value MPO activity was expressed as units per gram tissue weight, as an enzyme unit is defined as the amount of enzyme that produces an increase of 1 absorbance unit per min [222]**.**

NE activity was measured according to the protocol described in [224] using N-methoxysuccinyl-Ala-Ala-Pro-Val p–nitroanilide (Sigma Chemicals, US) as substrate. Briefly, supernatants of wound tissue homogenates was incubated at 37 °C for 24 h with 1 mM substrate prepared in 0.1 M Tris–HCl buffer (pH 8.0) containing 0.5 M NaCl and the amount of p-nitroanilide liberated was measured spectrophotometrically at 405 nm and NE activity was expressed as nmol/mg/24 h.

### 7.3.5 *Nitrite and VEGF-A measurements in wound tissue*

In wounds, during the inflammatory phase (day 3 p.w.) a peak NO level occurs which is mainly due to the migrated macrophages [4,7]. NO is rapidly oxidized to nitrite [225]. Therefore, nitrite level was measured in tissue homegnates of non diabetic as well as diabetic mice, according to the protocol described in [ 225]. For measurements on nitrite level, the tissues were first pulverized in liquid nitrogen with the help of mortar/ pestle. The tissue fragments were mixed (1; 5, w/v) with 0.1 M chilled

potassium phosphate buffer (pH 7.4), homogenized (3500 rpm, 5 min) and then sonicated at ~20 kHz, 10 s for 4 times, with gap of 10 s (Model CPX 130, Cole Parmer,US). Briefly, a 50 µl of tissue supernatant of each test sample was mixed with 50 µl of freshly prepared Griess reagent [0.1% N-(1-naphthyl)ethylenediamine dihydrochloride, 1% sulphanilamide and 5 % phosphoric acid in a 1:1:1 ratio] in 96 microwell plate and then the plate was incubated for 30 min at room temperature. The absorbance of the colored reaction product was measured at 550 nm using a microplate reader (Powerwave 340, Microtek, USA). Concentration of nitrate in samples was determined from the standard curve obtained by measuring the absorbance of known concentration of sodium nitrite (0- 500 µg/ml) and Griess reagent. The total protein content of the wound lysate was estimated by BCA assay [160], using BSA as standard. The nitrite values (µg nitrite/ml) of samples obtained, was normalized with protein concentration (µg/ml) and were expressed as µg nitrite /mg protein

Levels of VEGF-A in the wound tissue supernatant was estimated by following the protocol described in the ELISA kit (Sigma-Aldrich, USA). Briefly, the powdered tissues were mixed with lysis buffer provided along with the ELISA kit and kept on ice for 30 min. The lysates were sonicated by keeping on ice and then centrifuged (5000 rpm, 10 min, 4$^{o}$C).The supernatant was collected, divided into two aliquots. One aliquot was used for determination of VEGF-A by ELISA and the other aliquot was used for protein estimation by BCA [160]. For the determining total VEGF-A content, supernatants of tissue samples were diluted (1:1) with the sample diluent buffer and incubated in the capture antibody coated microwells provided along with the kit for 18h at 4$^{0}$C. Following the incubation, the assays were carried out

according to the protocol described in the kit and absorbance of the final product was recorded at 450 nm in a microplate reader (Powerwave 340, Mircotek). VEGF-A concentration (pg/ml) in the samples was calculated from the slope of the linear fit of the standard curve prepared using the absorbance values of the known concentrations of VEGF-A (10 pg - 10 ng/ml ) provided along with the kit and values obtained was normalized with the respective protein concentration of the tissue and expressed as pg VEGF-A/mg tissue protein.

### 7.3.6 *Masson's trichrome staining and Abramov Scoring*

In order to study the response of wounds to diabetes and infection, wounded tissues from mice of different groups excised on day 18 p.w. were fixed in 10 % neutral buffered formalin for 24 h, following which all the tissue sections were processed using a standard histological procedure. The deparafinized sections were processed for Masson's trichrome staining. The slides were examined under a microscope to determine tissue changes such as inflammation, reepithelialization, and arrangement of collagen fibers [99, 182, 203]. Scoring was carried out according to the Abramov scoring [226] with some modifications, as described in [227], by three individuals who were blinded to the sample groups and the time of wounding. In each microscopic slide the sections were scored on a scale of 0–3 for inflammatory cells (0 : no inflammatory cells, 1: scant , ~10 % of the total cells were inflammatory cells , 2 : moderate, ~20-50 % of the cells in each microscopic view are inflammatory cells, 3 : abundant, more than 50 % of the cells in each microscopic view are inflammatory cells) [100,226,227]. At least 15 microscopic views were scored per group. The

inflammatory scores of each group obtained by the individuals were averaged to obtain mean inflammation score.

### 7.3.7 *Statistical analysis*

Data were analyzed using Origin 8.5 scientific plotting software. The data were expressed as mean and SD. Statistical comparison between means was carried out using one way ANOVA. To quantify the correlation between the wound nitrite level and wound closure time, we used the regression coefficient 'R' from the linear regression analysis . $p<0.05$ were considered significant.

## 7.4 Results

### 7.4.1 *Effect of APDT on bacterial load of wounds of diabetic and non diabetic mice*

Figure 7.1 A shows bacterial load in wounds of diabetic mice assessed on day 3 p.w (24 h post APDT) after treating with two different concentrations of pl-cp6 and irradiated at a light fluence ~ 60 J/cm$^2$. Results show that APDT efficacy increases with increase in pl-cp6 concentration. In figure 7.1.B we show bacterial load in wounds assessed immediately (day 2 p.w.) and 24 h post APDT (day 3 p.w.) for the wounds of diabetic and non diabetic mice treated with 200 μM pl-cp6 and exposed to light at fluence of ~120 J/cm$^2$. The results show that although immediately after APDT the reduction in the bacterial load in the wounds of the non diabetic and diabetic mice, are comparable, at 24 h post APDT (day 3 p.w.), the wounds of diabetic mice show a much higher ($p < 0.05$) bacteria regrowth compared to that of

non diabetic mice. Bacterial regrowth is observed to vary with increase in glucose levels in diabetic mice. In the wounds of diabetic mice with blood glucose level >500 mg/dl the bacterial load increased by ~ 5 fold on day 3 p.w (fig 7.1 B).

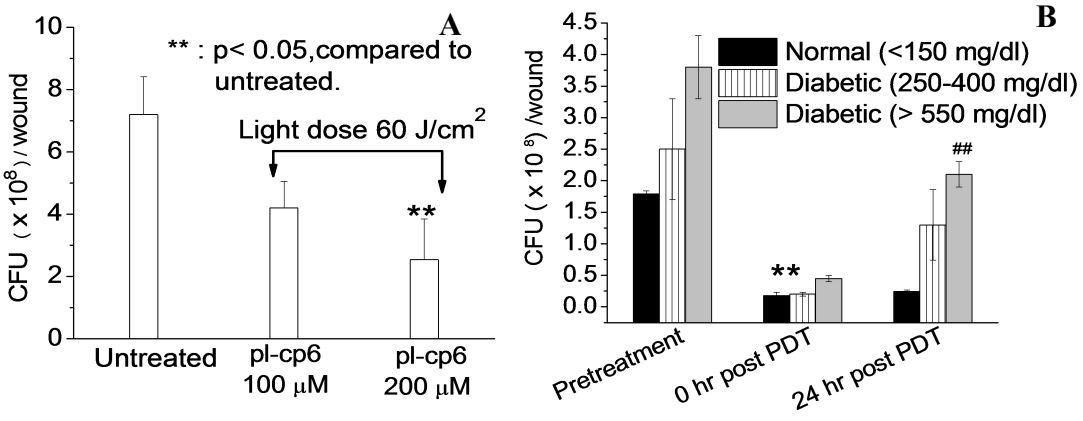


**Figure 7.1** (A) Effect of APDT induced by pl-cp6 and red light on bacterial load of wounds of diabetic mice as a function of pl-cp6 concentration. (B) Comparison of photobactericidal efficacy of APDT in wounds of diabetic and non diabetic mice. In non diabetic and diabetic mice, wounds were infected with ~$10^8$ and $10^7$ CFU MRSA, respectively. **: p <0.05 compared to respective pretreatment group . Data represent mean values of three different assays performed in 8 animals of non diabetic and diabetic group.

To further check whether higher regrowth of bacteria observed in photodynamically treated wounds of diabetic mice was due to high level of glucose in blood, we studied the effect of increasing glucose concentration in LB medium on bacterial growth. When glucose concentration was increased to 0.4 %, enhancement in growth of bacteria (fig 7.2 A) was marginal (~15 % higher OD).

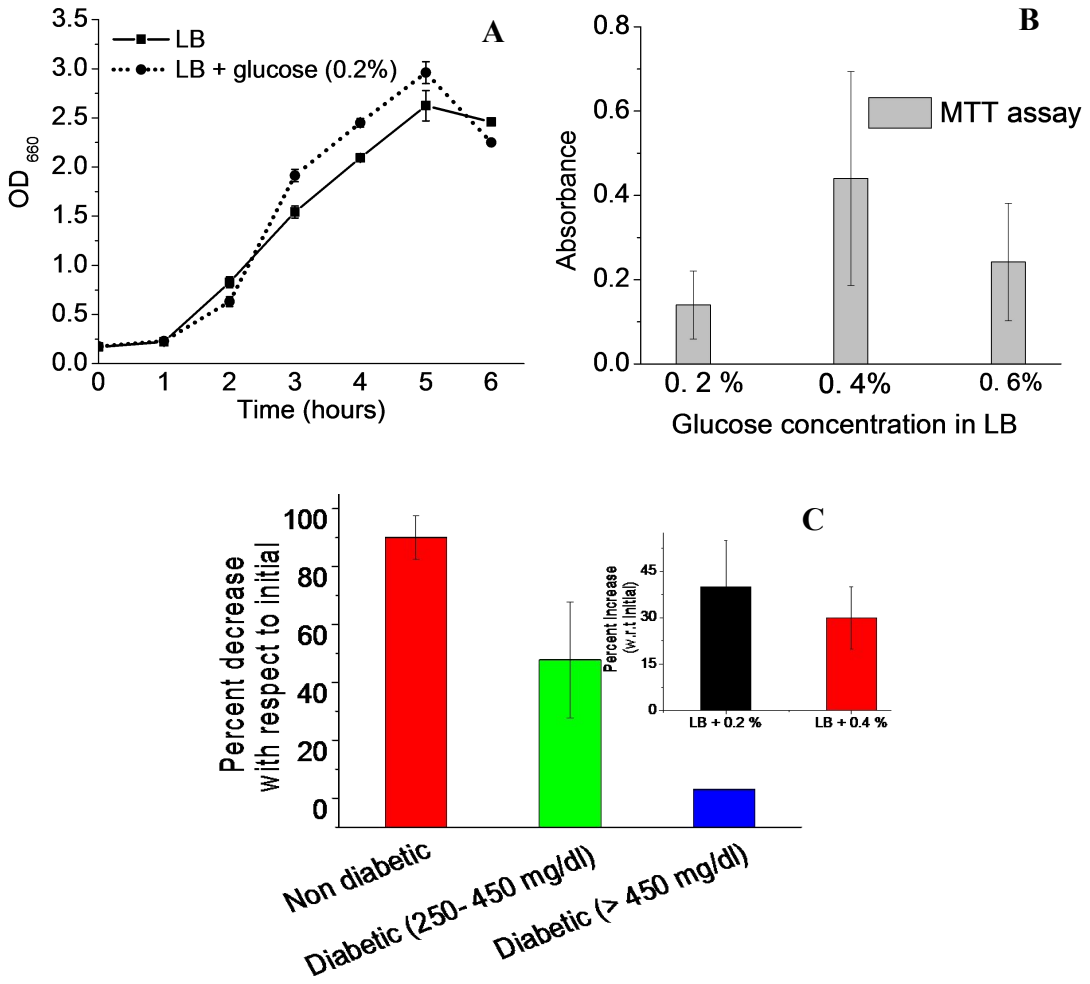


**Figure 7.2** Effect of glucose on MRSA growth in suspension culture (A) and biofim (B) Biofilms were grown in presence of LB medium containing different glucose concentration on fibrinogen coated polystyrene surface. (C) Bactericidal activity of blood from non diabetic and diabetic mice against ~$10^5$ CFU MRSA, represented as percent decrease in bacteria load with respect to (w.r.t) initial number. (Inset) Percent increase in bacteria number observed at 120 min incubation w.r.t initial number, in LB medium with different glucose concentrations. The data represent the mean values of 3 different experiments performed on 6 non diabetic and 6 diabetic mice (day 30 post STZ treatment) of each group.

Similarly, biofilm growth enhanced only by 10-15 % with increse in glucose concentration (fig 7.2 B). The PDT effect on bacteria grown in suspension and biofilms was also not different in presence and absence of 0.4 % glucose.

Neutrophils from diabetic patients have been shown to exhibit impaired bactericidal activity [206, 208]. To determine whether the leukocytes from STZ treated diabetic mice exhibit a similar decrease in bacteria killing capability, we studied the bactericidal action of blood derived from non diabetic and diabetic mice and compared with bacteria growth in LB alone and LB with 0.4 % glucose (fig. 7.2 C). Results showed that while the blood of non diabetic, moderately diabetic (glucose level 250-450 mg/dl) killed ~90 % and ~ 40 % MRSA, respectively, after 120 min, the bacterial counts in blood derived from highly diabetic mice (glucose level > 450 mg/dl), decreased by ~ 5 %. Also, it may be noted that when MRSA was incubated, in LB alone or LB with 0.4 % glucose for the same period, the growth of bacteria increased by ~ 40 % and ~35 %, respectively. To further verify whether the observed decrease in bactericidal effect of blood of diabetic mice with high glucose level was due to change in WBC counts, their number was enumerated in blood. In contrast to the expectation, the WBC count (2-3 x $10^6$/ml) of diabetic mice was ~10-15 % higher than the counts observed in case of non diabetic mice. These results suggested antibacterial defense capability of diabetic mice was much lower [213]. This could have resulted in increased bacteria regrowth in APDT wounds of diabetic mice with blood glucose level > 450 mg/dl.

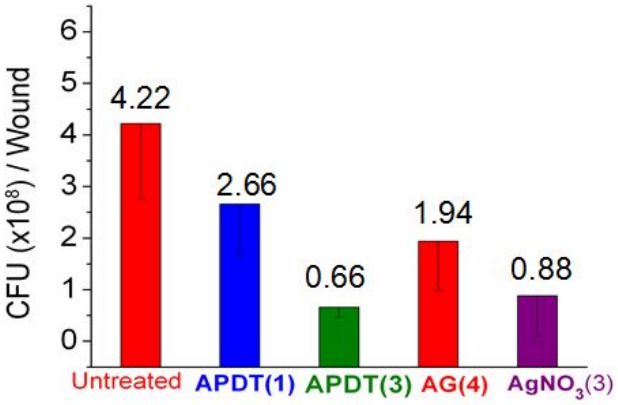


**Figure 7.3** Effect of multiple APDT (thrice), AG (4 times) and $AgNO_3$ (thrice) on bacterial load in wounds of diabetic mice with blood glucose level >500 mg/dl. Wounds were infected with ~ $10^7$ CFU/wound MRSA. Treatment frequency is indicated in parentheses.Topical APDT and $AgNO_3$ treatment were given on day 1-3 p.w. at 24 h intervals. AG treatment (intraperitoneal) was initiated 6 h before wound creation and continued for next 3 days at 24 h interval.

To reduce the regrowth of MRSA in wounds of diabetic mice, we investigated the effect of multiple APDT given during day 1-3 p.w. (figure 2.1) using light fluence ( ~ 60 J/cm$^2$) and compared the relative wound healing efficacy of multiple APDT with that of multiple treatment of AG and $AgNO_3$. AG was chosen because it is an inhibitor of AGE formation and is known to improve healing in diabetic conditions although it has no direct antibacterial action. $AgNO_3$ was selected because of its antibacterial property [155, 214]. Effect of these three treatments on bacterial load of wounds of diabetic mice is shown in figure 7.3. It is evident from the figure among all the treatments, multiple APDT of wound induced by 200 µM pl-cp6 and ~ 60 J/cm$^2$

red light was the most effective for inhibiting bacterial regrowth in wounds of diabetic mice.

| **Group** | TBARS (nmol/mg protein) | PC (nmol/mg protein) | GSH (mmol/mg protein) | MPO (U/gm) | NE (nmol/mg/24 hr) |
|---|---|---|---|---|---|
| Skin non diabetic mice | 0.4 ± 0.02 | 0.04 ± 0.005 | 0.15 ± 0.03 | 0.026 ± 0.002 | 154.5 ± 2.5 |
| Skin diabetic mice*** | 2.8 ± 0.2*** | 0.08 ± 0.003*** | 0.114 ± 0.01 | 0.12 ± 0.01*** | 93.41 ± 7.9 *** |
| Wound non diabetic mice | 0.51 ± 0.04 | 0.07 ± 0.004 | 0.27 ± 0.025 | 0.75 ± 0.06 | 889.1 ± 133.24 |
| Wound diabetic mice ** | 0.2 ± 0.02 | 0.06 ± 0.002 | 0.08 ± 0.02 ** | 1.6 ± 0.2 | 395 ± 11..9 |
| Wound non diabetic mice and PDT (~ 120 J/cm$^2$)* | 1.5 ± 0.2* | 0.085* | 0.43 ± 0.03 | 1.3 ± 0.3 | 1214 ± 36 |
| Wound diabetic mice and PDT ( ~120 J/cm$^2$ ) ## | 0.35 ± 0.01 | 0.076 ± 0.01 | 0.11 ± 0.012 | 0.7 ** | 394 ** |
| MRSA infected wound diabetic mice | 0.11 ± 0.004 | 0.025 ± 0.003 | 0.05 ± 0.01 | 11.3 ±1.3 | 288.5 |
| MRSA infected wound diabetic mice and PDT (thrice, ~ 60 J/cm$^2$) +++ | 0.3 ± 0.007 | 0.04 ± 0.01 | 0.08 | 25 ± 1.7 | 436.5 |

Table 7.1 Effect of APDT on oxidative events and inflammatory cell response of early wound healing phase [228]. *,##,++,+++ : $p < 0.005$ , one way ANOVA .

### 7.4.2 *Effect of APDT on oxidative markers level*

Effect of APDT on oxidative markers (TBARS, PC) and level of antioxidant (GSH) was studied in wounds of diabetic and non diabetic mice. The results presented in table 7.1 show that as compared to non diabetic mice, cutaneous tissues of diabetic mice have higher levels of oxidative markers, but lower levels of GSH. However,as compared to the wounds of non diabetic mice [228], in wounds of diabetic mice on day 3 p.w., levels of TBARS, PC and GSH were reduced considerably ($p < 0.05$, one way ANOVA). Infection of wounds of the diabetic mice was seen to result in a further reduction in the levels of PC, TBARS and GSH .

However, in response to APDT at a fluence of ~120 J/cm$^2$, PC, TBARS and GSH levels increased in both uninfected and infected wounds of non diabetic and diabetic mice. (Table 7.1). Levels of TBARS, PC and GSH in MRSA infected wounds of diabetic mice subjected to multiple APDT at fluence ~60 J/cm$^2$, were comparable to that of non diabetic mice skin. It should be noted that as compared with other treatments, multiple $AgNO_3$ treatment led to significant increase (~2 times) in TBARS level (0.35 nmol/mg). However, as compared to untreated control and photodynamically treated counterparts, ~ 30 % decrease in GSH level was observed in these wounds. At the same time, as compared to untreated controls, no significant change in the GSH (~0.042 mmol/mg) and TBARS (~0.13 nmol/mg) levels were observed in MRSA infected wounds of mice treated with AG.

### 7.4.3 *Effect of APDT on inflammatory cell sequestration level*

The level of inflammatory markers (MPO, NE) in skin and wounds of diabetic and non diabetic mice is shown in table 7.1. The results show that MPO levels in skin and wounds (uninfected and infected) of diabetic mice was higher than the levels observed in wounds of non diabetic mice. In infected wounds of both non diabetic and diabetic mice, MPO levels increased further with the values were higher for wounds of diabetic mice . However, compared to untreated controls, although APDT at fluence ~120 J/cm$^2$ led to significant increase in level of MPO in uninfected wounds of non diabetic mice, in the wounds of diabetic mice MPO level decreased significantly. Compared to untreated or pl-cp6 treated controls, MPO levels in infected wounds of diabetic mice subjected to multiple APDT at lower fluence (~60 J/cm$^2$) increased by a factor of ~ 2.5 ( table 7.1). In contrast, multiple $AgNO_3$ and AG treatment of MRSA infected wounds of diabetic mice, led to increase in MPO levels by factors of ~5 and ~ 3 , respectively.

Our investigations on the NE level in wounds show that as compared to the level observed in skin and wounds of non diabetic mice, in diabetic mice, NE level was reduced ~2 times. Infection in wounds lowered the levels of NE further. In wounds subjected to APDT, NE level was higher compared to their respective untreated control or only pl-cp6 treated control (table 7.1).

### 7.4.4 *Effect of APDT on total nitrite content and VEGF-A level of wounds*

It is known that levels of NO and VEGF-A are reduced in diabetes [7] and studies have shown that low levels of ROS can upregulate both NO and VGEF-A levels [212]. Therefore, we assessed the effect of APDT on NO and VEGF-A level of wounds. In table 7.2 we show comparison of the level of NO and VEGF-A in wounds of non diabetic and diabetic mice. The level of NO in wounds of diabetic mice was considerably reduced (~ 4-5 times). MRSA infection led to further reduction in the NO level in diabetic mice, However, APDT of wounds led to increase in levels of both NO and VEGF-A (table 7.2.).

| Sample | VEGF-A (pg) / mg protein | Nitrite ( µg) /mg protein |
|---|---|---|
| | Mean ± S.D. | Mean ± S.D. |
| Wound non diabetic mice | 3634.5 ± 160 | 20.5 ± 1.4 |
| Wound Diabetic mice ** | 2024 ± 73.5 | 4.37 ± 0.8 |
| Wound non diabetic mice and APDT (~60 J/cm$^2$) * | 4090.5 ± 49 | 17.6 ± 0.9 |
| Wound Diabetic mice and APDT ( ~60 J/cm$^2$ ) ## | 3593 ± 94 | 16.7 ± 2 |
| MRSA infected wound diabetic mice | 2437 ± 224 | 2.9 ± 0.2 |
| MRSA infected wound diabetic mice and APDT (thrice, ~60 J/cm$^2$) +++ | 3637 ± 322 | 6.7 ± 0.9 |

**Table 7.2** Effect of APDT on VEGF-A and nitrite level of wounds on day 3 p.w.

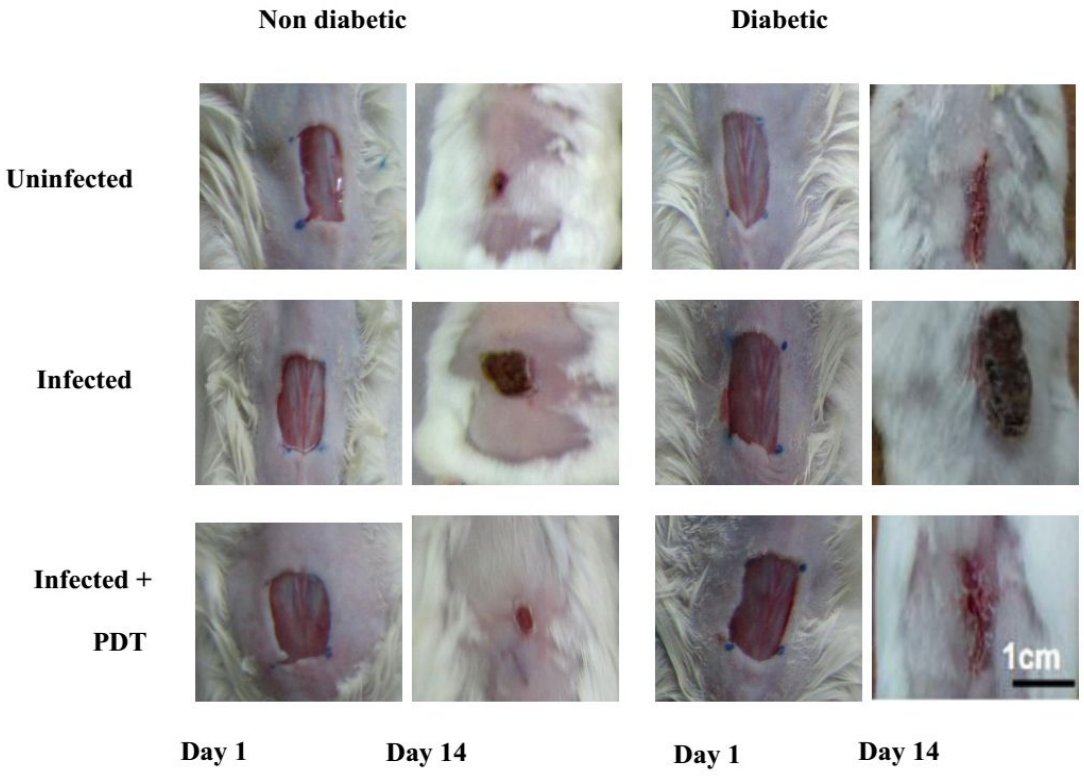


**Figure 7.4** Effect of APDT on wound closure.

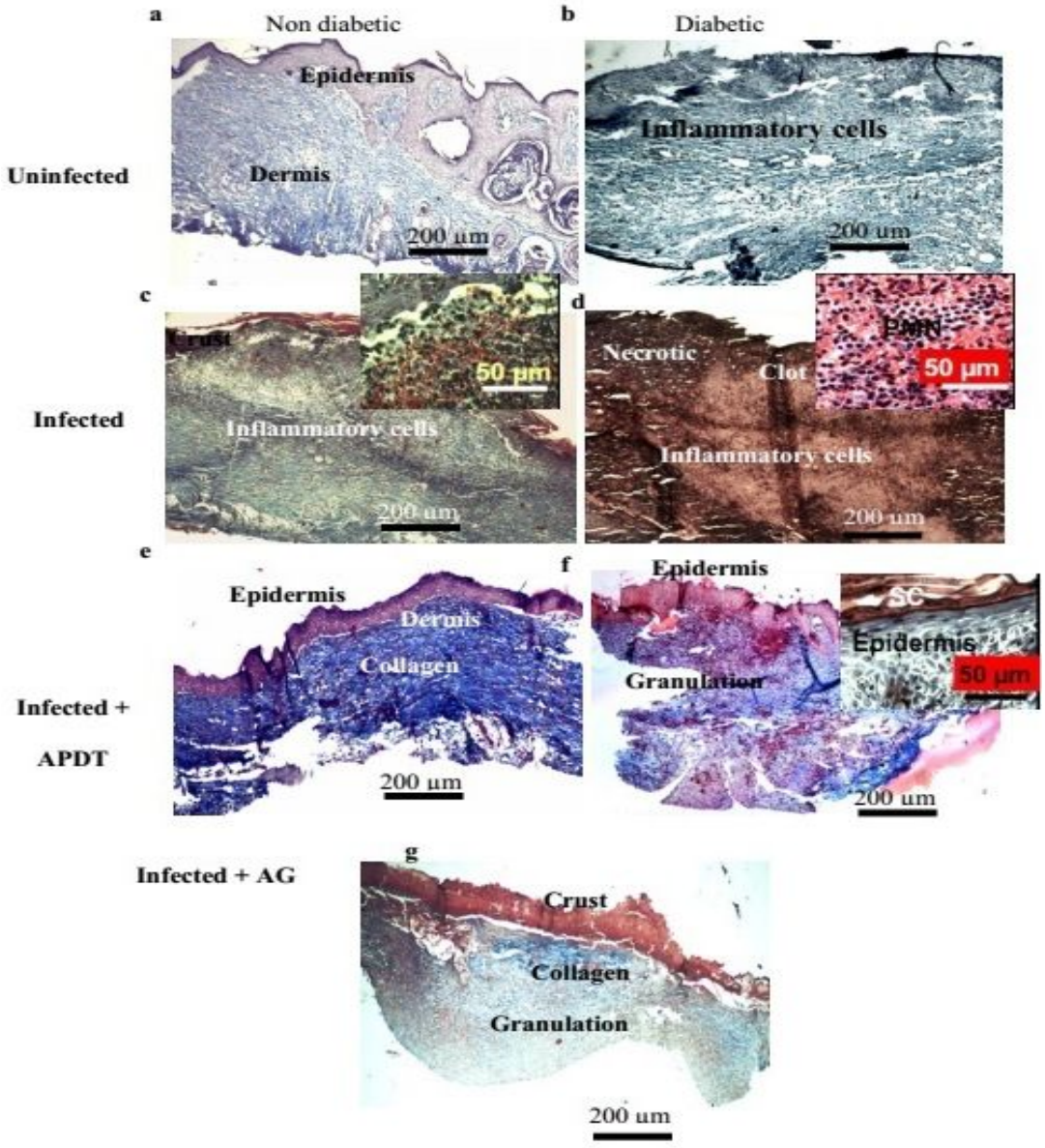


**Figure 7.5** Photomicrograph of Masson's trichrome stained deparafinized sections of wounds of non diabetic (a, b, e) and diabetic mice (c, d, f) excised on day 18 p.w., respectively. Panels; (a, c) uninfected wounds, (b, d); infected untreated wounds; (e), infected wounds of non diabetic mice treated with pl-cp6 and exposed to light fluence of ~ 120 J/cm$^2$ ; (f) infected wounds of moderately diabetic mice exposed to single APDT fluence of ~ 120 J/cm$^2$ ; g: AG treated wounds. SC : Stratum corneum. PMN : polymorphonuclear leukocytes.

The results presented in table 7.2 show that VEGF-A level is reduced considerably in wounds of diabetic mice. However, following APDT treatment their level was increased by ~ 60 % in both uninfected and infected wounds of diabetic mice on day 3. It may be noted that the enhancement in VEGF-A level was better in wounds of diabetic mice wounds as compared to non diabetic animals.

We also compared the effects of multiple APDT with multiple AG and $AgNO_3$ treatments for MRSA infected wounds of high diabetic mice. Further, as compared to the level observed in untreated wounds, while the wounds treated with APDT and AG showed ~3 and ~2 times increase in the NO level, the wounds treated with $AgNO_3$ exhibited no significant change in NO.

### 7.4.5 *Effect of APDT on healing response of MRSA infected wounds of diabetic mice*

In figure 7.4 we show the morphology of wound. The histomicrographic features of the wounds excised on day 14 p.w (non diabetic) and day 18 p.w (diabetic) are shown in fig. 7.5 and the semi quantitative scores on inflammation obtained following Abramov scoring pattern, are shown in table 7.3.

| Experimental group | | Inflammation score |
|---|---|---|
| Non diabetic mice (blood glucose < 150 mg/dl) | Uninfected wounds | 0.4 ± 0.06 |
| | Untreated infected wounds | 1.26 ± 0.18 |
| | Infected wounds and APDT (pl-cp6 and ~ 120 J/cm$^2$, once) | 0.75 ± 0.33** |
| Diabetic mice (blood glucose 250-450 mg/dl) | Uninfected wounds | 1.2 ± 0.3 |
| | Untreated infected wounds | 2.5 ± 0.29 |
| | Infected wounds and APDT (pl-cp6 and ~ 120 J/cm$^2$, once) | 1.75 ±0.25## |
| Diabetic mice (blood glucose > 450 mg/dl) | Untreated infected wounds | 2.8 ± 0. 3 |
| | Infected wounds and multiple APDT (pl-cp6 and ~ 60 J/cm$^2$, thrice) | 1.5 ± 0.3++ |
| | Infected wounds and AG (4 times (100 mg/kg, i.p.) | 2.1 ± 0.34*** |

**Table 7.3** Effect of APDT on inflammatory cells level, as scored by Abramov histological scoring method. The data represent mean ± SD.**,##,++ : $p < 0.05$ compared to untreated wounds (one way ANOVA). ***: $p > 0.05$ compared to untreated infected wounds.

While the uninfected wounds of non diabetic mice show complete healing on 14$^{th}$ day p.w, as evidenced by completely formed epithelium layer and ordered collagen fibers (fig. 7.5 a), the healing in uninfected (fig. 7.5 b) wounds of diabetic mice and all the infected wounds was compromised. In the infected wounds of non diabetic mice on day 14 p.w (fig. 7.5 c), one could observe random deposition of collagen fibers along

with higher numbers of immune cells and incomplete reepithelialization (table 7.3). For the infected wounds of diabetic mice, even on day 18 p.w, a thick abscess, higher number of inflammatory cells, necrotic regions and complete lack of collagen fibers were observed (fig. 7.5 d). APDT at a fluence of ~120 J/cm$^2$ led to complete healing of the infected wounds of non diabetic mice, on day 14 p.w (fig. 7.5 e). However, for infected wounds in diabetic mice, the outcome was observed to depend on blood glucose level. While in moderately diabetic mice (fig. 7.5 f), there was partial recovery as suggested by presence of moderate inflammatory cells(table 7.3), in highly diabetic mice single APDT did not lead to significant improvement in wound repair outcome. However, multiple APDT at fluence of ~60 J/cm$^2$, led to better healing response , also evident in the results presented in table 7. 3. In MRSA infected wounds of high diabetic mice subjected to multiple AG treatment, (fig. 7.5 g), much lesser inflammatory exudates ( table 7.3) were observed. Further, the results presented in figure 7.6 which show a correlation between NO and wound closure times suggest that wound closure time decreases with increase in NO level of wounds.

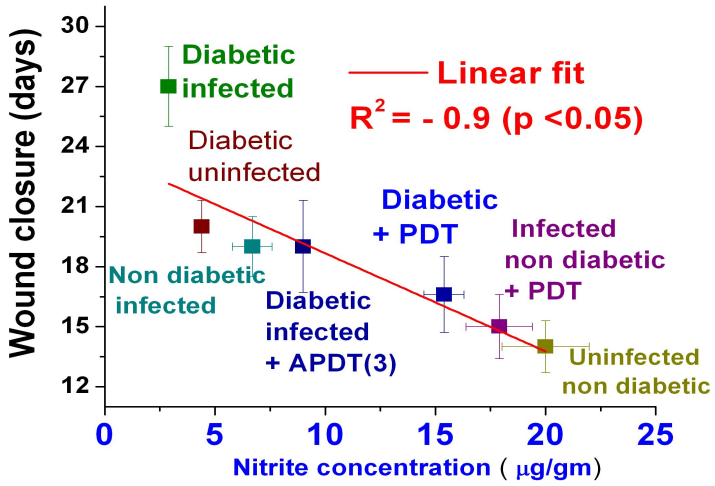


**Figure 7.6** Correlation of wound closure (days) with wound NO level. NO level was ascertained by measuring nitrite level. The data points and error bars represent mean and SD, respectively.

## 7.5 Discussion

The objective of this study was to evaluate the use of APDT for infected wounds of diabetic mice. In this respect, it is known that hyperglycemia and oxidative stress can directly activate cell adhesion molecules, pro and anti-inflammatory molecules, VEGF signaling, inflammatory cell sequestration and neutrophil degranulation. In this study, we therefore emphasized on the possible effects of APDT on cellular response of wound healing like oxidative events, inflammatory and angiogenesis in addition to studying the photobactericidal effect.

The results presented in figures 7.1 B and table 7.1 show that though there is higher inflammatory cells in wounds of diabetic mice, the bacterial load in untreated wounds of diabetic mice is higher than the non diabetic mice and shows dependence on blood

glucose level. Our data are consistent with the reduction in bactericidal effect observed in the blood drawn from the diabetic mice (fig. 7.1 C) as well as the reduced levels of oxidative markers TBARS, PC and NE observed in wounds of diabetic mice (table 7.1). These data are in accordance with previous studies wherein it has been shown that in diabetes, despite of increased inflammatory cell migration [229] there is impaired oxidative burst [207-209, 229, 230] , reduced superoxide [224], NE [231] and NO production by inflammatory cells [7, 21, 22, 202, 232]. One of the reasons for the decreased oxidative markers levels could be depletion of NADPH [207, 232], the latter being a cofactor for NAPDH oxidase, i-NOS and glutathione reductase [232]. The other reason for decreased GSH and NO in wounds could be the fact that during diabetes, persistent hyperglycemia can cause increased production of free radicals and oxidative stress via autoxidation of glucose and also via glycation of nonenzymatic proteins [212]. It has also been demonstrated that decreased glutathiolation of cellular proteins is also related to decreased NO availability in diabetic rats [232]. We also observed that compared to non diabetic mice, in cutaneous tissue of diabetic mice there are higher levels of oxidative stress markers but decreased level of antioxidants.

In infected wounds, compared to the uninfected wounds, there is a further decrease in levels of oxidants and NE levels despite of increased MPO level. This may be because of the *S.aureus* toxin mediated apoptotic cell death response in macrophages [233-235], which are potential source of ROS and NO[7]. Increased MPO level in infected wounds suggests prolonged presence of phagocytosis defective neutrophils in the wounds [43, 207, 209, 236]. One would presume that even in absence of functional phagocytosis of bacteria by neutrophils of diabetic mice, the released MPO can directly bind and kill extracellular bacteria or form neutrophil/macrophage

extracellular traps (NET/MET) [237, 238]. However, bacterial killing by MPO or by NET/MET would require an optimum level of oxidants as well as NE. Therefore, the increase in MPO alone is not of much significance and there is a higher bacterial growth in wounds of diabetic mice, causing further sequestration of higher number of phagocytosis defective neutrophils to wounds. This delays the arrival of macrophages and inflammation resolution at the wound site. The impaired inflammation resolution processes lead to elevated proinflammatory cytokines levels in the wound, which may interfere further with the cellular signaling of neutrophils [42], inducing either a delayed apoptotic response [43] or necrotic response [44]. All these processes culminate in release of more and more proteases in wounds that could induce apoptosis of host cells, delay collagen remodeling and wound repair [46], evidenced by the presence very high number of neutrophils even on day 18 p.w. in the histology images of infected wounds , in our study .

Results presented in figure 7.1 A shows that although pl-cp6 mediated single APDT (~ 120 J/cm$^2$) reduced bacteria load by ~ 1.5 log in wounds, high bacteria regrowth was observed in wounds of diabetic mice with glucose level > 450 mg/dl. This is not solely because of the reduced immune cell functions. The observed decrease in MPO level indicates that PDT could have caused oxidative damage to the inflammatory cells [201]. Since, bacterial phagocytosis by the immune cells is crucial for complete elimination of the pathogens post treatment, the decrease in MPO level in wounds combined with the high level of oxidative stress and the already reduced NE levels might have contributed to bacterial regrowth, elicit a prolonged neutrophil presence which would further augment inflammation and tissue damage. In addition, the reduced inflammatory cell content at the early inflammation phase is also a signal for

suboptimal response in the release of critical growth stimulatory signals necessary for neovascularization, epithelialization, keratinocyte migration and proliferation at the later stages [239]. Therefore, the reduced MPO indicate that the high fluence APDT not only affects the inflammation but also other cellular response. The higher inflammation, incomplete reepithelialization (fig. 7.5 f, table 7.2) and delayed wound closure (fig. 7. 4, 7.5 B) observed in wounds subjected to APDT fluence of ~120 J/cm$^2$ are suggestive of the delay in wound closure response.

Data presented in this study (fig. 7.3) show that bactericidal effect is better in wounds subjected to multiple APDT than the wounds subjected to single APDT. This could be due to enhanced inflammatory cell sequestration and lower damage to these cells due use of lower light fluence for PDT. This contention was consistent with the enhancement in levels of MPO and NE observed in these wounds as compared to single APDT group. This increased inflammatory cell sequestration can arise due to the PDT induced destruction of *S.aureus*, its toxins and release of bacterial cellular contents like DNA [240]. Indeed, it has been reported that bacterial products such as DNA, LPS, flagella, pilli, can elicit inflammatory and antimicrobial response [43]. Improvement in MPO, NE levels can also arise due to PDT induced ROS generation [237, 238], leading to increased permeability of the azurophilic granules to cations [241], dissociation of the glycosaminoglycans bound NE [237]. Increase in NE, MPO will help in infection resolution as these two enzymes are part of the antibacterial defense mechanisms like NET/MET [237]. Our data in fact suggest a new way by which PDT can also lead to generation of enhanced antibacterial response which could have contributed to faster inflammation resolution, reepithelialization and wound closure (fig. 7.4 A) observed for the multiple APDT group. In addition, our

results show multiple APDT also led to increase in GSH levels of wounds. The observed increase in level of GSH of wounds because of APDT are qualitatively similar to the effects of AGE inhibitor [216], plant extracts [242] and growth factor treatment [243]. This is also expected to benefit wound repair outcome, because GSH is known to reduce MMP / TIMP leading to timely extracellular matrix production, possibly via redox dependent signaling [5] or increase in proliferation response [6,7].

Our results on APDT induced inflammatory reaction are consistent with the results of previous studies [201] where the use of APDT for treatment of MRSA infection induced arthritis in mice was investigated. In the study, while APDT carried out at very low fluence (~5 or 20 J/cm$^2$) was observed to lead to insufficient bacteria inactivation, high fluence (~120 and 160 J/cm$^2$) resulted in synovial microvessls damage, reduced neutrophil accumulation and higher bacterial regrowth. The best outcome (high inflammatory cell sequestration to the infected site and low bacteria load) was obtained at a moderate light fluence of ~50 J/cm$^2$. In this context, our results suggested that use of an optimum fluence can also contribute to inflammation response.

The results presented in this study (table 7.2) also showed that level of both the angiogenic markers (NO, VEGF-A) in the wounds of diabetic mice are significantly lowered compared with that of non diabetic mice. This may be due to impairment of iNOS activity due to hyperglycemia induced depletion of NADPH [244,245]. Reduced NO and VEGF levels observed in infected wounds is suggestive of the delay in onset of proliferation phase of wound healing. It is known that *S. aureus* infection can delay angiogenesis [77] by inducing prolonged presence of neutrophils [236,246],

apoptosis in macrophages [247], which reduces NO levels as well as downregulates VEGF signaling [248], and reduced VEGF stability in the wound environment [77]. The enhancement in angiogenic markers VEGF-A and NO observed in infected diabetic mice in response to multiple PDT, could have occured due to higher macrophage recruitment to the wound site as a result of inactivation of *S. aureus* toxins such as the alpha toxins and other proteases This would result increased NO production. The other possible explanations for increased NO level in wounds due to PDT may be activation of i-NOS [3], oxidative denitrosylation of proteins [249]. It is also possible that ROS induced by PDT may regulate VEGF signaling, which in turn can operate in a feedback loop to increase NO production [5-7] via i-NOS upregulation.

Our results of the studies carried out to compare the efficacy of multiple APDT with $AgNO_3$ and AG treatment on wound healing suggest that APDT has better healing enhancing response in diabetic mice. This is evident from the fact that though, AgNO3 caused a comparable reduction in bacterial regrowth in bacteria in wounds of diabetic mice, the oxidative damage to wounded tissue was enhanced as indicated by significant enhancement in TBARS and reduction in GSH level. Although, multiple intraperitoneal AG treatment (4 times) leads to reduced bacteria load and enhanced NO level, the bactericidal effect of AG was not comparable to wounds subjected to multiple APDT (fig. 7.3) in diabetic mice. This may be because, although AG promotes the migration and respiratory burst of neutrophils [216], has no direct bactericidal action. In addition, the response of AG is slow which is evident from the fact that infected wounds of diabetic mice that received AG treatment, showed higher inflammatory infiltrates on day 18 p.w. (table 7.3), compared to that of the wounds

subjected to APDT. Our results suggest that for diabetic animals with blood glucose >550 mg/dl , APDT could be better options as this approach reduces the bacterial regrowth considerably and also increases the NO, GSH level. However, the levels of inflammatory cells (table 7.3) in photodynamically treated wounds are still higher than that of uninfected counterparts. This is because though APDT causes local alterations in wound healing biomarkers, the systemic abnormalities in case of diabetes like reduced bactericidal action of neutrophils/macrophages still persists. Therefore, a possible combined approach like use of AG or NO donor [21, 22] alongwith low fluence APDT ensuring optimum inflammatory, proangiogenic and collagen remodeling response may be more useful for management of infected wounds in diabetes.

## 7.6 Conclusion

APDT induced by pl-cp6 causes inactivation of MRSA in wounds of moderately diabetic mice. Further, PDT efficacy can be improved in wounds of diabetic mice with blood glucose level > 550 mg/dl by treating wounds with multiple fluences of APDT without affecting inflammatory cell sequestration and function. Results of this study also suggest that apart from inactivating bacteria, APDT may contribute to healing of the wound tissue by increasing proangiogenic response and recruitment of inflammatory cells. In addition, APDT induced alteration in non enzymatic antioxidants may help in faster closure of healing of wounds of diabetic mice.

# 8. Summary and future scope

## 8.1 Summary

The main objective of thesis was to investigate the photo bactericidal efficacy of poly lysine conjugate of chlorin p6 (cp6) and to explore its use for photodynamic treatment of bacteria infected wounds in normal and diabetic mice. Cp6 is a chlorophyll derivative which possesses many characteristics of an ideal PS such as (i) high triplet yield which is important for ROS generation (ii) a strong absorbance in the red region to minimize the energy deposition in host tissue. However, to improve bactericidal efficacy of cp6 which is anionic in nature poly-L-lysin a cationic peptide was conjugated. The important findings of the present thesis can be summarized as follows:

1. Studies on phototoxicity of cp6 and pl-cp6 on MRSA (Gram positive), *P. aeruginosa* (Gram negative) showed that conjugation of cp6 with pl-cp6 led to significant enhancement of photobactericidal efficacy for MRSA and *P. aeruginosa* which were resistant to photoinactivation with cp6.

2. Studies carried out on the mechanism of bacterial cell damage induced by APDT mediated by cp6, pl-cp6 and a standard phenothiazinium, toluidine blue O (TBO) on *S. aureus* and *P.aeruginosa* by using AFM showed that cp6 treatment did not result in significant morphological alterations in bacteria. For *S.aureus* and *P. aeruginosa,* APDT mediated by both TBO and pl-cp6 resulted in a significant reduction in the mean cell height, flattening of Gram negative bacteria

(*P.aeruginosa, E.coli*) suggesting damage to the bacterial membrane and reduction of cell volume due to the loss of cytoplasmic materials. For *S.aureus,* the change in morphology observed subsequent to APDT mediated by TBO and pl-cp6 was significantly different. While the major effect of TBO mediated APDT was breakage in the contact between the cell wall and the membrane, pl-cp6 mediated APDT resulted in damage primarily to outer peptidoglycan layer.

3. Studies on the effect of pl-cp6 mediated topical APDT on healing of *P.aeruginosa* infected wounds showed that at 96 h post APDT (day 5 p.w.), inflammatory cytokines like IL-6 and TNF-α were reduced significantly in addition to decrease in bacterial load (~1.5 log). This suggested that reduction in hyperinflammatory response in wounds contribute to faster healing of wounds.

4. Effect of pl-cp6 mediated topical APDT on collagen remodeling response of MRSA and *P. aeruginosa* infected wounds studied by using PSOCT as well as by measurements on hydroxyproline content and MMP-8,-9 level in wounds showed that APDT restored collagen remodeling in bacteria infected wounds of mice by attenuating excessive MMP-8/9 levels. This also enhanced epithelial layer migration, hydroxyproline content, and collagen fibril arrangement.

5. Effect of APDT studied in MRSA infected wounds of diabetic mice showed a light fluence dependent decrease in bacteria and healing response. While the use of higher fluence of ~120 J/cm $^2$ led to higher oxidative stress and bacteria regrowth 24 h post APDT, a multiple APDT with lower fluence of ~ 60 J/cm$^2$ showed a better response in terms of decreased bacteria regrowth, increase in the levels of antioxidants and proangiogenic molecules such as NO and VEGF-A. These

observations suggested that multiple APDT with lower fluence may be more effective in controlling bacterial growth and reducing host cell damage as well as inflammatory cell sequestration and granulation in wounds. In summary, studies carried out in the thesis demonstrate that APDT enhance the growth factor levels which is essential for healing of diabetic wounds.

## 8.2 Future scope

The work presented in the thesis show the potential of pl-cp6 mediated APDT for applications in wound healing. Futher research may be aimed at addressing following points.

- For clinical application, suitable formulation for photosensitizer such as use of gel matrix like collagen may improve the efficacy of PS by protecting the conjugate from degradation in chronic wounds rich with proteases.
- Recent clinical studies suggest that Low level light therapy (LLLT) can promote healing in infected foot ulcers of diabetic patients after the bacteria load is brought down to a manageable level by antibiotic treatment. Therefore, use of APDT to reduce antibiotic resistant bacteria load prior to LLLT should be a explored for management of wound healing in diabetes.

# 9. References


[1]. S. Enoch, D.J. Leaper, "Basic science of wound healing.Surgery." (Oxford). **26**, 31–37 (2008).

[2]. A.J. Singer, R.A. Clark, "Cutaneous wound healing." N Engl J Med. **341**, 738–746 (1999).

[3]. A.S. Weyrich, G.A. Zimmerman, "Platelets: signalling cells in the immune continuum." Trends Immunol. **25**, 489–495 (2004).

[4]. S.A. Eming, T. Krieg, J.M. Davidson,"Inflammation in wound repair: molecular and cellular mechanisms." J Invest Dermatol. **127**, 514–525(2007).

[5]. C.K. Sen, S. Roy,"Redox signals in wound healing," Biochim Biophys Acta. **1780**, 1348-1361(2008).

[6]. P. Bao, A. Kodra, M. Tomic-Canic, M.S. Golinko, H.P. Ehrlich, H. Brem, "Role of VEGF during wound healing." J Surg Res.**153**, 347-358 (2009).

[7]. M.B. Witte, A. Barbul, "Role of nitric oxide in wound repair." Am J Surg. **183**, 406-412 (2002).

[8]. W.K. Stadelmann, A.G. Digenis, and G.R. Tobin "Physiology and healing dynamics of chronic cutaneous wounds." Am J Surg. **176** (Suppl 2A):26S -38S (1998).

[9]. G. Henry and W.L. Garner, "Inflammatory mediators in wound healing." Surg. Clin. N. Am. **83**, 483-507 (2003).

[10]. S. Werner and R. Grose, "Regulation of wound healing by growth factors and cytokines." Physiol Rev. **83**, 835-870 (2003).

[11]. B.A. Mast and G.S. Schultz, “Interactions of cytokines, growth factors, and proteases in acute and chronic wounds.” Wound Rep Reg. **4**, 411-420(1996).

[12]. B. Douraiswami, P.K. Dilip, B.N. Harish, M.C. Jagdish, “Reactive protein and interleukin-6 levels in the early detection of infection after open fractures.” J Orthop Surg (Hong Kong). **20**, 381-385(2012).

[13]. Y. Han, T. Tuan, M. Hughes, H. Wu, and W.L. Garner, “Transforming growth factor-beta and tumor necrosis factor- alpha mediated induction and proteolytic activation of MMP-9 in human skin.” J Biol Chem. **276**, 22341-22350 (2001).

[14]. A.M. Manicone , J. K. McGuire, “Matrix metalloproteinases as modulators of inflammation.” Semin Cell Dev.Biol. **19**, 34–41(2008).

[15]. E.A. Rayment, Z. Upton, G.K. Shooter, “Increased matrix metalloproteinase-9 (MMP-9) activity observed in chronic wound fluid is related to the clinical severity of the ulcer.” Br J Dermatol. **158**, 951-961( 2008).

[16]. M. S. Hayden, S. Ghosh, “Shared principles in NF-kappa B signaling,” Cell. **132,** 344-362 (2008).

[17]. G. Gloire, S. Legrand-Poels, J. Piette, “NF-kappaB activation by reactive oxygen species: fifteen years later.” Ochem Pharmacol. **72**, 1493-1505(2006).

[18]. T.N. Demidova-Rice, M.R. Hamblin, I.M. Herman, “Acute and impaired wound healing: pathophysiology and current methods for drug delivery, part 1: normal and chronic wounds: biology, causes, and approaches to care.” Adv Skin Wound Care. **25**, 304-314 (2012).

[19]. F. Xu, C. Zhang, D.T. Graves, “Abnormal Cell Responses and Role of TNF-α in Impaired Diabetic Wound Healing.” Biomed Res Int. **2013**, 754802(2013).

[20]. H. Brem, M. Tomic-Canic, “Cellular and molecular basis of wound healing in diabetes.” J Clin Invest. **117**, 1219-1222(2007).

[21]. M.R. Schäffer, U. Tantry, P.A. Efron, G.M. Ahrendt, F.J. Thornton, A. Barbul. “Diabetes-impaired healing and reduced wound nitric oxide synthesis: a possible pathophysiologic correlation.” Surgery. **121**, 513-519 (1997).

[22]. M.B. Witte, F.J. Thornton, U. Tantry, A. Barbul. “L-Arginine supplementation enhances diabetic wound healing: involvement of the nitric oxide synthase and arginase pathways.” Metabolism. 5**1**, 1269-1273(2002).

[23]. R.D. Wolcott, D.D. Rhoads, S.E. Dowd. “Biofilms and chronic wound inflammation.” J Wound Care, **17**, 333-341(2008).

[24]. T. Okamoto, T. Akaike, M. Suga, S. Tanase, H. Horie, S. Miyajima, M. Ando, Y. Ichinose, H. Maeda, “Activation of human matrix metalloproteinases by various bacterial proteinases.” J Biol Chem. **272**, 6059–6066(1997).

[25]. K. Iwatsuki, O. Yamasaki, S. Morizane, T. Oono, “Staphylococcal cutaneous infections: invasion, evasion and aggression, a review.” J Dermatol Sci **42**, 203–214 (2006).

[26]. D.J.Harrington, “Bacterial collagenases and collagen-degrading enzymes and their potential role in human disease.” Infect. Immun. **64,** 1885–1891(1996).

[27]. R. Rao, S. Sumathi, K. Anuradha, D. Venkatesh, S. Krishna, “Bacteriology of postoperative wound infections.” Int J Pharm Biomed Res. **4**, 72-76(2013).

[28]. H.K. Kim, V. Thammavongsa, O. Schneewind, D. Missiakas, “Recurrent infections and immune evasion strategies of Staphylococcus aureus.” Curr Opin Microbiol**. 15**, 92-99(2012).

[29]. D. Kraus, A. Peschel, “Staphylococcus aureus evasion of innate antimicrobial defense.” Future Microbiol. **3**, 437-451(2008).

[30]. S.A. Grimble, T.R. Magee, R.B. Galland, “Methicillin resistant Staphylococcus aureus in patients undergoing major amputation.” Eur J Vasc Endovasc Surg. **22**, 215–218(2001).

[31]. N. Tentolouris, E.B. Jude, I. Smirnof, E.A. Knowles, A.J. Boulton, “Methicillin resistant Staphylococcus aureus: an increasing problem in a diabetic foot clinic.” Diabet Med. **16,** 767–71(1996).

[32]. A. Wagner, H. Reike, B. Angelkort, “Highly resistant pathogens in patients with diabetic foot syndrome with special reference to methicillin-resistant Staphylococcus aureus infection.” Dtsch Med Wochenschr. **126**, 1353–1356(2001)

[33]. P.D. Lister, D.J. Wolter, N.D. Hanson, ”Antibacterial resistant Pseudomonas aeruginosa: clinical impact and complex regulation of chromosomally encoded resistance mechanisms.” Clin Microbiol Rev, **22** , 582-610(2009).

[34]. M. Muller, Z. Li, P.K. Maitz, “Pseudomonas pyocyanin inhibits wound repair by inducing premature cellular senescence: role for p38 mitogen-activated protein kinase.” Burns. **35**, 500-508(2009).

[35]. L.W. Heck, K. Morihara, W.B. McRae and E.J. Miller, “Specific cleavage of human type III and IV collagens by Pseudomonas aeruginosa elastase.” Infect Immun. **51**, 115–118(1986).

[36]. D. Wildeboer, K.E. Hill, F. Jeganathan, D.W. Williams, A.D. Riddell, P.E. Price, D.W. Thomas, P. Stephens, R.A. Abuknesha, R.G. Price,“Specific protease activity indicates the degree of Pseudomonas aeruginosa infection

in chronic infected wounds." Eur J Clin Microbiol Infect Dis. **31**, 2183-2189 (2012).

[37]. A. Jahoor, R. Patel, A. Bryan, C. Do, J. Krier, C. Watters, W. Wahli, G. Li, S.C. Williams, K.P. Rumbaugh, " Peroxisome proliferator-activated receptors mediate host cell proinflammatory responses to Pseudomonas aeruginosa autoinducer." J Bacteriol. **190**, 4408-4415(2008).

[38]. G.R. Cornelis, "The type III secretion injectisome." Nat Rev Microbiol **4**, 811-825(2006).

[39]. S.R. Schooling, T.J. Beveridge, "Membrane vesicles: an overlooked component of the matrices of biofilms." J Bacteriol. **188**, 5945-5957(2006).

[40]. H. Zhang, D.W. Niesel, J.W. Peterson, G.R. Klimpel, "Lipoprotein release by bacteria: potential factor in bacterial pathogenesis." Infect Immun. **66**, 5196-5201(1998).

[41]. D. Hart, P. Latzin, P. Hordijk, V. Marcos, C. Rudolph, M. Woischnik, S. Krauss-Etschmann, B. Koller, D. Reinhardt, A.A. Roscher, D. Roos, M. Griese, "Cleavage of CXCR1 on neutrophils disables bacterial killing in cystic fibrosis lung disease." Nat Med. **13**, 1423-1430(2007).

[42]. K. Guzik, M. Bzowska, J. Smagur, O Krupa, M Sieprawska, J Travis, J Potempa, "A new insight into phagocytosis of apoptotic cells: proteolytic enzymes divert the recognition and clearance of polymorphonuclear leukocytes by macrophages." Cell Death Differ. **14**, 171-182(2007).

[43]. J. Baran, K. Guzik, W. Hryniewicz, M. Ernst, H.D. Flad, J.Pryjma,"Apoptosis of monocytes and prolonged survival of granulocytes as a result of phagocytosis of bacteria." Infect Immun. **64**, 4242-4248(1996).

[44]. A. do Vale, C. Costa-Ramos, A. Silva, D.S. Silva, F. Gärtner, N.M. dos Santos, M.T.Silva, "Systemic macrophage and neutrophil destruction by secondary necrosis induced by a bacterial exotoxin in a Gram negative septicaemia." Cell Microbiol. **9**, 988-1003(2007).

[45]. P. Birrer, N.G. McElvaney, A. Rudeberg , C.W. Sommer, S. Liechti-Gallati, R. Kraemer, R. Hubbard, R.G. Crystal, "Protease-antiprotease imbalance in the lungs of children with cystic fibrosis." Am J Respir Crit Care. Med. **150**, 207-213(1994).

[46]. J.J. Yang, R. Kettritz, R.J. Falk, J.C. Jennette, M.L. Gaido "Apoptosis of endothelial cells induced by the neutrophil serine proteases proteinase 3 and elastase." Am J Pathol. **149**, 1617-1626 (1996).

[47]. J. Davies, D. Davies, "Origins and evolution of antibiotic resistance." Microbiol. Mol. Biol. Rev. **74**, 417-33 (2010).

[48]. R. C. Owens, "Antimicrobial Stewardship: Concepts and Strategies in the 21st Century." Diagn Microbiol Infect. Dis. **61**, 110-128(2008).

[49]. S. Ganesh Kumar, C. Adithan, B. N. Harish, S. Sujatha, G. Royn and A. Malini,"Antimicrobial resistance in India , a review." J Nat Sci Biol Med. **4**, 286–291(2013).

[50]. P.W. Taylor, P.D. Stapleton, P.J. Luzio, "New ways to treat bacterial infections." Drug Discov Today. **7**, 1086–1090(2002).

[51]. V. Nizet, "Antimicrobial peptide resistance mechanisms of human bacterial pathogens." Curr Issues Mol Biol. **8**, 11-26(2006).

[52]. T. Maisch "A new strategy to destroy antibiotic resistant microorganisms: antimicrobial photodynamic treatment." Mini Rev. Med Chem. **9**, 974-983 (2009).

[53]. M. Wainwright, "Photodynamic antimicrobial chemotherapy (PACT)." J. Antimicrob Chemother. **42** , 13–28(1998).

[54]. N. Komerik, M. Wilson, "Factors influencing the susceptibility of Gram negative bacteria to toluidine blue O-mediated lethal photosensitization." J.of Appl. Microbiol. **91**, 1-7(2001).

[55]. Kirikae T, F. Kirikae, S.Saito K. Tominaga ,H. Tamura, Y. Uemura, T. Yokochi, M.Nakano, "Biological Characterization of Endotoxins Released from Antibiotic-Treated Pseudomonas aeruginosa and Escherichia coli, Antimicrob Agents Chemother. May; **42**, 1015–1021(1998).

[56]. M. Sharma, H. Bansal, P.K. Gupta, "Virulence of Pseudomonas aeruginosa cells surviving photodynamic treatment with toluidine blue." Curr Microbiol. **50**, 277–280(2005).

[57]. N. Kömerik, M. Wilson, S. Poole, "The effect of photodynamic action on two virulence factors of Gram negative bacteria." Photochem Photobiol. **72**, 676–680(2007).

[58]. S.Tubby, M.Wilson, and S. P.Nair, "Inactivation of Staphylococcal Virulence Factors Using a Light-Activated Antimicrobial Agent." BMC Microbiol **9**, 211(2009).

[59]. A. Tavares, C.M. Carvalho, M.A. Faustino, M.G. Neves, J.P. Tomé, A.C. Tomé, J.A. Cavaleiro, A. Cunha, N.C. Gomes, E. Alves, A. Almeida, "Antimicrobial

photodynamic therapy: study of bacterial recovery viability and potential development of resistance after treatment." Mar Drugs. **8**, 91-105(2010).

[60]. M. Sharma, L. Visai, F. Bragheri, I. Cristiani, P.K. Gupta, P. Speziale, "Toluidine Blue Mediated Photodynamic Effects on Staphylococcal Biofilms." Antimicrob Agents Chemother. **52**, 299-305(2008).

[61]. P. Braham, C. Herron, C. Street, R.Darveau, P. Braham, C. Herron, C. Street, R. Darveau "Antimicrobial Photodynamic Therapy May Promote Periodontal Healing Through Multiple Mechanisms." J Periodontol. **80**, 1790-1798(2009).

[62]. S. Packer, M. Bhatti, T. Burns, M. Wilson "Inactivation of Proteolytic Enzymes from Porphyromonas gingivalis Using Light Activated Agents." Lasers Med Sci. **15**, 24–30(2000)

[63]. G. Jori, C. Fabris, M. Soncin, S. Ferro, O. Coppellotti, D. Dei, L. Fantetti, G. Chiti, G. Roncucci,"Photodynamic therapy in the treatment of microbial infections: Basic principles and perspective applications," Lasers Surg Med **38**, 468 – 481(2006).

[64]. E. Alves , M.A. Faustino, M.G. Neves, A. Cunha, J. Tome, A. Almeida, "An insight on bacterial cellular targets of photodynamic inactivation." Future Med Chem. **6**:141-164 (2014).

[65]. K.A. Craig-Mylius and A. A. Weiss, "Antibacterial Agents and Release of Periplasmic Pertussis Toxin from Bordetella pertussis." Antimicrob Agents Chemother **44**, 1383-1386(2000).

[66]. M.Bhor, C. J.Thomas, N. Surolia, A.Surolia, "Polymyxin B: An Ode to an Old Antidote for Endotoxic Shock." Mol BioSyst. **1**, 213-222(2005).

[67]. K. Matsuzaki, “Control of cell selectivity of antimicrobial peptides.” Biochim Biophys Acta. **1788,** 1687-1692(2009).

[68]. M.W. Leach, R.J. Higgins, S.A. Autry J.E. Boggan, S.J. Lee K.M. Smith. “In vitro photodynamic effects of lysyl chlorin p6: cell survival, localization and ultrastructural changes.” Photochem Photobiol. **58** , 653-660(1993).

[69]. M.N. Usacheva, M.C. Teichert, M.A. Biel, “The role of the methylene blue and toluidine blue monomers and dimers in the photoinactivation of bacteria.” J. Photochem. Photobiol. B **71**, 87–98(2003).

[70]. G.P. Tegos , K. Masago , F. Aziz , A. Higginbotham , F.R. Stermitz , M.R. Hamblin “Inhibitors of bacterial multidrug efflux pumps potentiate antimicrobial photoinactivation.” Antimicrob Agents Chemother. **52**,3202-3209(2008).

[71]. R.A. Prates, I.T. Kato, M.S. Ribeiro, G.P. Tegos, M.R Hamblin, “Influence of multidrug efflux systems on methylene blue-mediated photodynamic inactivation of Candida albicans.” J Antimicrob Chemother. **66**,1525-1532 (2011).

[72]. A. Datta, A. Dube, B. Jain, A. Tiwari, P.K. Gupta, “The effect of pH and surfactant on the aggregation behavior of chlorin p6: a fluorescence spectroscopic study. Photochem Photobiol.” **75**, 488-494(2002).

[73]. A. Dube , S. Sharma, P.K. Gupta. “Tumor regression induced by photodynamic treatment with chlorin p(6) in hamster cheek pouch model of oral carcinogenesis: Dependence of mode of tumor cell death on the applied drug .” Oral Oncol. **47**, 467-471(2011).

[74]. V.S. Müller Campanile, C. Giannopoulou, G. Campanile, J.A. Cancela, A.Mombelli "Single or repeated antimicrobial photodynamic therapy as adjunct to ultrasonic debridement in residual periodontal pockets: clinical, microbiological, and local biological effects." Lasers Med Sci. **30**,27–34 (2015).

[75]. P.F. Andrade, G.P. Garlet, J.S. Silva, Fernandes PG, Milanezi C, Novaes AB Jr, D.B. Palioto, M.F. Grisi, M. Taba Jr, S.L. Souza. "Adjunct effect of the antimicrobial photodynamic therapy to an association of non-surgical and surgical periodontal treatment in modulation of gene expression: a human study." J Photochem Photobiol B.**126**, 119-125(2013).

[76]. M.C.Hashimoto, , R.A.Prates, , I.T.Kato, , S.C.Nu´n˜ez, , L.C. Courrol, M.S..Ribeiro. "Antimicrobial photodynamic therapy on drug resistant Pseudomonas aeruginosa induced infection. An in vivo study." Photochem Photobiol. **88**, 590–595(2012).

[77]. O.Simonetti, O.Cirioni, F.Orlando, C Alongi, G Lucarini, C Silvestri, A Zizzi, L Fantetti, G Roncucci, A Giacometti, A Offidani, M Provinciali, "Effectiveness of antimicrobial photodynam ic therapy with a single treatment of RLP068/Cl in an experimental model of Staphylococcus aureus wound infection." Br J Dermatol. **164**, 987–995(2011).

[78]. P.S.Zolfaghari, , S.Packer, , M.Singer, S.P. Nair, J. Bennett, C. Street, M. Wilson, "In vivo killing of Staphylococcus aureus using a light activated antimicrobial agent." BMC Microbiol. **9**, 27 (2009).

[79]. T.W. Wong, Y.Y. Wang, H.M. Sheu, Y.C. Chuang, "Bactericidal effects of toluidine blue mediated photodynamic action on Vibrio vulnificus." Antimicrob Agents Chemother. **49**, 299–305(2005).

[80]. D.Vecchio, , T. Dai, , L.Huang, , L. Fantetti, , G. Roncucci, , and M.R.Hamblin, "Antimicrobial photodynamic therapy with RLP068 kills methicillin resistant Staphylococcus aureus and improves wound healing in a mouse model of infected skin abrasion." J Biophotonics **6**, 733–742(2012).

[81]. F.F.Sperandio, A.Simo˜es, A.C.Aranha, , L.Correˆa, , S.C. Orsini Machado de Sousa, "Photodynamic therapy mediated by methylene blue dye in wound healing." Photomed Laser Surg. **28**, 581–587(2010).

[82]. S.G. Parekh, K.B. Trauner, B. Zarins, T.E.Foster, and R.R. Anderson, "Photodynamic modulation of wound healing with BPD-MA and CASP." Lasers Surg Med. **24**, 375–381(1999).

[83]. A. Kubler, R.K. Finley, I.A. Born, T.S. Mang,. "Effect of photodynamic therapy on the healing of a rat skin flap and its implication for head and neck reconstructive surgery." Lasers Surg Med. **18**, 397–405(1996).

[84]. S. Morley, J. Griffiths, G. Philips, H. Moseley, C. O'Grady, K. Mellish, C.L. Lankester, B. Faris, R.J. Young, S.B. Brown, L.E. Rhodes "Phase IIa randomized, placebo-controlled study of antimicrobial photodynamic therapy in bacterially colonized, chronic leg ulcers and diabetic foot ulcers: a new approach to antimicrobial therapy." Br. J. Dermatol. **168**, 617-624(2013).

[85]. S. Brown, "Clinical antimicrobial photodynamic therapy: phase II studies in chronic wounds." J. Natl Compr Canc Netw. **10** ,Suppl 2,S80-3(2012).

[86]. M.M. Dinges, P.M. Orwin, P.M. Schlievert, "Exotoxins of Staphylococcus aureus." Clin. Microbiol Rev. **13**, 16-34(2000).

[87]. J. Travis , J. Potempa, "Bacterial Proteinases as Targets for the Development of Second-Generation Antibiotics." Biochim Biophys Acta. **1477**, 35-50(2000).

[88]. B. Fournier and D. Philpott "Recognition of Staphylococcus aureus by the Innate Immune System." Clin Microbiol Rev. **18**, 521-540(2005).

[89]. J.K. Hoober, T.W. Sery, and N. Yamamoto, "Photodynamic sensitizers from chlorophyll:purpurin-18 and chlorin p6," Photochem Photobiol **48**, 579–582 (1988).

[90]. T. Dai, G.B. Kharkwal, M. Tanaka, Y.Y. Huang, V.J. Bil de Arce and M.R. Hamblin, "Animal models of external traumatic wound infections." Virulence. **2**, 296-315(2011).

[91]. K. Srinivasan and P. Ramarao "Animal models in type 2 diabetes research: an overview." Indian J Med Res. **125**, 451-72(2007).

[92]. S.G. Paik, N. Fleischer, S.I. Shin, "Insulin-dependent diabetes mellitus induced by subdiabetogenic doses of streptozotocin: obligatory role of cell mediated autoimmune processes." Proc Natl Acad Sci. USA **77**, 6129–6133(1980).

[93]. S. Arora, S. K. Ojha and D. Vohora. "Characterization of streptozotocin induced Diabetes Mellitus in Swiss albino mice." Glob J Pharmac. **3**, 81-84 (2009).

[94]. Y. Bai, D.K. Ann, and W.C. Shen, "Recombinant granulocyte colony-stimulating factor-transferrin fusion protein as an oral myelopoietic agent." Proc Natl Acad Sci. USA **102**, 7292-6(2005).

[95]. K. Sahu, Y. Verma, M. Sharma, K.D. Rao and P.K. Gupta. "Non-invasive assessment of healing of bacteria infected and uninfected wounds using optical coherence tomography." Skin Res Technol. **16**, 428-437(2010).

[96]. A.F. Zuluaga, B.E. Salazar, C.A Rodriguez, A.X. Zapata, M. Agudelo and O. Vesga, "Neutropenia induced in outbred mice by a simplified low-dose

cyclophosphamide regimen: characterization and applicability to diverse experimental models of infectious diseases." BMC Infect Dis. **6**, 55(2006).

[97]. R.J. Mc Ripley and R.R. Whitney,"Characterization and quantitation of experimental surgical-wound infections used to evaluate topical antibacterial agents." Antimicrob Agents Chemother. **10**, 38–44(1976).

[98]. G.K. Reddy, C.S. Enwemeka, "A simplified method for the analysis of hydroxyproline in biological tissues." Clin Biochem. **29**, 225-9(1996).

[99]. G.C. Meireles, J.N. Santos, P.O. Chagas, A.P. Moura and A.L. Pinheiro, "Effectiveness of laser photobiomodulation at 660 or 780 nanometers on the repair of third-degree burns in diabetic rats." Photomed Laser Surg. **26**, 47-54 (2008).

[100]. C. Sevimli-Gür, I. Onbaşılar, P. Atilla, R. Genç, N. Cakar, I. Deliloğlu-Gürhan and E. Bedir, "In vitro growth stimulatory and in vivo wound healing studies on cycloartane-type saponins of *Astragalus* genus." J Ethnopharmacol. **134**, 844-50 (2011).

[101]. T. Dai, G.P. Tegos, T. Zhiyentayev, E. Mylonakis and M.R. Hamblin, "Photodynamic therapy for methicillin-resistant Staphylococcus aureus infection in a mouse skin abrasion model." Lasers Surg Med. **42**, 38-44(2010).

[102]. M.R. Hamblin, D.A. O'Donnell, N. Murthy, C.H. Contag and T. Hasan, "Rapid control of wound infections by targeted photodynamic therapy monitored by in vivo bioluminescence imaging." Photochem Photobiol 75, 51–57(2002).

[103]. M.R. Hamblin and T. Hasan "Photodynamic therapy: a new antimicrobial approach to infectious disease?" Photochem Photobiol Sci. **3**, 436-450(2004).

[104]. M.L. Embleton, S.P. Nair, B.D. Cookson and M. Wilson, "Selective lethal photosensitization of methicillin-resistant Staphylococcus aureus using an IgG-tin (IV) chlorin e6 conjugate," J Antimicrob Chemother. **50**,857-864(2002).

[105]. N.S. Soukos, L.A. Ximenez-Fyvie, M.R. Hamblin, S.S. Socransky, and T. Hasan, "Targeted antimicrobial photochemotherapy." Antimicrob Agents Chem. **42**, 2595-2601(1998).

[106]. G.P. Tegos, M. Anbe, C. Yang, T.N. Demidova, M. Satti, P. Mroz, S. Janjua, F. Gad , M.R. Hamblin, "Protease stable polycationic photosensitizer conjugates between polyethyleneimine and chlorin(e6) for broad-spectrum antimicrobial photoinactivation," Antimicrob Agents Chemo. **50**, 1402-1410 (2006).

[107]. M.R. Hamblin, T. Zahra, C.H. Contag, A.T. McManus and T. Hasan, "Optical monitoring and treatment of potentially lethal wound infections in vivo," J Infect Dis. **187**, 1717-1725(2003).

[108]. I. Kralic and S. El Mohsni. "A new method for the detection of singlet oxygen in aqueous solution," Photochem Photobiol **28**, 577–581(1978).

[109]. Y. Yamakoshi, , N. Umezawa, A. Ryu, K. Arakane, N. Miyata, Y. Goda, T. Masumizu and T. Nagano, "Active oxygen species generated from photoexcited fullerene (C60) as potential medicines: $O2^{-\cdot}$ versus $_1O^2$," J Am Chem Soc. **125**, 12803–12809(2003).

[110]. E. Alves, L. Costa, C.M. Carvalho, J.P. Tomé, M.A. Faustino, M.G. Neves, A.C. Tomé, J.A. Cavaleiro, A. Cunha and A. Almeida, "Charge effect on the photoinactivation of Gram negative and Gram positive bacteria by cationic meso-substituted porphyrins" BMC Microbiol. **9**, 70(2009).

[111]. M. Vaara "Agents that increase the permeability of the outer membrane." Microbiol Rev. **56**, 395-411(1992).

[112]. D. A. Devine and R. E. Hancock, "Cationic peptides: distribution and mechanisms of resistance," Curr Pharm Des. **8**,703–714(2002).

[113]. R.E. Hancock, "The Pseudomonas aeruginosa outer membrane permeability barrier and how to overcome it." Antibiot Chemother **36**, 95–102(1985).

[114]. F. Gad, T. Zahra, T. Hasan , M.R. Hamblin, "Effects of growth phase and extracellular slime on photodynamic inactivation of Gram-positive pathogenic bacteria," Antimicrob Agents Chemother. **48**, 2173-2178(2004).

[115]. M. Wilson and J. Pratten "Lethal photosensitisation of Staphylococcus aureus in vitro: effect of growth phase, serum, and pre-irradiation time," Lasers Surg Med. **16**, 272-276(1995).

[116]. W. Sabra, E.J. Kim and A.P. Zeng "Physiological responses of Pseudomonas aeruginosa PAO1 to oxidative stress in controlled microaerobic and aerobic cultures," Microbiol. **148**, 3195–3202(2002).

[117]. R.L Soon, R.L. Nation, P.G. Hartley, I. Larson , J. Li, "Atomic force microscopy investigation of the morphology and topography of colistin-heteroresistant Acinetobacter baumannii strains as a function of growth phase and in response to colistin treatment," Antimicrob Agents Chemother. **53**, 4979-4786(2009).

[118]. S.L. Walker, J.E. Hill, J.A. Redman and M. Elimelech, "Influence of growth phase on adhesion kinetics of Escherichia coli D21g." Appl Environ Microbiol. **71**, 3093–3099(2005).

[119]. M. Sharma, A. Dube, H. Bansal and P. K. Gupta, "Effect of pH on uptake and photodynamic action of chlorin p6 on human colon and breast adenocarcinoma cell lines," Photochem Photobiol Sci. **3**, 231-235(2004).

[120]. F. Gad, T. Zahra, K.P. Francis, T. Hasan and M.R. Hamblin, "Targeted photo-dynamic therapy of established soft-tissue infections in mice," Photochem Photobiol Sci. **3**, 451(2004).

[121]. M. N. Usacheva, M.C. Teichert and M.A. Biel, "Comparison of the methylene blue and toluidine blue photobactericidal efficacy against Gram positive and Gram negative microorganisms." Lasers Surg Med**. 29**, 165–173(2001).

[122]. M. Salmon-Divon, Y. Nitzan and Z. Malik, "Mechanistic aspects of Escherichia coli photodynamic inactivation by cationic tetra-meso(N-methylpyridyl)porphine, Photochem Photobiol Sci. **3**, 423-429(2004).

[123]. M.R. Hamblin, D.A. O'Donnell, N. Murthy, K. Rajagopalan, N. Michaud, M.E. Sherwood and T. Hasan, "Polycationic photosensitizer conjugates: effects of chain length and Gram classification on the photodynamic inactivation of bacteria." J Antimicrob Chemother. **49**, 941-951(2002).

[124]. J. Ubbinka nad P.Scha¨r-Zammaretti, "Probing bacterial interactions: integrated approaches combining atomic force microscopy, electron microscopy and biophysical techniques." Micron. **36**, 293-320(2005).

[125]. A da Silva, O Teschke, "Dynamics of the antimicrobial peptide PGLa action on Escherichia coli monitored by atomic force microscopy." World J Microbiol. Biotechnol. **21**, 1103-1110(2005).

[126]. M. Firtel and T. J. Beveridge, "Scanning Probe Microscopy in Microbiology." Micron. **26**, 347-362(1995).

[127]. D. Robichon, J.C. Girard, Y. Cenatiempo and J. F. Cavellier, "Atomic force microscopy of dead or living bacteria." C. R. Acad. Sci. III **322**, 687-693(1999).

[128]. A.V. Bolshakova, O.I. Kiselyova, A.S. Filonov, O.Y. Frolova, Y.L. Lyubchenko and I.V. Yaminsky, "Comparative study of bacteria with an atomic force microscopy operating in different modes." Ultramicroscopy **86**, 121-128(2001).

[129]. C.J. Sullivan, J.L. Morrell, D.P. Allisona, M.J. Doktycz, "Mounting of Escherichia coli spheroplasts for AFM imaging." Ultramicroscopy **105**, 96–102 (2005).

[130]. M. Meincken., D.L. Holroyd ,M. Rautenbach, "Atomic Force Microscopy Study of the Effect of Antimicrobial Peptides on the Cell Envelope of Escherichia coli." Antimicrob Agents Chemother. **49**, 4085–4092(2005).

[131]. J. Varkey, S. Singh, R. Nagaraj, "Antibacterial activity of linear peptides spanning the carboxy-terminal beta-sheet domain of arthropod defensins." Peptides **27**, 2614-2623 (2006).

[132]. A. Li , P.Y. Lee , B. Ho, J.L. Ding, C.T. Lim, "Atomic force microscopy study of the antimicrobial action of Sushi peptides on Gram negative bacteria." Biochim Biophys Acta **1768**, 411-418 (2007).

[133]. H.L. Alakomi, A. Paananen, M.L. Suihko, I.M. Helander, M.Saarela, "Weakening Effect of Cell Permeabilizers on Gram Negative Bacteria Causing Biodeterioration, Appl Env Microbiol. **72**, 4695–4703 (2006).

[134]. P.C. Bragga and D.Ricci, "Differences in the susceptibility of Streptococcus pyrogenes to rokitamycin and erythromycin A revealed by morphostructural atomic force microscopy." J. Antimicrob Chemother. **50**, 457-460(2002).

[135]. J. Lin, L.J. Bi, Z.G. Zhang, Y.M. Fu, T.T. Dong "Toluidine blue-mediated photodynamic therapy of oral wound infections in rats." Lasers Med Sci. **25**, 233-238 (2010).

[136]. M. Bhatti, A. MacRobert, S. Meghji, B. Henderson, M. Wilson, "A study of the uptake of toluidine blue O by Porphyromonas gingivalis and the mechanism of lethal photosensitization." Photochem Photobiol. 68 370-376(1998).

[137]. J.A. Williams, G.J. Pearson, M.J. Colles, M.Wilson "The photo-activated antibacterial action of toluidine blue O in a collagen matrix and in carious dentine." Caries Res. **38** (6): 530-536 (2004).

[138]. C. Z. Chen, S. L. Cooper. "Interactions between dendrimer biocides and bacterial membranes." Biomaterials 233359–3368 (2002).

[139]. Y. Kim, S. Farrah, R. Baney, "Membrane damage of bacteria by silanol treatment." Electronic Journal of Biotechnology **10.** 253-259 (2007).

[140]. N. Katsui, T. Tsuchido, R. Hiramatsu, S. Fujikawa, M. Takano, I. Shibasaki. "Heat-Induced blebbing and vesiculation of the outer membrane of Escherichia coli." J Bacteriol. **151**, 1523-1531(1982).

[141]. Z. Malik, T. Babushkin, S. Sher, J. Hanania, H. Ladan, Y. Nitzan, S. Salzberg, "Collapse of the K+ and ionic balance during photodynamic inactivation of leukemic cells, erythrocytes and Staphylococcus aureus." Int J Biochem. **25**, 1399-1406 (1993).

[142]. T.W.Wong,Y.Y.Wang, H.M. Sheu, Y.C. Chuang, "Bactericidal Effects of Toluidine Blue-Mediated Photodynamic Action on Vibrio vulnificus." Antimicrob Agents Chemother. **49,** 299–305 (2005).

[143]. N. A. Romanova, L. Y. Brovko, L. Moore, E. Pometun, A. P. Savitsky, N. N. Ugarova, and M. W. Griffiths, "Assessment of photodynamic destruction of Escherichia coli O157:H7 and Listeria monocytogenes by using ATP bioluminescence." Appl Environ Microbiol **69,** 6393-6398(2003).

[144]. M.R. Burns, Jenkins SA, Wood SJ, Miller K, David SA. "Structure-activity relationships in lipopolysaccharide neutralizers: design, synthesis, and biological evaluation of a 540-membered amphipathic bisamide library." J Comb Chem., **8**,32-43 (2006).

[145]. Hoess, A., Watson, S., Siber, G. R., and Liddington, R. "Crystal structure of an endotoxin-neutralizing protein from the horseshoe crab." Limulus anti-LPS factor, at 1.5 Å resolution. EMBO J. **12**, 3351–3356 (1993).

[146]. M. Ansermino, C.Hemsley, "Intensive care management and control of infection." BMJ **329,** 220–223(2004).

[147]. A. Hoess, S. Watson, G.R. Siber and R. Liddington, "Crystal structure of an endotoxin-neutralizing protein from the horseshoe crab, Limulus anti-LPS factor, at 1.5 Å resolution." EMBO J. **12**, 3351–3356 (1993).

[148]. S. Guo, L.A. Dipietro, "Factors affecting wound healing." J Dent Res. **89,** 219 –229 (2010).

[149]. C. Van Delden, B.H. Iglewski, "Cell-to-cell signaling and Pseudomonas aeruginosa infections." Emerg Infect Dis. **4**, 551-560 (1998).

[150]. B.A. Pruitt Jr, A.T. McManus, S.H. Kim, C.W. Goodwin, "Burn wound infections: current status." World J Surg. **22,** 135 – 145 (1998).

[151]. B. Moriyama, S.A. Henning, R. Childs, S.M. Holland, V.L. Anderson, J.C. Morris, W.H. Wilson, G.L. Drusano, T.J. Walsh, "High-fluence continuous

infusion beta-lactam antibiotics for the treatment of resistant Pseudomonas aeruginosa infections in immunocompromised patients." Ann Pharmacother. **44** (2010) 929-935.

[152]. T. Bjarnsholt, K. Kirketerp-Møller, P.Ø. Jensen , K.G. Madsen , R. Phipps , K. Krogfelt , N. Høiby , M.Givskov, "Why chronic wounds will not heal: a novel hypothesis." Wound Rep Regen. **16**, 2 –10 (2008).

[153]. J.P. Heggers, "Assessing and controlling wound infection." Clin Plast Surg. **30,** 25 – 35 (2003).

[154]. M. Firczuk, D. Nowis, J. Gołąb, "PDT-induced inflammatory and host responses." Photochem Photobiol Sci. **10,** 653-63 (2011).

[155]. K. Dunn, V. Edwards-Jones, "The role of Acticoat with nanocrystalline silver in the management of burns. " Burns. **30,** Suppl 1**,** S1-9 (2004).

[156]. M.R. Hamblin, T. Zahra, C.H. Contag, A.T. McManus, T. Hasan, "Optical monitoring and treatment of potentially lethal wound infections in vivo." J Infect Dis. **187,** 1717– 1725 (2003).

[157]. D.A. Caminos, M.B. Spesia, E.N. Durantini, "Photodynamic inac-tivation of Escherichia coli by novel meso-substituted porphyrins by 4-(3-N, N, N-trimethylammoniumpropoxy)phenyl and 4-(trifluoro-methyl)phenyl groups." Photochem Photobiol Sci. **5,** 56–65 (2006).

[158]. D. Bryan, K.B. Walker, M. Ferguson, R. Thorpe, "Cytokine gene expression in a murine wo und healing model." Cytokine **31,** 429 – 438 (2005).

[159]. J. Deng, B.R.Younge, R.A. Olshen, J.J. Goronzy, C.M. Weyand, "Th17 and T h1 T- cell responses ingiant cell arthritis." Circulation. **23,** 906–915 (2010).

[160]. P.K. Smith, R.I. Krohn, G.T. Hermanson, A.K. Mallia , F.H.Gartner, M.D.Provenzano,E.K. Fujimoto, N.M.Goeke, B.J.Olson, D.C. Klenk. "Measurement of protein using bicinchoninic acid." Anal Biochem. **150,** 76 – 85 (1985).

[161]. K. Ipaktchi, A. Mattar, A.D. Niederbichler et al, "Topical p38 MAPK inhibit ion reduces bacterial growth in an in vivo burn wound model." Surgery **142,** 86 –93 (2007).

[162]. E. Kanno, K. Kawakami, M. Ritsu K. Ishii, H. Tanno, S. Toriyabe, Y. Imai, R. Maruyama, M.Tachi, "Wound healinging skin promoted by inoculation with Pseudomonas aeruginosa PAO1: the critical role of tumor necrosis factor-α secreted from infiltrating neutrophils." Wound Repair Regen. **19**, 608 – 621 (2011).

[163]. S.O. Gollnick, S.S. Evans, H. Baumann, B. Owczarczak, P. Maier, L. Vaughan, W.C. Wang, E. Unger, B.W. Henderson, "Role of cytokines in photodynamic therapy-induced local and systemic inflammation." Br J Cancer. **88**, 1772– 1779 (2003).

[164]. M.R. Fogle, J.A. Griswold, J.W. Oliver, A.N. Hamood, "Anti-ETA IgG neutralizes the effects of Pseudomonas aeruginosa exotoxin A." J Surg Res. **106,** 86 – 98 (2002).

[165]. A.N. Neely, D.L. Hoover, I.A. Holder, A.S. Cross, "Circulating levels of tumour necrosis factor, interleukin 6, and proteolytic activity in a murine model of burn and infection." Burns. **22**, 524 –530 (1996).

[166]. R.S. Smith, S.G. Harris, R. Phipps, B. Iglewski, "The Pseudomonas aeruginosa quorum-sensing molecule N -(3-oxododeca-noyl) homoserine

lactone contributes to virulence and induces inflammation in vivo." J Bacteriol. **184,** 1132 –1139 (2002).

[167]. S. de Bentzmann, M. Polette, J.M. Zahm, J. Hinnrasky, C. Kileztky, O. Bajolet, J.M. Klossek, A. Filloux, A. Lazdunski, E. Puchelle, "Pseudomonas aeruginosa virulence factors delay airway epithelial wound repair by altering the actin cytoskeleton and inducing overactivation of epithelial matrix metalloproteinase-2." Lab Invest. **80,** 209-219 (2000).

[168]. E. Frithz-Lindsten, Y. Du, R. Rosqvist, A. Forsberg, "Intracellular targeting of exoenzyme S of Pseudomonas aeruginosa via type III-dependent translocation induces phagocytosis resistance, cytotoxicity and disruption of actin microfilaments." Mol. Microbiol. **25**, 1125-1139 (1997).

[169]. T.F. Bruno, D.E. Woods, C.H. Mody, "Exoenzyme S from Pseudomonas aeruginosa induces apoptosis in T lymphocytes." J Leukoc Biol. **67,** 808-816 (2000).

[170]. M. Aepfelbacher, M. Essler, "Disturbance of endothelial barrier function by bacterial toxins and atherogenic mediators: a role for Rho/Rho kinase." Cell Microbiol. **3,** 649-658 (2001).

[171]. M. Arditi, J. Zhou, R. Dorio, G.W. Rong, S.M. Goyert, K.S. Kim, "Endotoxin-mediated endothelial cell injury and activation: role of soluble CD14." Infect Immun. **61**, 3149-56 (1993).

[172]. L.F. Fajardo, H.H. Kwan, J. Kowalski, S.D. Prionas, A.C. Allison, "Dual role of tumor necrosis factor alpha in angiogenesis." Am J Pathol. **140**, 539 – 554 (1992).

[173]. Y.P. Han, T.L. Tuan, H. Wu, M. Hughes, W.L. Garner, "TNF-alpha stimulates activation of pro-MMP2 in human skin through NF-(kappa) B mediated induction of MT1-MMP." J Cell Sci. **114**, 131–139 (2001).

[174]. R. Liu, H.S. Bal, T. Desta, Y. Behl, D.T. Graves, "Tumor necrosis factor alpha mediates diabetes enhanced apoptosis of matrix producing cells and impairs diabetic healing." Am J Pathol. **168,** 757–764 (2006).

[175]. W.L. Biffl, E.E. Moore, F.A. Moore, V.M. Peterson, "Interleukin-6 in the injured patient. Marker of injury or mediator of inflammation?" Ann Surg. **224,** 647 – 664 (1996).

[176]. J.B. Wright, K. Lam, M.E. Olson, R.E. Burrell, "Is antimicrobial efficacy sufficient? A question concerning the benefits of new dressings." Wounds. **15,** 133 – 142 (2003).

[177]. D. Kjolseth, J.M. Frank, J.H. Barker et al, "Comparison of the effects of commonly used wound agents on epithelialization and neovascularization." J Am Coll Surg. **179,** 305 –312 (1994).

[178]. R. Mori, T. Kondo, T. Ohshima, Y. Ishida, N. Mukaida, "Accelerated wound healing in tumor necrosis factor receptor p55-deficient mice with reduced leukocyte infiltration. FASEB J **16,** 963 –974 (2002).

[179]. T Okamoto, Akaike T, M Suga, S Tanase, H. Horie , S. Miyajima, M. Ando, Ichinose Y, Maeda H. "Activation of human matrix metalloproteinases by various bacterial proteinases. " J Biol Chem. **272**, 6059-6066 (1997).

[180]. O. Simonetti, O. Cirioni, G. Lucarini et al, "Tigecycline accelerates staphylococcal-infected burn wound healing through matrix

metalloproteinase-9 modulation." J Antimicrob Chemother. **67**, 191-201 (2012).

[181]. Z. Metzger, D. Nitzan, S. Pitaru, T. Brosh, S. Teicher, "The effect of bacterial endotoxin on the early tensile strength of healing in surgical wounds." J Endod. **28**, 30–33 (2002).

[182]. K. Sahu, M. Sharma, H. Bansal, A. Dube, P.K. Gupta, "Topical photodynamic treatment with poly-L-lysine-chlorin p6 conjugate improves wound healing by reducing hyperinflammatory response in Pseudomonas aeruginosa infected wounds of mice." Lasers Med Sci. **28**, 465-471 (2013).

[183]. S. Rajagopalan, X.P.Meng ,S. Ramasamy,D.G.Harrison, Z.S. Galis . "Reactive oxygen species produced by macrophage-derived foam cells regulate the activity of vascular matrix metalloproteinases in vitro." Implications for atherosclerotic plaque stability. J Clin Invest. **98,** 2572–2579 (1996).

[184]. F. Kheradmand , E. Werner ,P. Tremble , M.Symons , Z. Werb , "Role of Rac1 and oxygen radicals in collagenase-1 expression induced by cell shape change." Science. **280,** 898–902 (1998).

[185]. J.W. Madden, E.E. Peacock Jr, "Studies on the biology of collagen during wound healing. Dynamic metabolism of scar collagen and remodeling of dermal wounds." Ann Surg. **174**, 511-520 (1971).

[186]. M.J. Cobb, Y. Chen, R.A. Underwood, M.L. Usui, J. Olerud, X. Li, "Noninvasive assessment of cutaneous wound healing using ultrahigh-resolution optical coherence tomography." J Biomed Opt. **11**, 064002–064011 (2006).

[187]. J.T. Oh, S.W. Lee, Y.S. Kim, K.B. Suhr, B.M. Kim, "Quantification of the wound healing using polarization-sensitive optical coherence tomography." J Biomed Opt. **11**, 041124 (2006).

[188]. K.H. Kim, M.C. Pierce, G. Maguluri, B.H. Park, S.J. Yoon, M. Lydon, R. Sheridan, J.F. de Boer, "In vivo imaging of human burn injuries with polarization-sensitive optical coherence tomography." J Biomed Opt. **17**, 066012 (2012).

[189]. C.K. Hitzenberger, E. Gotzinger, M. Sticker, M. Pircher, A.F. Fercher, "Measurement and imaging of birefringence and optic axis orientation by phase resolved polarization sensitive optical coherence tomography." Opt Express. **9**, 780–790.

[190]. K. Sahu, Y. Verma, M. Sharma, K.D. Rao, P.K. Gupta, "Non-invasive assessment of healing of bacteria infected and uninfected wounds using optical coherence tomography." Skin Res Technol. **16**, 428-437 (2010).

[191]. Y.P. Han, T.L. Tuan, H. Wu, M. Hughes, W.L. Garner, "TNF-alpha stimulates activation of pro-MMP2 in human skin through NF-(kappa) B mediated induction of MT1-MMP." J Cell Sci. **114**, 131–139 (2001).

[192]. C.A. Wesson, J. Deringer, L.E. Liou, K.W. Bayles, G.A. Bohach, W.R. Trumble, "Apoptosis Induced by Staphylococcus aureus in Epithelial Cells Utilizes a Mechanism Involving Caspases 8 and 3." Infect Immun. **68**, 2998-3001 (2000).

[193]. P. Kulig, B.A. Zabel, G. Dubin, S.J. Allen, T. Ohyama, J. Potempa, T.M. Handel, E.C. Butcher, J. Cichy, "Staphylococcus aureus-derived staphopain B,

a potent cysteine protease activator of plasma chemerin." J Immunol. **178**, 3713-3720 (2007).

[194]. T. Sasaki, R. Kano, H. Sato, Y. Nakamura, S. Watanabe, A. Hasegawa, "Effects of staphylococci on cytokine production from human keratinocytes." Br J Dermatol. **148**, 46-50 (2003).

[195]. A.M. Calander, S. Starckx, G. Opdenakker, P. Bergin, M. Quiding-Järbrink, A. Tarkowski, "Matrix metalloproteinase-9 (gelatinase B) deficiency leads to increased severity of Staphylococcus aureus triggered septic arthritis." Microbes Infect. **8**, 1434-1439 (2006).

[196]. P. Greenwel, S. Tanaka, D. Penkov et al, "Tumor necrosis factor alpha inhibits type I collagen synthesis through repressive CCAAT/enhancer-binding proteins." Mol Cell Biol. **20**, 912-918 (2000).

[197]. Y.P. Han, T.L. Tuan, H. Wu, M. Hughes, W.L. Garner, "TNF-alpha stimulates activation of pro-MMP2 in human skin through NF-(kappa) B mediated induction of MT1-MMP." J Cell Sci. **114**, 131–139 (2001).

[198]. M.J. Reiss, Y.P. Han, E. Garcia et al, "Matrix metalloproteinase-9 delays wound healing in a murine wound model." Surgery. **147**, 295 – 302 (2010).

[199]. M. Wolman, F.H. Kasten, "Polarized light microscopy in the study of the molecular structure of collagen and reticulin." Histochemistry. **85**, 41-49 (1986).

[200]. N.Z. Cantürk, N. Esen, B. Vural, Z. Cantürk, G. Kirkali, G. Oktay, S. Solakoglu, "The relationship between neutrophils and incisional wound healing." Skin Pharmacol Appl Skin Physiol. **14**, 108-116 (2001).

[201]. M. Tanaka, P. Mroz, T. Dai, L. Huang, Y. Morimoto, M. Kinoshita, Y. Yoshihara, K. Nemoto, N. Shinomiya, S. Seki, M.R. Hamblin, "Photodynamic therapy can induce a protective innate immune response against murine bacterial arthritis via neutrophil accumulation." PLoS One. **7,** e39823 (2012).

[202]. J.W. Burrow, J.A. Koch, H.H. Chuang, W. Zhong, D.D. Dean,V.L. Sylvia, "Nitric oxide donors selectively reduce the expression of matrix metalloproteinases-8 and -9 by human diabetic skin fibroblasts." Journal of Surgical Research. **140**, 90–98 (2007).

[203]. V. Rapozzi, E. Della Pietra, S. Zorzet, M. Zacchigna, B. Bonavida, L.E. Xodo, "Nitric oxide mediated activity in anti-cancer photodynamic therapy." Nitric Oxide. **30,** 26-35 (2013).

[204]. U.S. Pettersson, G. Christoffersson, S. Massena, D. Ahl, L. Jansson, J. Henriksnäs, M. Phillipson, "Increased recruitment but impaired function of leukocytes during inflammation in mouse models of type 1 and type 2 diabetes. " PLoS One. **6**, e22480 (2011).

[205]. K. Sahu, M. Sharma, P. Sharma, Y. Verma, K.D. Rao, H. Bansal, A. Dube, P.K. Gupta, "Effect of poly-L-lysine-chlorin P6-mediated antimicrobial photodynamic treatment on collagen restoration in bacteria-infected wounds." Photomed Las Surg. **32,** 23-29 (2014).

[206]. K.K. Griendling, G.A. FitzGerald, "Oxidative stress and cardiovascular injury : par t ii: animal and human studies." Circulation. **108**, 2034–2040 (2003).

[207]. Ana Tellechea, Ermelindo Leal, Aristidis Veves and Eugénia Carvalho, "Inflammatory and Angiogenic Abnormalities in Diabetic Wound Healing:

Role of Neuropeptides and Therapeutic Perspectives." The Open Circulation and Vascular Journal. **3**, 43-55 (2010).

[208]. W. Marhoffer, M. Stein, L. Schleinkofer, K. Federlin, "Evidence of ex vivo and in vitro impaired neutrophil oxidative burst and phagocytic capacity in type 1 diabetes mellitus." Diabetes Res. Clin. Pract. **19**, 183-188 (1993).

[209]. S. Rossi, M. D'Amico, A. Capuano, M. Romano, P. Petronella, C. Di Filippo, "Hyperglycemia in streptozotocin-induced diabetes leads to persistent inflammation and tissue damage following uveitis due to reduced levels of ciliary body heme oxygenase-1." Mediators Inflamm. 2006; 2006(4):60285.

[210]. J. Berlanga-Acosta, G.S. Schultz, E. López-Mola, G. Guillen-Nieto, M. García-Siverio, L. Herrera-Martínez, "Glucose toxic effects on granulation tissue productive cells: the diabetics' impaired healing." Biomed Res Int. 2013;2013:256043.

[211]. A.M. Rasik, A. Shukla, "Antioxidant status in delayed healing type of wounds." Int J Exp Pathol. **81,** 257-63 (2000).

[212]. X Zhang,F Jiang,S N Kalkanis, Z Zhang, X Hong,H Yang,M Chopp, "Post-acute response of 9L gliosarcoma to Photofrin-mediated PDT in athymic nude mice." Lasers Med Sci **22**, 253-259 (2007).

[213]. J. Rich, J.C. Lee, "The pathogenesis of Staphylococcus aureus infection in the diabetic NOD mouse." Diabetes." **54**, 2904-2910 (2005).

[214]. B.B. Atiyeh, M. Costagliola, S.N. Hayek, S.A. Dibo, "Effect of silver on burn wound infection control and healing: review of the literature." Burns. **33**, 139-148 (2007).

[215]. A. Ozturk , C. Fırat , H. Parlakpınar, A. Bay-Karabulut, H. Kirimlioglu, A. Gurlek, "Beneficial effects of aminoguanidine on skin flap survival in diabetic rats." Exp Diabetes Res. **2012**, 721256 (2012).

[216]. M. Tian, C. Qing, Y. Niu, J. Dong, X. Cao, F. Song, X. Ji, S. Lu, "Effect of aminoguanidine intervention on neutrophils in diabetes inflammatory cells wound healing." Exp Clin Endocrinol Diabetes. **121**, 635-642 (2013).

[217]. H.G. Utley, F. Bernheim, P. Hochstein, "Effect of sulfhydryl reagents on peroxidation in microsomes." Arch Biochem Biophys. **118,**29–32(1967).

[218]. P. Kehkashan, R. Khan, W. A. Siddiqui, "Antidiabetic effects afforded by Terminalia arjuna in high fat fed and streptozotocin induced type 2 diabetic rats." Int J Diabetes and Metab **19**,23-33 (2011).

[219]. R.L. Levine, J.A. Williams, E.R. Stadtman, E. Shacter, "Carbonyl assays for determination of oxidatively modified proteins." Methods Enzymol. **233**, 346-357 (1994).

[220]. G.L. Ellman, "Tissue sulphydryl groups." Arch Biochem Biophys. **82,** 70-77 (1959).

[221]. J. Drobnik, D. Slotwinska, S. Olczak, D. Tosik, A. Pieniazek,K. Matczak, A. Koceva-Chyla, A. Szczepanowska, "Pharmacological doses of melatonin reduce the glycosaminoglycan level within the infarcted heart scar." J Physiol Pharmacol. **62**, 29-35 (2011).

[222]. J. Seguí, M. Gironella, M. Sans, S. Granell, F. Gil, M. Gimeno, P. Coronel , J.M. Piqué, j. Panés, "Superoxide dismutase ameliorates TNBS-induced colitis by reducing oxidative stress, adhesion molecule expression, and leukocyte recruitment into the inflamed intestine." J Leukoc Biol. **76,** 537-544 (2004).

[223]. P. Wanikiat, A. Panthong, P. Sujayanon, C. Yoosook, A.G. Rossi, V. Reutrakul, "The anti inflammatory effects and the inhibition of neutrophil responsiveness by Barleria lupulina and Clinacanthus nutans extracts." J Ethnopharmacol. **116**, 234-244 (2008).

[224]. T. Hagio, K. Kishikawa, K. Kawabata, S. Tasaka, S. Hashimoto, N. Hasegawa, A.Ishizaka, "Inhibition of neutrophil elastase reduces lung injury and bacterial count in hamsters." Pulm Pharmacol Ther. **21**,884-891 (2008).

[225]. G C Jagetia,G K Rajanikant,K V Rao Mallikarjun,"Ascorbic acid increases healing of excision wounds of mice whole body exposed to different doses of gamma radiation." Burns **33**, 484-494 (2007)..

[226]. Y. Abramov, B. Golden, M. Sullivan, S.M. Botros, J.J.R. Miller, A. Alshahrour, R.P. Goldberg, P.K. Sand, "Histologic characterization of vaginal vs. abdominal surgical wound healing in a rabbit model." Wound Rep Regen **15**, 80–86 (2007).

[227]. C. Sevimli-Gür, I. Onbaşılar, P. Atilla, R. Genç, N. Cakar, I. Deliloğlu-Gürhan, E. Bedir, "In vitro growth stimulatory and in vivo wound healing studies on cycloartane-type saponins of Astragalus genus." J Ethnopharmacol., **134**, 844-850 (2011).

[228]. H. Jain "Effect of photodynamic therapy on oxidative marker level of wounds of diabetic mice" M. Phil. thesis submitted to DAVV, Indore (2013).

[229]. U.S. Pettersson, G. Christoffersson, S. Massena, D. Ahl, L. Jansson, J. Henriksnäs, M. Phillipson, "Increased recruitment but impaired function of leukocytes during inflammation in mouse models of type 1 and type 2 diabetes. " PLoS One. **6**, e22480 (2011).

[230]. Y. Kannan, M. Tokunaga, M. Moriyama, H. Kinoshita, Y.Nakamura, "Beneficial effects of troglitazone on neutrophil dysfunction in multiple low-dose streptozotocin induced diabetic mice." Clin Exp Immunol.**137**, 263-271 (2004).

[231]. M.B. Joshi, A. Lad, A.S. Bharath Prasad, A. Balakrishnan, L. Ramachandra, K. Satyamoorthy, "High glucose modulates IL-6 mediated immune homeostasis through impeding neutrophil extracellular trap formation." FEBS Lett. **587**, 2241-2246(2013) .

[232]. F. Giacco, M. Brownlee, "Oxidative stress and diabetic complications." Circ Res. **107**, 1058-1070 (2010).

[233]. H. Bantel, B. Sinha, W. Domschke, G. Peters, K. Schulze-Osthoff and R.U. Jänicke, "Alpha-Toxin is a mediator of Staphylococcus aureus-induced cell death and activates caspases via the intrinsic death pathway independently of death receptor signaling," J. Cell. Biol. **155**, 637-48(2001).

[234]. S.S. Im, T.F. Osborne,"Protection from bacterial-toxin-induced apoptosis in macrophages requires the lipogenic transcription factor sterol regulatory element binding protein 1a." Mol Cell Biol. **32**, 2196-202(2012).

[235]. R. Liu, T. Desta, H. He, D.T. Graves, "Diabetes alters the response to bacteria by enhancing fibroblast apoptosis." Endocrinology **145**, 2997-3003(2004).

[236]. F. Hanses, S. Park, J. Rich, J.C. Lee, "Reduced neutrophil apoptosis in diabetic mice during staphylococcal infection leads to prolonged Tnfα production and reduced neutrophil clearance." PLoS One **6**, 23633(2011).

[237]. V. Papayannopoulos, K.D. Metzler, A. Hakkim, A. Zychlinsky, "Neutrophil elastase and myeloperoxidase regulate the formation of neutrophil extracellular traps." J. Cell. Biol. **191**, 677-91(2010).

[238]. Y. Nishinaka, T. Arai, S. Adachi, A. Takaori-Kondo, K. Yamashita, "Singlet oxygen is essential for neutrophil extracellular trap formation." Biochem. Biophys. Res. Commun. **413**, 75-79 (2011).

[239]. Devalaraja RM, Nanney LB, Du J, Qian Q, Yu Y, Devalaraja MN, Richmond A. Delayed wound healing in CXCR2 knockout mice. J Invest Dermatol. **115**, 234-244(2000).

[240]. K. Sahu, H. Bansal, C. Mukharjee, M. Sharma, P.K. Gupta, "Atomic force microscopic study on morphological alterations induced by photodynamic action of Toluidine Blue O in Staphylococcus aureus and Escherichia coli." J. Photochem. Photobiol. B **96**, 9–16 (2009).

[241]. E.P. Reeves, H. Lu, H.L. Jacobs, C.G. Messina, S. Bolsover, G. Gabella, E.O. Potma, A. Warley, J. Roes, A.W. Segal, "Killing activity of neutrophils is mediated through activation of proteases by K+ flux." Nature. **416**, 291-297 (2002).

[242]. E. Collard and S. Roy, "Improved function of diabetic wound-site macrophages and accelerated wound closure in response to oral supplementation of a fermented papaya preparation." Antioxid Redox Signal. **13,** 599-606 (2010).

[243]. K. Kaltalioglu, S. Coskun-Cevher, F. Tugcu-Demiroz, N. Celebi, "PDGF supplementation alters oxidative events in wound healing process: a time course study." Arch Dermatol Res. **305**, 415-422 (2013).

[244]. Kim YW, Byzova TV, "Oxidative stress in angiogenesis and vascular disease." Blood. **123**, 625-631 (2014) .

[245]. J.D. Luo , A.F Chen, "Nitric oxide: a newly discovered function on wound healing." Acta Pharmacol Sin. **26**, 259-64(2005) .

[246]. T. Shibata ,K. Nagata ,Y. Kobayashi, "The mechanism underlying the appearance of late apoptotic neutrophils and subsequent TNF-α production at a late stage during Staphylococcus aureus bioparticle-induced peritoneal inflammation in inducible NO synthase deficient mice." Biochim Biophys Acta. **1802**,1105-1111 (2010) .

[247]. S.S. Im ,T.F. Osborne, "Protection from bacterial toxin induced apoptosis in macrophages requires the lipogenic transcription factor sterol regulatory element binding protein 1a." Mol Cell Biol. **32**,2196-2202 (2012) .

[248]. Power C., J.H. Wang , S. Sookai , J.T. Street , H.P. Redmond, "Bacterial wall products induce down-regulation of vascular endothelial growth factor receptors on endothelial cells via a CD14-dependent mechanism: implications for surgical wound healing" J Surg Res. **101**,138–145 (2001).

[249]. Gladwin M.T., D. B.Kim-Shapiro, "The functional nitrite reductase activity of the heme-globins." Blood. **112**, 2636-47(2008).